REPORT DOCUMENTATION PAGE

1a. REPORT SECURITY CLASSIFICATION UNCLASSIFIED	1b. RESTRICTIVE MARKINGS
2a. SECURITY CLASSIFICATION AUTHORITY	3 DISTRIBUTION / AVAILABILITY OF REPORT Approved for public release; distribution is unlimited.
2b. DECLASSIFICATION / DOWNGRADING SCHEDULE	
4. PERFORMING ORGANIZATION REPORT NUMBER(S) TR 7997	5. MONITORING ORGANIZATION REPORT NUMBER(S)
6a. NAME OF PERFORMING ORGANIZATION Naval Underwater Systems Center 6b. OFFICE SYMBOL (If applicable) Code 3315	7a. NAME OF MONITORING ORGANIZATION
6c. ADDRESS (City, State, and ZIP Code) New London Laboratory New London, CT 06320	7b. ADDRESS (City, State, and ZIP Code)
8a. NAME OF FUNDING / SPONSORING ORGANIZATION 8b. OFFICE SYMBOL (If applicable)	9. PROCUREMENT INSTRUMENT IDENTIFICATION NUMBER
8c. ADDRESS (City, State, and ZIP Code)	10. SOURCE OF FUNDING NUMBERS PROGRAM ELEMENT NO. / PROJECT NO. / TASK NO. / WORK UNIT ACCESSION NO.

11. TITLE (Include Security Classification)
OPTIMAL AND CONVENTIONAL SPACE-TIME PROCESSING IN FLOW NOISE

12. PERSONAL AUTHOR(S)
Dr. John W. Fay

13a. TYPE OF REPORT	13b. TIME COVERED	14. DATE OF REPORT (Year, Month, Day)	15. PAGE COUNT
Ph.D Thesis	FROM 1983 TO 1986	10 November 1987	204

16. SUPPLEMENTARY NOTATION

17 COSATI CODES		
FIELD	GROUP	SUB-GROUP
17	01	

18. SUBJECT TERMS (Continue on reverse if necessary and identify by block number)
Conventional Processing
Eckart Filtering
Flow Noise
Gaussian Signal Detection
Likelihood Ratio
Line Array

19 ABSTRACT (Continue on reverse if necessary and identify by block number)

A systematic approach is developed as a means of characterizing optimal and conventional space-time detection of a Gaussian signal in colored Gaussian flow noise with line arrays. Discrete arrays of sensors, as well as continuous finite observation intervals, are considered. Using the likelihood ratio as a starting point, exact solutions are formulated, specifying the optimal instrumentation for a rational noise model. These solutions provide the theoretical framework to determine upperbound detection performance and permit examination of the role played by the noise spectra in influencing the optimal instrumentation and its performance.

The study describes potential gains achievable with optimal processing over conventional processing. Flow noise spectral parameters are identified, for which either the detection gains with optimal processing are significant or conventional processing is sufficiently close to optimal. In many cases of practical interest,

20. DISTRIBUTION / AVAILABILITY OF ABSTRACT ☒ UNCLASSIFIED/UNLIMITED ☐ SAME AS RPT. ☐ DTIC USERS	21. ABSTRACT SECURITY CLASSIFICATION UNCLASSIFIED
22a. NAME OF RESPONSIBLE INDIVIDUAL John W. Fay	22b. TELEPHONE (Include Area Code) (203) 440-4176 22c. OFFICE SYMBOL Code 3315

DD FORM 1473, 84 MAR 83 APR edition may be used until exhausted.
All other editions are obsolete.

18. SUBJECT TERMS (Cont'd.)

Noise Model
Noise Spectra
Optimal Processing
Sensor Performance
Space-Time Processing
Wavenumber Spectra

19. ABSTRACT (Cont'd.)

one finds that the best narrowband robust performance is nearly achieved with conventional processing alone, especially if the spatial bandwidth-length product is large.

We examined a novel, but simple, modification of basic Eckart frequency filtering at a conventional beamformer output. We show that this modification recovers a substantial part of the detection loss incurred with basic Eckart filtering and conventional beamforming.

Examining performance under constraints of a limited number of sensors that affect the choice of array geometry, we find that, with groups of tightly spaced sensors, one can get a much higher array gain at certain frequencies. Thus, one achieves greatly improved detector performance (either optimal or conventional) over the performance achieved by spreading available sensors out so that the noise is uncorrelated from sensor to sensor.

With regard to the sensitivity of performance to differences between assumed and actual noise spectra, we find, with continuous observations, that wideband performance with conventional beamforming followed by modified Eckart filtering remains essentially invariant as the noise model ranges over a large class of rational spectra, including a simple Butterworth spectrum at one extreme and a Gaussian spectrum at the other.

NUSC Technical Report 7997
10 November 1987

Optimal and Conventional Space-Time Processing in Flow Noise

John W. Fay
Surface Ship Sonar Department

Naval Underwater Systems Center
Newport, Rhode Island / New London, Connecticut

Preface

This study was prepared as a dissertation for the degree of Doctor of Philosophy in Electrical Engineering from Yale University. It was funded under NUSC Project Nos. A75010 (Independent Research and Independent Exploratory Development) and 632Y00. Work was also supported by the Office of Naval Research under Contract No. N0014-80-C-0092.

The Technical Reviewer for this report was I. B. Cohen (Code 33A).

Reviewed and Approved: 10 November 1987

W. A. Von Winkle

W. A. Von Winkle
Associate Technical Director for Technology

TABLE OF CONTENTS

TABLE OF CONTENTS (Cont'd)

LIST OF ILLUSTRATIONS

LIST OF ILLUSTRATIONS (Cont'd)

GLOSSARY

TBL	Turbulent boundary layer
ν_k	Convective center wavenumber
U_c	Convective noise speed
λ_k	Noise wavelength at frequency ω_k
$y(t,x)$	Received space-time waveform
$s(t,x)$	Signal component of received waveform
$n(t,x)$	Noise component of received waveform
x	Point in the array
t	Time
A	Indicator function
L	Spatial observation interval
T	Temporal observation interval
H_1	Target-present hypothesis
H_0	Noise-only-present hypothesis
$\underline{\tilde{r}}$	Data vector of space-time samples
N	Number of positive frequencies
M	Number of spatial measurements
E	Expected value
W	Signal bandwidth
$\underline{r}$	Data vector of frequency space samples
$Y(\omega,x)$	Received waveform Fourier coefficient at ω and x
ω	Radian frequency
W	Processing bandwidth
K	Covariance matrix for received process

GLOSSARY (Cont'd)

$\delta_{n,m}$	Kronecker delta
$*$	Transpose conjugate operation
$K(\omega_j)$, K_j	Covariance matrix for received process at frequency ω_j
$\underline{r}_n$	Data vector of space samples at frequency n
$S(\omega_k,x)$	Fourier coefficient of signal at ω_k and x
$\omega_k\left(\frac{2\pi k}{T}\right)$	kth radian frequency
k	Frequency index
c	Speed of sound in water
$\underline{\delta}$	Unit vector in direction of signal propagation
$\underline{x}$	Vector from origin of array to point x in array
Ψ	Transformation variable vector from origin of array to point x
ν_s	Signal wavenumber
$S(\omega_k)$	Signal Fourier coefficient at ω_k
$s_k(x)$	Deterministic spatial function for signal
$\underline{s}(t)$	Received signal vector
θ_s	Signal arrival angle relative to array axis
$R_s(\omega_k,\omega_1;x-y)$, $R_s(\omega_k,\omega_1;\Omega)$	Signal space-time covariance function
Ω	x - y
S_k, $S(\omega)$	Power spectrum of signal process
$S(\omega_k,\nu)$	Signal wavenumber spectrum at ω_k
s_{ok}	Signal voltage at kth frequency
ν	Wavenumber (spatial frequency)
$\delta(\nu)$	Dirac delta function

GLOSSARY (Cont'd)

$K_s(\omega_k)$	Signal covariance matrix at ω_k
P_k	Normalized signal covariance matrix
$\underline{V}_k$, $\underline{V}(\omega)$	Steering vector
$\tilde{\lambda}_1$	Eigenvalue of signal covariance matrix
$\tilde{\lambda}_i$	itn eigenvalue of signal covariance matrix
$n_c(t,x)$	Flow noise component received waveform
$w(t,x)$	Uncorrelated noise component received waveform
$N(\omega_k,x)$	Noise Fourier coefficient at ω_k and x
$R_n(t-\sigma;x-y)$	Space-time covariance function of noise
$q(\omega_k,\omega_1;x-y)$	Space-frequency covariance function of noise
$q_k(x-y)$, $q(\omega;x-y)$	Noise space covariance function at kth frequency
N_k, $N(\omega)$	Noise power spectrum
$Q_k(\nu)$	Wavenumber-frequency density for total noise at ĸtn frequency
$F_k(\nu)$	First-order Butterworth wavenumber function at ĸtn frequency
I_k	Flow noise component of noise power spectrum N_k
β_k	Spatial bandwidth
α	Fractional bandwidtn, β_k/ν_k
$\tilde{\rho}_k(\Omega)$	First-order Butterwortn space covariance. function
δ_{ij}	Kronecker delta (δ) function
W_k	Spectral level for uncorrelated noise at ω_k

GLOSSARY (Cont'd)

$f(\Omega)$	Spatial function for uncorrelated noise
$\underline{r}/H_o$, $\underline{r}_k/H_o$	Data vector of noise-only frequency-space samples
K_n	Covariance matrix for received noise
$L(\underline{r})$	Likelinood ratio
$p(\underline{r}/H_i)$	Condition probability density of $\underline{r}$ under hypotnesis i
z	Log likelihood ratio
K_s	Covariance matrix for received signal
$K_n(\omega_k)$	Covariance matrix for received noise at ω_k
Q_k, $Q(\omega)$	Normalized-noise-only covariance matrix at single frequency
G_{ko}, $G_o(\omega)$	Optimal array gain
z_s	Small-signal likelinood ratio test
f_k	Variable cnange
z_s^k	ktn component small-signal likelihood ratio test
i, j	Integers
g_{kj}	Variable change, f_{kj}/Δ
Δ	Uniform sensor spacing
v_{ki}	ith element of steering vector at kth frequency
r_{kj}	jtn element of data vector of frequency-space samples
Q_{ij}	Element ij of normalized noise covariance matrix
$g_k(x)$, $g(\omega,x)$	Integral equation solution
$r_k(x)$, $r(\omega,x)$	Continuous data observation

GLOSSARY (Cont'd)

d^2	Detection index
z/H_i	Likelihood ratio test under hypothesis i
$\underline{H}_k$	Arbitrary matrix filter
G_k	Array gain at frequency ω_k
λ_1	First noise eigenvalue
ϕ_1	Eigenvector associated with largest eigenvalue λ_1
C_k, $C(\omega)$	Multiplicative scalar constant
$\underline{H}_k \mid opt$	Optimal matrix filter
$\underline{H}_k \mid con$	Conventional matrix filter
G_{kc}	Conventional array gain
p, r	Integers
Q_r, Q_{1-p}	Elements of noise-inverse normalized covariance matrix
d_o^2	Optimal detection index
A_k	Signal power at matrix filter output
B_k	Square of noise power at matrix filter output
C	Frequency invariant constant
b_o, c_o	Constants needed to satisfy endpoint boundary conditions
ν_d	Wavenumber difference, $\nu_k - \nu_s$
n	Integer
d_c^2	Conventional detection index
$F_{ka}(\nu)$	Wavenumber spectrum of sampled Butterworth covariance function

GLOSSARY (Cont'd)

ω_1	Lower signal frequency
ω_2	Upper signal frequency
ν_c	Cut-off wavenumber
ρ_k	Normalized covariance function
$\frac{W\Delta}{U_c}, \frac{\omega_{k\Delta}}{U_c}$	Normalized frequencies
G_{kT}	Overall array gain with beamforming on extended sensors
$G_{kc\|sub}$	Subarray gain
$G_{kc\|sub\ c}$	Extended sensor array gain
S_c	Extended sensor response to signal
$G_{ko\|sub}$	Large β_k l (optimal) extended sensor array gain
u	Variable
$\delta(r)$	rth derivative of Dirac delta function
$Q_n(\nu)$	Arbitrary homogeneous noise spectra
λ_s	Signal wavelength
G_{kD}	Overall array gain with conventional beamforming on subarrays
$\hat{S}$	Subarray response to signal discrete sensors
ν_D	Cluster steering wavenumber
$G_k$clus	Cluster array gain
M_1	Number of sensors per cluster
N_1	Number of subarrays in [-L/2, L/2]
$\tilde{Q}_n(\frac{\nu_k-\nu}{\beta_k})$	General spectral function independent of temporal frequency

CHAPTER ONE

INTRODUCTION

1.1 Physical Problem

We are concerned with the problem of passive sonar processing in mobile sonars, such as towed line arrays. The physical mechanism motivating the study is hydrodynamic noise, which often interferes with sonar (Sound Navigation Ranging) performance. It defines a class of noises arising from the flow of water over hydrophones or the hydrophone housing [1]. Flow noise, considered a member of this class, remains after all other sources of hydrodynamic noise have been accounted for. Its energy levels increase with tow speed, and hydrophones are usually directly coupled to the excitation. Hence, flow noise is often a major source of interference at low frequencies and high tow vessel speeds.

The flow noise components of primary concern to us are caused by turbulent flow in a turbulent boundary layer (TBL). The TBL existing between the free stream flow and the array creates random pressure fluctuations and transmits them to the hydrophones. These pressure fluctuations are usually seen as additive, often predominant, noise components, independent of the signal.

In the usual sonar application, the hydrophones in Fig. 1.1 simultaneously sense the signal and noise pressure field. Hydrophone data are then sent to data processing. The processed data are presented to an observer, who must decide whether or not a target is present. Uncertainty in this decision process is obviously increased by the presence of corrupting flow noise. The problem is to eliminate as much of the unwanted flow noise as possible without destroying target information.

Usual methods of reducing direct-coupled TBL noise (flow noise) in towed arrays fall into the category of "mechanical" processing. One such method that has had some success is referred to as hosewall attenuation. It embeds the sensors in material that tends to flatten the flow noise wavenumber spectrum. If the hosewall sufficiently whitens the noise spectrum, then conventional beamforming on the sensor outputs is optimum. The hosewall may also sufficiently attenuate the high wavenumber components so that flow noise is no longer the predominant noise component. When the remaining noise is spatially white, then conventional beamforming is again nearly optimal. If it is desired to improve signal-to-noise ratio, then hosewall attenuation must preferentially attenuate flow noise while passing the signal undistorted.

We shall argue on the basis of an assumed, but physically reasonable, flow noise model that hosewall attenuation gains nothing

over conventional processing on space-continuous apertures if the aperture contains a sufficient number of noise correlation lengths. Thus, space-continuous extended sensors essentially whiten the flow wavenumber spectrum with an insignificant effect on signal. Hence, a detector that uses conventional beamforming on extended sensor outputs can, with noise uncorrelated from sensor to sensor, come close to achieving the best possible detection index with an extremely simple but "robust" instrumentation. The present investigation grew out of earlier work by a number of researchers. Pasupathy [2] analyzed space-time processing on a space-continuous finite observation interval. He established asymptotic conditions on noise spatial parameters under which optimal processing could be expected to yield significant detection improvement over simpler conventional processing, such as conventional beamforming. In the same manner, he established asymptotic conditions for which conventional processing is itself nearly optimal.

Although Pasupathy's results serve mainly as asymptotic check points for parameter values, such as the ratio of interference power to the white noise power in the interference band and the noise spatial bandwidth array length product (βL), they do not provide sufficient insight into the practical issues of the array design problem. Pasupathy's model included an additive spatially white noise

component, incoherent from point to point. This formally results in infinite power at a point; hence, it is not a realistic model of underlying flow noise processes. Nor can we derive meaningful inferences from Pasupathy's results applicable to the detection problem with discrete observations (arrays).

In recent years there have been extensive investigations of the TBL and its effect on sonar processing. Much of the work is classified. The following summarizes the most relevant unclassified work. Jorgensen and Maidanick [3] have examined signal-to-noise improvement in the TBL that is achievable by adjusting sensitivities and separations of two- and three-point transducer systems. Kennedy [4] considered the approach of Nuttall and Hyde [5] of fully optimal weighting of discrete sensor outputs clustered in TBL and isotropic noise. Motivated by these earlier studies, Fay and Owsley [6] proposed an extremely simple instrumentation that combined the outputs of two sensors, resulting in a simple noise cancellation instrumentation. They considered the concept of minimum variance complex weighting on clusters of point sensors for the class of TBL noise fields represented by a very simple exponential model with additive uncorrelated noise.

However, a number of issues remain unresolved. For instance, there is not yet an adequate characterization of the achievable gains to be made with optimal processing over conventional processing in a flow noise environment, especially with regard to wideband detector performance. It is also not clear what detector instrumentations are necessary to achieve the gains. Attainable optimal and conventional performance values are not known nor are the exact conditions on spectral and array parameters for which optimal processing can produce large gains over conventional processing. Insight into these issues is necessary for practical interpretation of proposed signal processing schemes for flow-noise-dominated environments.

Our results differ from previous work in several ways. In formulating the detection problem, we derive exact closed-form expressions for the optimal detector structure and also the best detection performance achievable on a space-continuous, finite observation interval. This is done by modeling TBL noise with a first-order Butterworth rational wavenumber spectrum consistent with TBL models used in [3], [4], and [6] and also with Pasupathy's model. Although we confine our attention to the TBL flow noise problem in sonar line arrays (towed line arrays), the general results have a wider application to other interfering noise sources. We omit discussion of such noise sources because their influence on sonar performance has been treated extensively in the literature [7] - [18]. We shall present a unified treatment of optimal and

conventional detector performance in passage from a discrete array of spatial measurements to a space-continuous observation interval. It is shown that an uncorrelated noise component has zero spectral level in the limit of continuous observations. Therefore, only spatially colored flow noise remains to limit detection capability on the space-continuous interval. Since even the slightest amount of uncorrelated noise brings conventional processing closer to optimal, our performance results represent the best possible performance and also the absolute upper-bound performance advantage attainable with optimal processing over conventional processing.

Once specific spectra have been assigned to the signal and noise processes, the binary detection problem of a coherent wavefront signal in spatially colored flow noise with continuous observations becomes a straightforward filtering problem. The object then is to secure maximum signal-to-noise ratio subject to the spatial bandwidth constraint imposed by the finite length array at each signal frequency. Determining the optimal filter (detector) involves solving Fredholm integral equations encountered in connection with the likelihood ratio test [19]. The resulting optimal instrumentation is realized as an inner product between the space-continuous data and the solution of the integral equation.

This optimum instrumentation obviously depends on the particular features of the typical flow noise spectrum and the way these features interact with array properties. It is well known that a narrowband conventional detector (i.e., a conventional beamformer) is formally optimal when the noise wavenumber spectrum is white. We shall show that array gain for the conventional beamformer is nearly optimal when the array length contains a large number of noise correlation lengths. Thus, the long array must reduce the problem to near-white noise in the wavenumber interval for which the beamformer response is significant.

The main interest here is, of course, in situations where the noise is not white but instead has a general bandpass behavior in wavenumber space. In such situations, gains with optimal processing over conventional processing on a finite interval can be significant.

Our formulation of the detection problem of a signal in flow noise with continuous observations reduces to a classical binary detection problem of a known spatial signal in Gaussian-colored noise. Location of the signal is assumed to be known. Distance to the signal from a reference point in the array is assumed to be sufficiently large so that the signal is in the farfield and thus presents a plane wave pressure field to the array. The signal is assumed to be Gaussian zero mean with known spectral properties. Noise is assumed to be Gaussian zero mean with known temporal and spatial spectra. Numerous detection problems of this kind have been

solved in the framework of temporal processing on a finite temporal observation interval [19], [20]. Here we deal with a space-time interval but use established mathematical procedures to solve the detection problem.

The binary detection problem with arrays of equally spaced discrete sensors encounters an unavoidable aliasing problem in a flow noise environment. Since the upper cutoff wavenumber of the typical flow noise wavenumber spectrum is very high, there will be severe folding of noise wavenumbers onto acoustic wavenumbers unless uniform sensor spacing is extremely tight. The resulting aliased noise level, at the signal wavenumber, is thus increased over the noise level with continuous observations; also, the aliased noise wavenumber spectrum is often flatter. As a consequence, optimal and conventional detection capabilities are degraded substantially relative to the best continuous performance. With the flatter spectrum, the conventional processor itself moves closer to being optimum. The spatial Nyquist rate of the inverse noise spatial bandwidth [21] associated with sampling a bandpass flow noise process is meaningless in the spatial case since it implies the generation of a Hilbert transform on a space-continuous interval. Once discrete sensors are introduced, the aliasing loss has happened and is irreversible.

In almost all sonar applications, the number of available sensors or telemetry channels is limited and not sufficient to fully populate

a given observation interval. This raises the question of efficient use of a given number of sensors aimed at achieving the best possible detection performance. We show that there are better ways of using a limited number of sensors than simply spacing them uniformly, making the noise uncorrelated from sensor to sensor. We consider the array construction method in [6], consisting of groups of tightly spaced sensors with noise correlated between sensors. By using such groups, one can get a much higher array gain at certain frequencies and hence achieve greatly improved detector performance (either optimal or conventional) over the performance achievable with the same number of sensors spread out in the observation interval so as to make the noise uncorrelated from sensor to sensor.

Finally, we note that array gain is frequently used to compare the performance of alternative array processing procedures. It specifies the postbeamforming signal-to-noise ratio at any given frequency in terms of the input signal-to-noise ratio and is, therefore, independent of the transfer function of a linear filter connected to the beamformer output. Wideband detector or tracker performance, on the other hand, is not independent of such a filter. Thus, even if two systems have the same array gain, their wideband performance can be quite different. Specifically, in the case of towed line arrays operating in flow noise that is heavily concentrated at very high wavenumbers, optimal and conventional detectors can have very different wideband detection indices. It is shown here that much

of the performance loss due to the use of conventional beamforming can be recovered by a simple modification of the Eckart filter usually placed at the beamformer output. For a uniform array that is long compared with the flow noise correlation distance, such a filter can reduce the difference between optimal and conventional beamformer performance to a negligible amount. The modified Eckart filter should be much easier to implement than a fully optimal beamformer and, at least in environments such as those considered here, should realize much of the available performance gain.

It is appropriate at this point to discuss briefly the general form of the flow noise model to be used in this study, saving the detailed analytic description for Chapter 2. It is known that the TBL pressure fluctuations are random in both space and time, but the underlying physical mechanisms are not well understood [22, p. 125]. This lack of complete knowledge is not overly restrictive in our case. We need only consider available measured statistical properties of the TBL processes in order to specify the optimal processor.

We shall characterize the TBL process by a zero mean, Gaussian model, completely described by its covariance function. There is reason to believe that TBL pressure fluctuations are Gaussian [22, p. 125]. More pragmatically, the Gaussian property greatly simplifies analysis, leading to a linear processor that is optimum for a large class of error criteria [19].

One may obtain insight into the TBL pressure fluctuations from a discussion by Strasberg [22]. Hydrophones (pressure sensors) in the moving array (see Fig. 1.1) respond to the local random pressure fluctuations generated by the turbulence. In the case of towed arrays, the turbulent flow results mainly from the motion of the tow vessel and hence from the array moving through the water. Turbulent motion is characterized by flow velocities, whose magnitude and direction vary randomly with time. These flow velocities are superimposed on the mean flow velocity, which, for the towed array, is of the order of a typical tow vessel speed (17-42 ft/sec).

Local velocity variations of the eddies associated with the turbulence, traveling at the mean flow velocity along the array, are sensed at various temporal frequencies. If U_c is the mean (convective) speed of the moving sensor relative to the flow, the wavenumber, ν_k, associated with frequency $\omega_k = 2\pi f_k$ is

$$\nu_k = \omega_k / U_c \ .$$

These local velocity variations give rise to pressure fluctuations along the array at a frequency f_k. These pressure fluctuations are associated with alternating high and low pressure values along the array. The correlation function, describing the velocity and hence

the pressure dependence between points in the array at frequency f_k, has an oscillatory behavior with spatial period $\lambda_k = 2\pi/\nu_k$. Since typical mean flow speed is of the order of 25 ft/sec, adjacent zeros of the correlation function are separated by distances of the order of inches.

The local velocity variations of the eddies are commonly believed to maintain their spatial shape or structure for some distance as they move along the array at the mean flow speed in the direction of flow. However, they eventually lose their structure and thus become uncorrelated over distances that are often very large compared with the correlation period λ_k but small compared with acoustical signal wavelengths at typical sonar frequencies.

Theoretical models of TBL spectra do exist [23], [24, p. 145] but do not agree well with measured spectra for general towed array conditions. Experimental measurements [25], [26] suggest that the TBL wavenumber spectrum assumes the form shown in Fig. 1.2. This representation also agrees with the experimental Corcos spectral model for TBL wall pressure [27], [28]. Available measurements assure us that the typical wavenumber spectrum is concentrated about the convective wavenumber

$$\nu_k = \frac{\omega_k}{U_c} .$$

Once again, convective speed is of the order of the free stream speed (e.g., tow vehicle speed), which, for sonar applications, is orders of magnitude slower than the speed of sound in water. Thus, ν_k is likely to be a high wavenumber, far removed from the acoustic region where signal and other noise components with wavenumbers characterized by the speed of sound are found. It is this large wavenumber difference between signal and flow noise that provides the principal mechanism for separating signal and interfering flow noise and, hence, potentially achieving large detection gains. The peak noise level at ν_k is typically orders of magnitude larger than the noise level at the signal wavenumber. The wavenumber spread about the peak is characterized here by the spatial bandwidth, β_k, which characterizes the correlation scale of the TBL pressure fluctuations along the array. Experimental results in [26] suggest that β_k has the form

$$\beta_k = \frac{\alpha\omega_k}{U_c} = \frac{\alpha 2\pi}{\lambda_k} .$$

Since both ν_k and β_k vary linearly with ω_k, the fractional bandwidth α is frequency independent. The convective wavelength is λ_k, which is frequency dependent. Experimental results [26] indicate that components of pressure fluctuations in the turbulent flow at frequency ω_k are essentially uncorrelated after traveling five convective wavelengths in the direction of flow. This corresponds to values of α of order 0.02.

The small correlation length scale of the turbulent pressure fluctuations, shown in Fig. 1.2c, has important practical implications in sonar applications where one tends to separate sensors by one-half of an acoustical wavelength. In such cases, one sees that the high wavenumber TBL noise process is essentially uncorrelated from sensor to sensor. This generally results in aliased flow noise wavenumber density everywhere in the acoustic wavenumber interval. Hence, detection capability is severely degraded relative to detection capability with extremely tight sensor spacing.

It is clear, as we shall demonstrate, that there are preferred sensor spacings for the typical flow noise spectrum in Fig. 1.2. For instance, if the sensor interval in Fig. 1.2c is π/ν_K, noise tends to cancel. Sensor spacings of $2\pi/\nu_K$ are bad because the flow noise adds conerently. This suggests that sensors should always be tightly spaced within the noise correlation length, but that the precise spacing is not unimportant if one desires to improve detection performance in a flow noise environment.

The flow noise power spectrum is thougnt to be flat at low temporal frequencies but to slope at a rate of approximately f^{-3} at high frequencies. The transition between low and high frequencies, given by the quotient of the free stream velocity to the boundary layer thickness, is usually in the hundreds of hertz [1, pp. 360-365]. We shall assume that the flat portion of the power spectrum is either coincident with or larger than the signal band of interest.

Thus, we are always dealing with a flat noise spectrum in the signal band with a power level that varies, according to [1], as the cube of the free stream speed.

1.2 Organization

The study covers material that can be divided into six parts. Chapter 2 provides the mathematical background, models, and terminology needed in the remaining chapters.

Chapter 3 examines the binary detection problem of a random conerent wavefront signal in Gaussian stationary flow noise modeled as a first-order Butterworth rational wavenumber spectrum. We evaluate, in detail, the performance and structure of the likelihood ratio test by solving Fredholm integral equations over a finite and continuous observation interval. This characterizes the spatial aspects of the optimum detector and provides definite values for the detection index in terms of tne spectral parameters of signal and flow noise and their interaction with the aperture parameters.

In Chapter 4 the continuous observation interval is discretized to model an array of equally spaced point hydrophones. Again, we specify the optimal instrumentation. Array gain and detection index are used to measure comparative detection performance of optimal and conventional detectors in tne flow noise environment. It is shown

that much of the performance loss due to the use of conventional beamforming can be recovered by a simple modification of the Eckart filter usually placed at the beamformer output.

Chapter 5 deals with array design considerations, notably the choice of array geometry. When sensors are continuous, the primary constraints concern their length and separation. When sensors are discrete, one is almost certainly restricted to a given number of sensors and must arrange these in a geometrical pattern, which maximizes their detection index, preferably without unduly complicating the instrumentation. Both optimal solutions and the compromises dictated by practical considerations are presented.

Chapter 6 summarizes the results and recommends research along related lines.

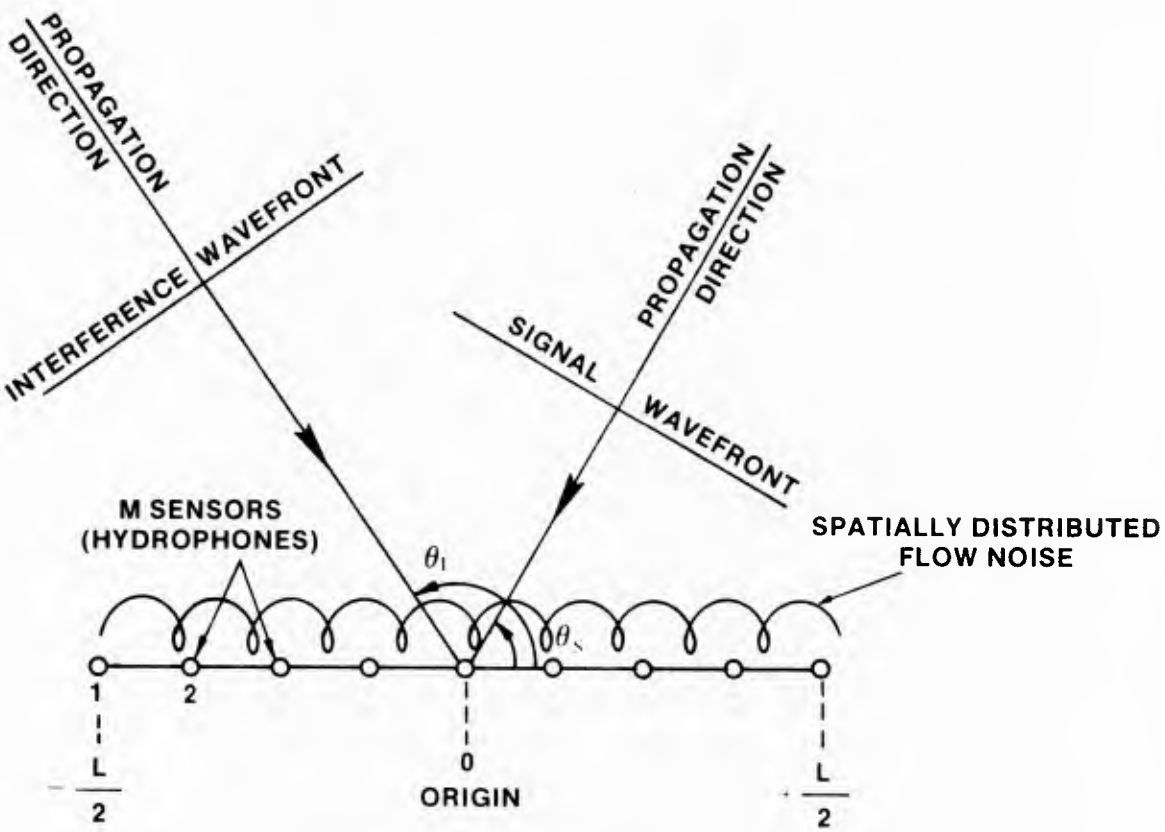

Fig. 1.1. Linear Array With Plane Wave Signal and Noises

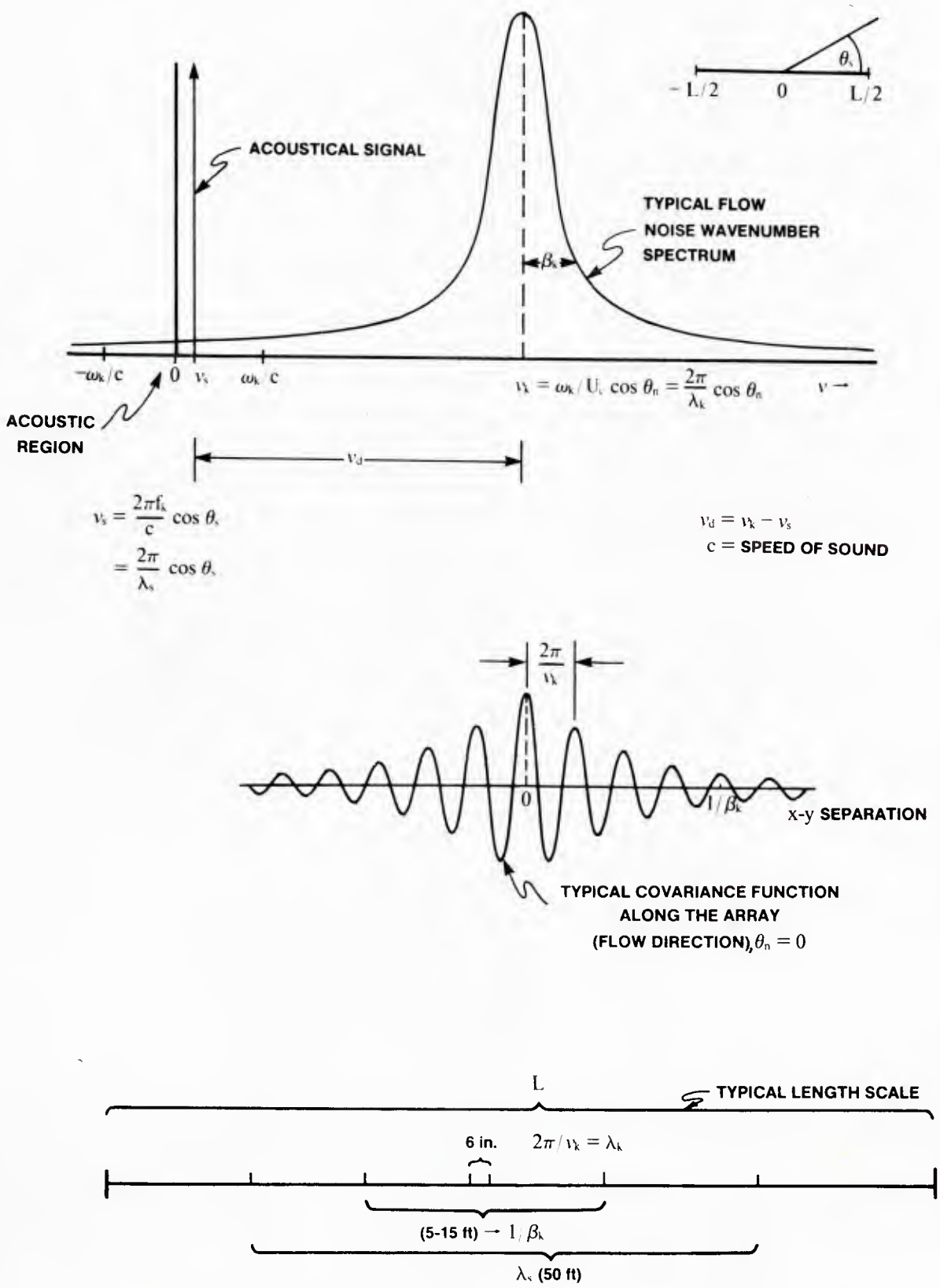

Fig. 1.2. Typical Narrowband Wavenumber Spectrum of Boundary Layer Pressure

CHAPTER TWO

MATHEMATICAL BACKGROUND

2.1 Mathematical Model

This chapter develops quantitative signal and noise models with mathematical properties to be used throughout the dissertation. It formulates the detection problem for discrete and continuous spatial observations and discusses the resulting integral equations.

The space-time processing model for target (signal) in a flow noise environment is shown in Fig. 2.1. The received pressure field is observed over the entire space-continuous array. Each point, x, in the array receives a space-time waveform,

$$y(t,x) = n(t,x) + A\, s(t,x), \qquad (2.1)$$

$$-\frac{L}{2} \le x \le \frac{L}{2}$$

$$-\frac{T}{2} \le t \le \frac{T}{2} \quad ,$$

which consists of signal $s(t,x)$ and additive noise $n(t,x)$. A is 1 if signal is present and 0 if it is absent. The received waveform is a realization of a random process parameterized by real numbers t and x. The realization contains target information when a target is present, and the noise usually consists of several components, such as

uncorrelated noise (electronic noise), farfield interference, and flow noise induced by movement of water past a mobile sonar array. We take special interest in the flow noise problem associated with high-speed towed line arrays and will generally ignore other noise components whose influence on the detection problem has been studied extensively [7] - [18].

2.2 Data Representation

2.2.1 Fourier Series Expansion

The received waveform is observed over a temporal-spatial observation interval, $[-T/2, T/2] \times [-L/2, L/2]$. The usual question in detection is whether or not the target signal is present in $y(t,x)$. This is a binary decision problem, with the following hypotheses on the received waveform (Van Trees [19]):

$$H_1 : \; y(t,x) = n(t,x) + s(t,x) \quad \text{(Target present)} \tag{2.2}$$

$$H_0 : \; y(t,x) = n(t,x) \quad \text{(Noise only present)} \; .$$

Signal and noise in (2.2) will be modeled as zero mean Gaussian random processes statistically independent of each other.

A data vector, $\underset{\sim}{\tilde{r}}$, is constructed by representing the received space-time pressure field in any convenient manner. An obvious, though not necessarily desirable, choice is a succession of space-time samples, $y(t_i,x_j)$:

$$\underset{\sim}{\tilde{r}} \triangleq \begin{bmatrix} y(t_1,x_1) \\ \vdots \\ y(t_1,x_M) \\ \vdots \\ y(t_N,x_1) \\ \vdots \\ y(t_N,x_M) \end{bmatrix} , \qquad (2.3)$$

where $i = 1, 2, \ldots, N$ and $j = 1, 2, \ldots, M$ so that there are N time samples at each of M spatial measurement points. The components of $\underset{\sim}{\tilde{r}}$ are zero mean and jointly Gaussian so that their statistical properties are specified by a covariance matrix with components:

$$E\left[y(t_i,x_l)\ y^*(t_j,x_m)\right] . \qquad (2.4)$$

The representation in (2.3) and (2.4) is cumbersome since it requires closely spaced time samples. For an observation interval T and bandwidth w, one generates a covariance matrix of dimension (M x 2wT) with little useful structure. The symbol * denotes a transpose conjugate operation and E represents statistical expectation.

A more convenient representation is available when all of the following conditions are satisfied: (a) the Tw product of the signal is large, a condition usually associated with passive sonar detection problems, (b) the signal wavefront travels across the aperture (array) in a time that is short compared with T, and (c) the turbulent boundary layer noise travels its correlation distance in a time that is short compared with T and the noise correlation time is also short compared with T. Then, Fourier coefficients at different frequencies are approximately uncorrelated [29], [30]. The Fourier representation, therefore, generates a block diagonal covariance matrix in (2.4) and hence reduces the effective dimensionality to M.

The data vector is now

$$\underline{r} \triangleq \begin{bmatrix} Y(\omega_1, x_1) \\ \vdots \\ Y(\omega_1, x_M) \\ \vdots \\ Y(\omega_N, x_1) \\ \vdots \\ Y(\omega_N, x_M) \end{bmatrix} , \tag{2.5}$$

where

$$Y(\omega_k, x_j) = \int_{-T/2}^{T/2} y(t, x_j) \frac{e^{-j\omega_k t}}{\sqrt{T}} \, dt , \quad \omega_k = \frac{2\pi k}{T} , \tag{2.6}$$

$$k = 1, 2, \ldots N .$$

The received waveforms are real so tnat $Y(-\omega_k, x_j) = Y^*(\omega_k, x_j)$. If $N \geq 2Tw$, then $\underline{r}$ should be an adequate representation of the continuous data over $(-T/2, T/2)$. The elements of $\underline{r}$ are jointly Gaussian since the Fourier series representation corresponds to a linear transformation on time samples. The process is thus characterized by its $(NM)x(NM)$ covariance matrix:

$$K \triangleq E[\underline{r}\,\underline{r}^*] . \tag{2.7}$$

Since Fourier coefficients associated with different frequencies are uncorrelated,

$$K_{n,m} \simeq K(\omega_n)\delta_{n,m} , \tag{2.8}$$

$$K_{n,m} \triangleq E\left[\underline{r}(\omega_n)\underline{r}(\omega_m)^*\right] , \tag{2.9}$$

$$\underline{r}_n \triangleq \underline{r}(\omega_n) \triangleq \begin{bmatrix} Y(\omega_n, x_1) \\ \vdots \\ Y(\omega_n, x_M) \end{bmatrix} , \tag{2.10}$$

and

$$K(\omega_n) \triangleq E\left[\underline{r}(\omega_n)\underline{r}(\omega_n)^*\right], \quad n = 1, 2, \ldots, N . \tag{2.11}$$

Consequently, the covariance matrix in (2.7) nas the following block diagonal form:

$$K = \begin{bmatrix} K_1 & 0 & \cdots & 0 \\ & K_2 & & \vdots \\ & & \ddots & \vdots \\ 0 & \cdots & 0 & K_N \end{bmatrix} , \tag{2.12}$$

where block matrices are defined by $K_j \triangleq K(\omega_j) = K(2\pi j/T)$.

2.3 Target Model

The target (signal) component of tne received waveform is modeled as shown in Fig. 2.2. The signal, s(t), originates at a source point that is assumed to satisfy farfield conditions. The signal pressure field propagates as a coherent wavefront from the source point, p, in the direction of the unit vector, $\underline{\delta}$, making an angle, θ_s, with the x axis, which coincides with the coordinate axis for the array. The following properties are assumed for the signal:

1. The signal s(t) is a stationary zero mean Gaussian random process characterized by known second moment properties.

2. The signal s(t) propagates undistorted from p to x, where it is represented as $s(t,x)$, $x \in (-\infty, \infty)$.

3. The signal s(t,x) is statistically independent of the noise processes n(t,x).

4. T is large compared with the signal correlation time and signal travel time across the spatial observation interval (array).

Fourier coefficients of the signal are given by

$$S(\omega_k,x) \triangleq \int_{-T/2}^{T/2} s(t,x) \frac{e^{-j\omega_k t}}{\sqrt{T}} dt , \quad \omega_k = \frac{2\pi k}{T} , \qquad (2.13)$$
$$k = 1, 2, \ldots, N ,$$

where $s(t,x) = s(t - \frac{\underline{\delta} \bullet \underline{x}}{c})$ are simply delayed versions of s(t) and c is the speed of sound in water. Note that $\frac{\underline{\delta} \bullet \underline{x}}{c}$ is the time delay at point x relative to a reference point at the origin, with

the vector from the origin to x defined by $\underline{x}$. Defining $\Psi \triangleq t - \frac{\underline{\delta} \cdot \underline{x}}{c}$, (2.13) can be written in the form

$$S(\omega_k, x) = \int_{-T/2 - \frac{\underline{\delta} \cdot \underline{x}}{c}}^{T/2 - \frac{\underline{\delta} \cdot \underline{x}}{c}} s(\Psi) \frac{e^{-j\omega_k (\Psi + \frac{\underline{\delta} \cdot \underline{x}}{c})}}{\sqrt{T}} d\Psi$$

$$= e^{-j\omega_k \frac{\underline{\delta} \cdot \underline{x}}{c}} \int_{-T/2 - \frac{\underline{\delta} \cdot \underline{x}}{c}}^{T/2 - \frac{\underline{\delta} \cdot \underline{x}}{c}} s(\Psi) \frac{e^{-j\omega_k \Psi}}{\sqrt{T}} d\Psi \quad . \tag{2.14}$$

Under assumption 4, (2.14) becomes

$$S(\omega_k, x) \simeq S(\omega_k)\, e^{-j\omega_k \frac{\underline{\delta} \cdot \underline{x}}{c}} , \tag{2.15}$$

where

$$S(\omega_k) \triangleq \int_{-T/2}^{T/2} s(t) \frac{e^{-j\omega_k t}}{\sqrt{T}} dt \quad . \tag{2.16}$$

Now define $s_k(x) = e^{j\nu_s x}$ with $\nu_s \triangleq \frac{\omega_k}{c} \cos \theta_s$; then

$$S(\omega_k,x) = S(\omega_k)s_k(x) \tag{2.17}$$

is the product of a Gaussian random variable, $S(\omega_k)$, describing temporal statistics of $s(t)$ and a deterministic function, $s_k(x)$, representing the spatial aspects of $s(t,x)$ at the kth frequency. Since $E[S(\omega_k)S(\omega_p)^*] = 0$ under assumption 4, the space-time covariance function for the signal is

$$R_s(\omega_k,\omega_l;x,y) \triangleq E\left[S(\omega_k,x)S(\omega_l,y)^*\right] = \begin{cases} E\left[\frac{|S(\omega_k)|^2}{T}\right]e^{j\nu_s(x-y)}, & \text{if } k = l \\ 0, & \text{if } k \neq l . \end{cases} \tag{2.18}$$

Again under assumption 4, $E\left[\frac{|S(\omega_k)|^2}{T}\right] \simeq S_k$ is the power spectrum of the radiated signal process. Fourier transforming (2.18) with respect to the variable $\mathbf{\Omega} = x - y$, one obtains the wavenumber spectrum for the signal:

$$S(\omega_k,\nu) \triangleq \int_{-\infty}^{\infty} R_s(\omega_k,\omega_l;\mathbf{\Omega})e^{-j\nu\mathbf{\Omega}}\, d\mathbf{\Omega} = \int_{-\infty}^{\infty} S_k\, e^{j(\nu_s-\nu)\mathbf{\Omega}}\, d\mathbf{\Omega}$$

$$= 2\pi\, S_k\, \delta(\nu - \nu_s) , \tag{2.19}$$

where $\delta(\nu)$ is a Dirac delta function. The frequency-wavenumber spectrum for the signal, at frequency ω_k, is thus modeled as a delta function at $\nu = \nu_s$ with known amplitude $2\pi\, S_k$.

Equation (2.15) characterizes the signal at x. The equivalent for a discrete set of sensors at $(x_1, x_2, \ldots, x_M)$ is

$$\underline{S}(\omega_k) = \int_{-T/2}^{T/2} \underline{s}(t) \frac{e^{-j\omega_k t}}{\sqrt{T}} dt = S(\omega_k) \begin{bmatrix} e^{-j\omega_k \frac{\underline{\delta} \bullet \underline{x}_1}{c}} \\ \vdots \\ e^{-j\omega_k \frac{\underline{\delta} \bullet \underline{x}_M}{c}} \end{bmatrix}, \quad (2.20)$$

which is a vector of essential spatial or geometric information scaled by the random variable $S(\omega_k)$. $\underline{S}(\omega_k)$ has the covariance matrix

$$K_s(\omega_k) \triangleq S_k \; P_k = S_k \; \underline{V}_k \; \underline{V}_k^* \quad , \quad (2.21)$$

where the "steering vector" $\underline{V}_k$ is defined by

$$\underline{V}_k \triangleq \begin{bmatrix} e^{-j\omega_k \frac{\underline{\delta} \bullet \underline{x}_1}{c}} \\ \vdots \\ e^{-j\omega_k \frac{\underline{\delta} \bullet \underline{x}_M}{c}} \end{bmatrix} . \quad (2.22)$$

Note that P_k is a rank one matrix with a single nonzero eigenvalue:

$$\tilde{\lambda}_1 = \text{trace } P_k = M \ , \tag{2.23}$$

$$\tilde{\lambda}_i = 0 \quad i \neq 1 \ . \tag{2.24}$$

2.4 Noise Model

We assume the following properties for the noise process $n(t,x) = n_c(t,x) + w(t,x)$, where $n_c(t,x)$ represents the flow component and $w(t,x)$ represents a spatially uncorrelated noise component. These assumptions are largely, but not entirely, equivalent to our earlier assumptions concerning the signal.

1. The noise components are assumed to be statistically independent of each other and of the signal.

2. $n(t,x)$ is a sample function from a zero mean Gaussian process characterized by known second moment properties, space homogeneity, and time stationarity.

3. The observation time T is large compared with the correlation time of the total noise process $n(t,x)$ and the time required for $n_c(t,x)$ to travel its correlation distance.

The noise spatial covariance function, at a pair of frequencies, is given by

$$q(\omega_k,\omega_l;x-y) \triangleq E\left[N(\omega_k,x)N^*(\omega_l,y)\right]$$

$$= \frac{1}{T}\int_{-T/2}^{T/2} dt \int_{-T/2}^{T/2} d\sigma\ E\left[n(t,x)n^*(\sigma,y)\right] e^{-j\omega_k t + j\omega_l \sigma}$$

$$= \frac{1}{T}\int_{-T/2}^{T/2} dt \int_{-T/2}^{T/2} d\sigma\ R_n(t-\sigma;x-y)e^{-j\omega_k x + j\omega_l \sigma} \quad , \qquad (2.25)$$

where

$$N(\omega_k,x) = \int_{-T/2}^{T/2} n(t,x)\frac{e^{-j\omega_k t}}{\sqrt{T}}\ dt \qquad (2.26)$$

and

$$R_n(t-\sigma;x-y) \triangleq E\left[n(t,x)\ n^*(\sigma,y)\right] \quad . \qquad (2.27)$$

Thus, when conditions 2 and 3 are satisfied,

$$q(\omega_k,\omega_l;x-y) = \begin{cases} \frac{1}{T}\int_{-T/2}^{T/2} dt \int_{-T/2}^{T/2} d\sigma\ R_n(t-\sigma;x-y)e^{-j\omega_k(t-\sigma)} = q_k(x-y), & \text{if } k = l \\ 0 , & \text{if } k \neq l . \end{cases}$$

(2.28)

Observe that the noise covariance function is homogeneous and thus depends only on the separation between spatial observations.

The power spectrum for the noise at a point is given by

$$\lim_{T\to\infty} q_k(o) = \lim_{T\to\infty} \frac{1}{T} \int_{-T/2}^{T/2}\int dt\, d\sigma\, R_n(t-\sigma;o)e^{-j\omega_k(t-\sigma)} = N_k \ . \quad (2.29)$$

The wavenumber-frequency power density for the noise, at frequency ω_k, is obtained by Fourier transforming the stationary covariance function in (2.28) with respect to $\boldsymbol{\Omega} = x - y$, yielding

$$Q_k(\nu) = \int_{\infty}^{\infty} q_k(\boldsymbol{\Omega})e^{-j\boldsymbol{\Omega}\nu}\, d\boldsymbol{\Omega} = \frac{1}{T}\int_{\infty}^{\infty} d\boldsymbol{\Omega} \int_{-T/2}^{T/2} dt \int_{-T/2}^{T/2} d\sigma\, R_n(t-\sigma;\boldsymbol{\Omega})e^{-j\omega_k(t-\sigma)-j\nu\boldsymbol{\Omega}} ,$$

$$k = 1, 2, \ldots, N \ . \quad (2.30)$$

The physical observations discussed in Chapter 1 indicate that the flow noise component of $Q_k(\nu)$ has the form of Fig. 2.3. For analytical purposes, we model the flow noise component of $Q_k(\nu)$ by the Butterworth function:

$$F_k(\nu) = \frac{2\beta_k I_k}{(\nu - \nu_k)^2 + \beta_k^2} \ , \quad (2.31)$$

$$k = 1, 2, \ldots, N \ .$$

Thus, ν_k characterizes the center wavenumber and β_k the bandwidth of the spatial spectrum with

$$\frac{\beta_k}{\nu_k} = \alpha \text{ , a constant,} \tag{2.32}$$

and

$$\nu_k = \frac{\omega_k}{\text{convective speed}} \triangleq \frac{\omega_k}{U_c} \text{ ;} \tag{2.33}$$

I_k is the flow noise spectral level at frequency ω_k. The flow noise component of $q_k(\boldsymbol{\Omega})$ is the inverse Fourier transform of (2.32):

$$\tilde{\rho}_k(\boldsymbol{\Omega}) = I_k \, e^{-\beta_k|\boldsymbol{\Omega}| + j\nu_k\boldsymbol{\Omega}} \text{ .} \tag{2.34}$$

Equation (2.31) is thus equivalent to the Corcos [27], [28] empirical model for a turbulent flow pressure field, which is a plausible model for the TBL noise observed by a towed array.

If, in addition to the flow noise, there is a spatially uncorrelated noise component of spectral level W_κ, then

$$q_k(x_i - x_j) = I_\kappa e^{-\beta_k |x_i - x_j| + j\,\nu_\kappa (x_i - x_j)} + W_\kappa \delta_{ij} \,, \qquad \kappa = 1, 2, \ldots, N \,, \tag{2.35}$$

where δ_{ij} is the Kronecker delta (δ) function. The Kronecker delta model for the uncorrelated noise process yields finite power density at each observation point. Thus, noise covariance matrices have finite traces.

Observe that the postulated noise model in (2.31) allows us to adjust all of the typically important variables (center wavenumber, bandwidth, and power level) discussed in Chapter 1. Because (2.31) is rational, solutions to the integral equations arising in the binary detection problem are obtained in a straightforward manner.

The uncorrelated noise makes no contribution to the wavenumber spectrum with continuous observations. To show this, we rewrite (2.35) in the form

$$q_\kappa(\boldsymbol{\Omega}) = I_\kappa e^{-\beta_k |\boldsymbol{\Omega}| + j\nu_k \boldsymbol{\Omega}} + W_\kappa f(\boldsymbol{\Omega}) \,, \tag{2.36}$$

where

$$f(\Omega) \triangleq \begin{cases} 1, & \text{if } \Omega = 0 \\ 0, & \text{if } \Omega \neq 0 \ . \end{cases} \tag{2.37}$$

Fourier transforming (2.36), we obtain

$$Q_k(\nu) = \int_{-\infty}^{\infty} I_k \, e^{-\beta_k|\Omega| + j(\nu_k - \nu)\Omega} d\Omega + W_k \int_{-\infty}^{\infty} f(\Omega) e^{-j\nu\Omega} d\Omega \ . \tag{2.38}$$

For finite W_k, the contribution from the second term is zero. As long as one is dealing with continuous observations, only the flow noise component of (2.35) need be considered. We must re-examine this issue when arrays of discrete sensors are discussed. We shall, however, argue for ignoring uncorrelated noise in this case, as well.

When there are M sensors, the noise wavesnapes are described by the M vector $\underline{n}(t)$ or the corresponding column vector of Fourier coefficients:

$$\underline{r}_k/H_o \triangleq \int_{-T/2}^{T/2} \underline{n}(t) \frac{e^{-j\omega_k t}}{\sqrt{T}} \, dt = \begin{bmatrix} N(\omega_k, x_1) \\ N(\omega_k, x_2) \\ \vdots \\ N(\omega_k, x_M) \end{bmatrix}, \quad k = 1, 2, \ldots, N \ . \tag{2.39}$$

Since the noise processes are jointly Gaussian, the vector process is described completely by the MN x MN covariance matrix

$$K_n \triangleq E\left[\underline{r}\,\underline{r}^*/H_0\right], \qquad k = 1, 2, \ldots, N, \tag{2.40}$$

consisting, for large Tw, of blocks of M x M matrices of the form in (2.12).

2.5 Likelihood Ratio.

2.5.1 Realization for Discrete Observations

Well-known analytical results [19] assert that the best detector forms the likelihood ratio

$$L(\underline{r}) = \frac{P(\underline{r}/H_1)}{P(\underline{r}/H_0)} \tag{2.41}$$

and compares it to a threshold. $P(\underline{r}/H_1)$ is the conditional probability density of the received data vector, $\underline{r}$, in (2.5) under hypothesis H_1.

The general form of the log likelihood ratio for Gaussian signals and noise is given by [19, pp. 296-116]. For the complex data vector in (2.5), the log likelihood ratio becomes [30]

$$\ln[L(\underline{r})] = \ln\left[\det\left[K_n\left(K_n + K_s\right)^{-1}\right]\right] + \underline{r}^* \left[K_n^{-1} - \left(K_n + K_s\right)^{-1}\right]\underline{r} \,, \tag{2.42}$$

where the covariance matrix under the noise-only hypothesis, from (2.40), is assumed to be nonsingular and

$$K_n + K_s = E\left[\underline{r}\,\underline{r}^*/H_1\right], \tag{2.43}$$

with

$$K_s = E\left[\underline{r}\,\underline{r}^*/\text{signal only}\right]. \tag{2.44}$$

Making use of the block diagonal structure of the covariance matrix in (2.12), an equivalent test statistic is

$$\begin{aligned} z &= \ln\left[L(\underline{r})\right] - \ln\left[\det\left[K_n(K_n + K_s)^{-1}\right]\right] \\ &= \sum_{k=1}^{N} \underline{r}_k^* \left[(N_k Q_k)^{-1} - (S_k P_k + N_k Q_k)^{-1}\right]\underline{r}_k \,, \end{aligned} \tag{2.45}$$

where

$$Q_k \triangleq K_n(\omega_k)/N_k \tag{2.46}$$

and P_k is defined by (2.21),

Appealing to Bartlett's identity [31],

$$(N_k Q_k + S_k P_k)^{-1} = (N_k Q_k)^{-1} - \frac{\frac{S_k}{N_k^2} Q_k^{-1} \underline{V}_k \underline{V}_k^* Q_k^{-1}}{1 + \frac{S_k}{N_k} \underline{V}_k^* Q_k^{-1} \underline{V}_k} . \tag{2.47}$$

Inserting this into (2.45), we obtain

$$z = \sum_{k=1}^{N} \frac{S_k / N_k^2}{1 + \frac{S_k}{N_k} G_{ko}} \left| \underline{V}_k^* \; Q_k^{-1} \; \underline{r}_k \right|^2 , \tag{2.48}$$

where

$$G_{ko} \triangleq G_o(\omega_k) = \underline{V}_k^* \; Q_k^{-1} \; \underline{V}_k \tag{2.49}$$

is the optimal array gain.

Significant detection problems exist primarily at low signal-to-noise ratios. With $S_k/N_k\ G_{ko} << 1$, one obtains the small signal likelihood ratio test:

$$z_s \triangleq \sum_{k=1}^{N} \left| \frac{\sqrt{S_k}}{N_k} \underline{V}_k^* \ Q_k^{-1} \ \underline{r}_k \right|^2 . \qquad (2.50)$$

If Q_k and the spectral functions are approximately constant over a frequency interval of length $(2\pi/T)$, the k sum can be approximated by an integral:

$$z_s = \frac{1}{\Delta\omega} \sum_{k=1}^{N} \left| \frac{\sqrt{S_k}}{N_k} \underline{V}_k^* \ Q_k^{-1} \ \underline{r}_k \right|^2 \Delta\omega \rightarrow \frac{T}{2\pi} \int_0^w \left| \frac{\sqrt{S(\omega)}}{N(\omega)} \underline{V}^*(\omega) Q(\omega)^{-1} \ \underline{r}(\omega) \right|^2 d\omega \ , \qquad (2.51)$$

with $\Delta\omega = \frac{2\pi}{T} \rightarrow d\omega$ and $N\Delta\omega \rightarrow w$, the upper end of the processed frequency band.

An implementation of the small signal test is shown in Fig. 2.4, where we have appealed to Parseval's theorem [21] to replace the frequency sum in (2.51) by a time sum.

2.5.2 Space-Continuous Observations

We now consider a heuristic, but direct, argument to derive the likelihood ratio test for space continuous observation in [-L/2, L/2]. The more rigorous argument is made in [32].

With the definition

$$\underline{f}_k^* \triangleq \sqrt{S}_k \, \underline{V}_k^* (N_k Q_k)^{-1} \quad , \tag{2.52}$$

the k^{th} component of (2.50) can be expressed as

$$z_s^k \triangleq \left| \sum_{j=1}^{M} f_{kj}^* \, r_{kj} \right|^2 = \left| \langle \underline{f}_k, \underline{r}_k \rangle \right|^2 \quad , \tag{2.53}$$

where the notation $\langle \bullet , \bullet \rangle$ denotes an inner product in the complex M space, C^M. Let f_{kj}, v_{kj}, and r_{kj} be the jth components of $\underline{f}_k$, $\underline{V}_k$, and $\underline{r}_k$, respectively. Now define

$$g_{kj} = \frac{f_{kj}}{\Delta} \quad , \; j = 1, 2, \ldots, M \; , \tag{2.54}$$

where Δ is the uniform spacing between observation points. Taking the transpose conjugate of (2.52) and then premultiplying by $N_k Q_k$, we have

$$\sum_{j=1}^{M} N_k Q_{ij} g_{kj} \Delta = \sqrt{S_k} v_{ki} \tag{2.55}$$

and

$$z_s^k = \left| \sum_{j=1}^{M} g_{kj}^* r_{kj} \Delta \right|^2 , \tag{2.56}$$

where

$i = 1, 2, \ldots, M,$
$k = 1, 2, \ldots, N,$ and
$M = \frac{L}{\Delta} + 1 ,$

with Q_{ij} the i^{th} j^{th} element of Q_k.

For $\Delta \to 0$ (arbitrarily tight sensor spacing on $[-L/2, L/2]$), with generalized function g and smoothly varying functions q and r, the sums in (2.55) and (2.56) can be approximated by integrals on $[-L/2, L/2]$ yielding

$$\int_{-L/2}^{L/2} q_k(x,y) g_k(y) dy = \sqrt{S_k}\, e^{j\nu_s x}, \quad -L/2 \le x \le L/2 , \tag{2.57}$$

and

$$z_s^{\kappa} = \left| \int_{-L/2}^{L/2} g_{\kappa}^{*}(x) r_{\kappa}(x) dx \right|^2 = \left| \left\langle g_{\kappa}(x),\ r_{\kappa}(x) \right\rangle \right|^2 \quad , \qquad (2.58)$$

where $$N_{\kappa} Q_{ij} \triangleq q_{\kappa}(x_i, y_j) \to q_{\kappa}(x,y) \ , \qquad (2.59)$$

$$\kappa = 1, 2, \ldots, N \ .$$

Equation (2.58) shows that the likelihood ratio test with continuous observations, at frequency ω_{κ}, is the magnitude-squared inner product between the data $r_{\kappa}(x)$ and the function $g_{\kappa}(x)$. To construct the optimal processor and thus the sufficient statistic z_s^{κ}, we need only determine $g_{\kappa}(x)$ from (2.57) for our Butterworth flow noise model from (2.34). Since we consider colored noise only, the relevant integral equations are Fredholm integral equations of the first kind.

Under the normal conditions for Riemann integrability, the sum over κ implied in (2.58) can be approximated by an integral for sufficiently large T:

$$z_s \doteq \frac{T}{2\pi} \int_0^W \left| \left\langle g(\omega,x),\ r(\omega,x) \right\rangle \right|^2 d\omega \quad , \qquad (2.60)$$

where $\Delta\omega = \frac{2\pi}{T} \to d\omega$ and $N\,\Delta\omega \to W$ as $T \to \infty$.

The more rigorous treatment of the transition from discrete to continuous observations in [32] shows that the solution of (2.55) converges formally to the solution of (2.57) if, and only if, the likelihood ratio test is nonsingular, a condition met in all problems of practical interest.

2.6 Likelihood Ratio Test Performance

2.6.1 Detection Index for General Detector

When the input covers a wide band of frequencies, the familiar detector structure in Fig. 2.4 is often characterized by a detection index, d^2, defined in terms of the output quantity z by the equation

$$d^2 = \frac{\left| E\left[z/H_1\right] - E\left[z/H_0\right] \right|^2}{\mathrm{Var}(z/H_0)} \quad . \tag{2.61}$$

Nuttall and Hyde [5] have obtained a general expression for d^2 in terms of an arbitrary matrix filter function $\underline{H}_k$:

$$d^2 = \frac{\left| \sum_k S_k \, \underline{H}_k^* \, \underline{V}_k \, \underline{V}_k^* \, \underline{H}_k \right|^2}{\sum_k \left| N_k \, \underline{H}_k^* \, Q_k \, \underline{H}_k \right|^2} \quad . \tag{2.62}$$

The narrowband performance of the general detector instrumentation is widely characterized by the array gain G_k at frequency ω_k. In physical terms, G_k is the signal-to-noise ratio at the matrix filter output (Point B in Fig. 2.4) divided by the signal-to-noise ratio at each sensor. Analytically, it takes the form [33]

$$G_k = \frac{\underline{H}_k^* \, \underline{V}_k \, \underline{V}_k^* \, \underline{H}_k}{\underline{H}_k^* \, Q_k \, \underline{H}_k} \quad . \tag{2.63}$$

$\underline{V}_k$ is the steering vector of the signal from (2.23). Again, $\underline{V}_k \, \underline{V}_k^*$ is the normalized spatial covariance matrix of the received signal.

If Q_k is positive definite and λ_1 is the largest eigenvalue of $Q_k^{-1} \, \underline{V}_k \, \underline{V}_k^*$, a well-known theorem of linear algebra asserts that

$$G_k \leq \lambda_1 \quad , \tag{2.64}$$

with equality if, and only if, $\underline{H}_k$ is an eigenvector, $\underline{\phi}_1$, associated with λ_1. Since $\underline{V}_k \, \underline{V}_k^*$ has rank 1, there is only one nonzero eigenvalue and $\underline{\phi}_1$ is unique to within a multiplicative constant, C_k. The fact that multiplication of $\underline{H}_k$ by a scalar constant, C_k, does not alter G_k is immediately obvious from (2.63).

Since

$$Q_k^{-1} \underline{V}_k \underline{V}_k^* \text{ has rank 1 ,}$$

$$\lambda_1 = \text{trace } (Q_k^{-1} \underline{V}_k \underline{V}_k^*) = \text{trace } (\underline{V}_k^* Q_k^{-1} \underline{V}_k) = \underline{V}_k^* Q_k^{-1} \underline{V}_k = G_{ko} \cdot \tag{2.65}$$

This is the familiar expression for the optimal array gain G_{ko}, first encountered in (2.49). The eigenvector ϕ_1 must satisfy

$$Q_k^{-1} \underline{V}_k \underline{V}_k^* \underline{\phi}_1 = \underline{V}_k^* Q_k^{-1} \underline{V}_k \underline{\phi}_1 \cdot \tag{2.66}$$

This equation is satisfied by $\underline{\phi}_1 = Q_k^{-1} \underline{V}_k$ so that

$$H_k|_{opt} = Q_k^{-1} \underline{V}_k , \tag{2.67}$$

unique to within a multiplicative constant, C_k.

Instead of using (2.67), conventional array processing procedures simply align the signal components of the received waveshape, which amounts to the choice

$$\underline{H}_k|_{con} = \underline{V}_k \cdot \tag{2.68}$$

Since $\left\|\underline{V}_k\right\|^2 = M^2$, (2.63) yields the conventional array gain

$$G_{kc} = \frac{M^2}{\underline{V}_k^* \, Q_k \, \underline{V}_k} \quad . \tag{2.69}$$

All of these results are familiar from the literature [33], [34]. Because of the invariance of G_k to scale changes in $\underline{H}_k$, one does not require equality of (2.68) and (2.67) to achieve equality of conventional and optimal array gains. Instead, one needs only

$$Q_k^{-1} \, \underline{V}_k = C_k \, \underline{V}_k \quad . \tag{2.70}$$

In other words, the steering vector $\underline{V}_k$ must be an eigenvector of Q_k^{-1} and hence of Q_k.

If the sensor separation is much larger than the noise correlation distance ($1 << \beta_k \Delta$), Q_k is an identity matrix and (2.70) is satisfied with $C_k = M$. If $\beta_k \Delta \leq 1$ but $\beta_k L >> 1$, it

follows that $M >> 1$. Since Q_k is a Toeplitz matrix, the left side of (2.70) has elements

$$Q_k^{-1} \underline{V}_k \Big|_l = \sum_{p=1}^{M} Q_{l-p} e^{j2\pi p\Delta\nu_s} = e^{j2\pi l\Delta\nu_s} \sum_{r=l-1}^{l-M} Q_r e^{-j2\pi r\Delta\nu_s} , \tag{2.71}$$

where $r = l - p$. Q_r differs from zero only for $r \leq \frac{1}{\beta_k \Delta}$.

Hence, the r sum is independent of l, except for edge effects near $l = 1$ and M. Except for these edge effects, (2.70) is therefore satisfied with

$$C_k = \sum_{r=-\infty}^{\infty} Q_r e^{-j2\pi r\Delta\nu_s} . \tag{2.72}$$

This somewhat informal argument suggests that the condition $\beta_k L >> 1$ is sufficient to ensure at least approximate equality of the optimal and conventional array gains of uniformly spaced linear arrays. Precise, but less general, calculations presented later will confirm this conclusion.

It is important to observe that a frequency-dependent rescaling of $\underline{H}_k$ by a scalar C_k will not, in general, leave d^2 unchanged. Thus, different instrumentations may have the same array gain but dramatically different detection indices.

According to a well-known result in detection theory [33], d^2 is maximized by the choice

$$\underline{H}_k = \frac{\sqrt{S_k}}{N_k} Q_k^{-1} \underline{V}_k \quad . \tag{2.73}$$

Thus, in addition to the spatial operation (2.67), the best processor uses the "Eckart filter" (see Fig. 2.4), with transfer function $\sqrt{S_k}/N_k$. Since it is common to all channels, it need be built only once and is inserted just ahead of the squaring operation in Fig. 2.4.

With the $\underline{H}_k$ given by (2.73), the optimum detection index becomes

$$d_o^2 = \sum_k \frac{S_k^2}{N_k^2} \left| \underline{V}_k^* Q_k^{-1} \underline{V}_k \right|^2 = \sum_k \frac{S_k^2}{N_k^2} G_{ko}^2 \quad . \tag{2.74}$$

For large T, one can make the usual integral approximation

$$d_o^2 \doteq \frac{T}{2\pi}\int_0^W \left|\frac{S(\omega)}{N(\omega)}\,\underline{V}^*(\omega)Q(\omega)^{-1}\,\underline{V}(\omega)\right|^2 d\omega$$

$$= \frac{T}{2\pi}\int_0^W \left|\frac{S(\omega)}{N(\omega)}\,G_o(\omega)\right|^2 d\omega \quad , \tag{2.75}$$

where again $G_o(\omega)$ is the optimal array gain at frequency ω.

Using the same Eckart filter with the conventional beamformer in (2.68),

$$\underline{H}_k = \frac{\sqrt{S_k}}{N_k}\,\underline{V}_k \quad . \tag{2.76}$$

Equation (2.62) becomes

$$d_c^2 = \frac{M^4\left|\sum_k \frac{S_k^2}{N_k^2}\right|^2}{\sum_k \frac{S_k^2}{N_k^2}\left|\underline{V}_k^*\,Q_k\,\underline{V}_k\right|^2} = \frac{\left|\sum_k \frac{S_k^2}{N_k^2}\right|^2}{\sum_k \frac{S_k^2}{N_k^2}\frac{1}{G_{kc}^2}} \quad . \tag{2.77}$$

G_{kc} is the conventional array gain given by (2.69).

The sum in (2.74) is dominated by frequencies where the optimal array gain G_{ko} (and hence the postbeamforming signal-to-noise ratio) is large. In contrast, the denominator sum in (2.77) is dominated by frequencies where G_{kc} is small. Low conventional array gain at some frequencies will, therefore, dramatically impair the performance of the conventional detector while it will only have a modest impact on the optimal detector. This statement remains true even when $G_{ko} = G_{kc}$ over the entire frequency band of interest (unless the two array gains are frequency independent). The only possible explanation is that the simple Eckart filter is well matched to the optimal processor but poorly matched to the conventional beamformer. The ideal postbeamformer filter (PBF) should be chosen according to its input signal and noise signal and noise spectra, not the element signal and noise spectra. The latter choice employs $\sqrt{S_k/N_k}$ as indicated in (2.76). We must, therefore, re-examine the issue of proper scalar filtering after the initial choice of the spatial filter has been made.

We now modify the detector structure in Fig. 2.4 by introducing the scalar filter $C(\omega)$, as shown in Fig. 2.5.

In what follows, we keep $\underline{H}(\omega)$ temporarily fixed and adjust $C(\omega)$ for the optimum detection index. Equation (2.62) now reads

$$d^2 = \frac{\left| \sum_k |C_k|^2 \, S_k \, \underline{H}_k^* \, \underline{V}_k \, \underline{V}_k^* \, \underline{H}_k \right|^2}{\sum_k |C_k|^4 \, N_k^2 \left| \underline{H}_k^* \, Q_k \, \underline{H}_k \right|^2} \quad . \tag{2.78}$$

$\underline{H}_k$ has simply been replaced by $C_k \, \underline{H}_k$.

Theorem:

$$\underset{C_k}{\text{Max}} \; d^2 = \sum_\kappa \frac{S_k^2}{N_k^2} \, G_k^2 \quad , \tag{2.79}$$

where G_k is given by (2.63) and the maximizing C_k satisfy

$$|C_k|^2 = \frac{S_k}{N_k^2} \frac{\underline{H}_k^* \, \underline{V}_k \, \underline{V}_k^* \, \underline{H}_k}{\left| \underline{H}_k^* \, Q_k \, \underline{H}_k \right|^2} \quad . \tag{2.80}$$

Proof:

$$\text{Let } A_k \equiv S_k \, \underline{H}_k^* \, \underline{V}_k \, \underline{V}_k^* \, \underline{H}_k \tag{2.81}$$

$$B_k \equiv N_k \, \underline{H}_k^* \, Q_k \, \underline{H}_k \quad . \tag{2.82}$$

Then (2.78) reads

$$d^2 = \frac{\left|\sum_K |C_K|^2 |A_K|^2\right|^2}{\sum_K |C_K|^4 B_K^2} \quad . \tag{2.83}$$

Rearranging the numerator and using the Schwartz inequality, one obtains

$$\left|\sum_k |C_k|^2 \; A_k\right|^2 = \left|\sum_K \frac{A_K}{B_K} |C_K|^2 \; B_K\right|^2$$

$$\leq \left(\sum_k \frac{A_K^2}{B_k^2}\right)\left(\sum_k |C_k|^4 \; B_K^2\right) \quad . \tag{2.84}$$

with equality if, and only if,

$$|C_k|^2 \; B_K = C \; \frac{A_k}{B_K} \quad , \tag{2.85}$$

where C is a frequency invariant constant. Substituting (2.85) into (2.83) and using (2.81), (2.82), and (2.63),

$$d^2 \leq \sum_k \frac{S_k^2}{N_k^2} \left| \frac{\underline{H}_k^* \underline{V}_k \underline{V}_k^* \underline{H}_k}{\underline{H}_k^* Q_k \underline{H}_k} \right|^2 = \sum_k \frac{S_k^2}{N_k^2} G_k^2 \quad . \tag{2.86}$$

Since the frequency invariant constant C does not affect the detection index, the maximizing $|C_k|^2$, i.e., the postbeamformer filter power transfer function, can be written as

$$|C_k|^2 = \frac{A_k}{B_k^2} = \frac{S_k}{N_k^2} \frac{\underline{H}_k^* \underline{V}_k \underline{V}_k^* \underline{H}_k}{|\underline{H}_k^* Q_k \underline{H}_k|^2} \quad . \tag{2.87}$$

This completes the proof.

With the optimal spatial filter $\underline{H}_k = Q_k^{-1} \underline{V}_k$, (2.87) becomes

$$|C_{ko}|^2 = \frac{S_k}{N_k^2} \quad . \tag{2.88}$$

Thus, we confirm that the simple Eckart filter is indeed optimal when matrix filtering is optimal. On the other hand, for the conventional beamformer $\underline{H}_k = \underline{V}_k$, the best frequency filter power transfer function is given by

$$\left|C_k\right|^2 = \frac{S_k}{N_k^2} \frac{M^2}{\left|\underline{V}_k^* Q_k \underline{V}_k\right|^2} = \frac{1}{M^2} \frac{S_k}{N_k^2} G_{kc}^2 \qquad (2.89)$$

The frequency invariant constant $1/M^2$ is, of course, immaterial. The important feature of (2.89) is the last factor: the best frequency filter voltage transfer function requires the weight G_{kc} in addition to the Eckart filter. With this weighting, the dependence of the detection index on the input signal-to-noise spectral ratio and array gain (2.79) is precisely the same for the optimal and conventional detector (or, for that matter, any detector with specified spatial filter $\underline{H}_k$). Differences in performance arise only because of differences between the optimal and suboptimal array gains, i.e., choices of $\underline{H}_k$.

The above ideas are easily extended to space-continuous observations. Using (2.52), we have from (2.74)

$$d_o^2 = \sum_k \frac{S_k^2}{N_k^2} \left|\underline{V}_k^* Q_k^{-1} \underline{V}_k\right|^2 = \sum_k S_k \left|\underline{f}_k^* \underline{V}_k\right|^2 . \qquad (2.90)$$

With the notation for g_{kj} in (2.54), the continuous formulation of optimal wideband detection performance follows easily:

$$d_o^2 = \sum_k \left| \left\langle g_k(x), \sqrt{S_k}\ e^{j\nu_s x} \right\rangle \right|^2$$

$$d_o^2 \doteq \frac{T}{2\pi} \int_0^W \left| \left\langle g(\omega,x), \sqrt{S(\omega)}\ e^{j\nu_s x} \right\rangle \right|^2 d\omega \ , \qquad (2.91)$$

with $g_k(x) \to g(\omega,x)$, $S_k \to S(\omega)$, and $N\Delta\omega \to W$.

Equation (2.91) says that optimal wideband detection performance in the continuous limit is specified completely by the inner product of the signal model $e^{j\nu_s x}$ and the function $g(\omega,x)$, which one obtains directly from (2.57). The inner product in (2.91) is over $[-L/2, L/2]$.

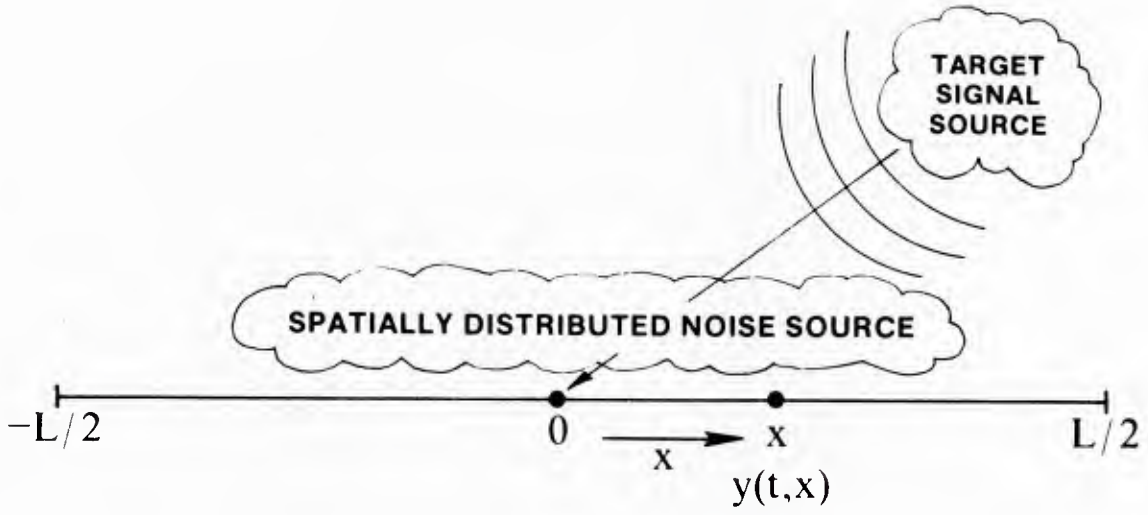

$$y(t,x) = n(t,x) + s(t,x)$$

Fig. 2.1. Aperture With Plane Wave Signal and Additive Colored Noise

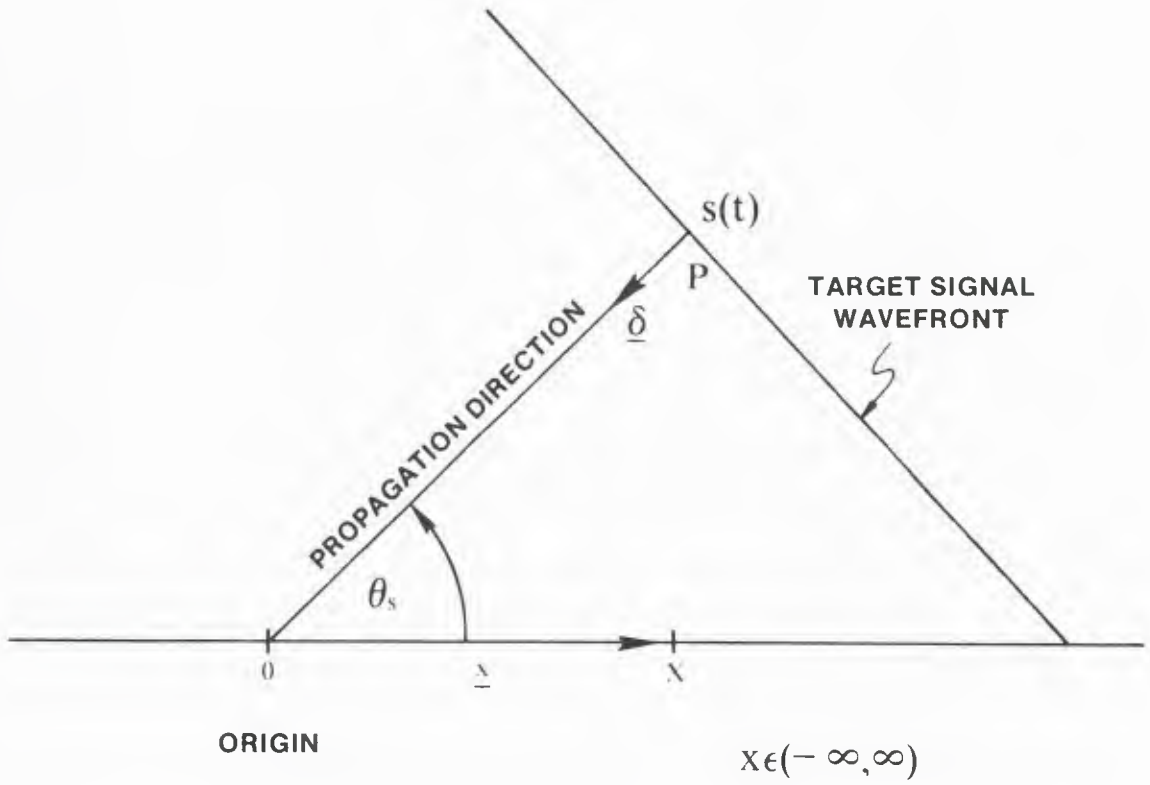

Fig. 2.2. Signal Model

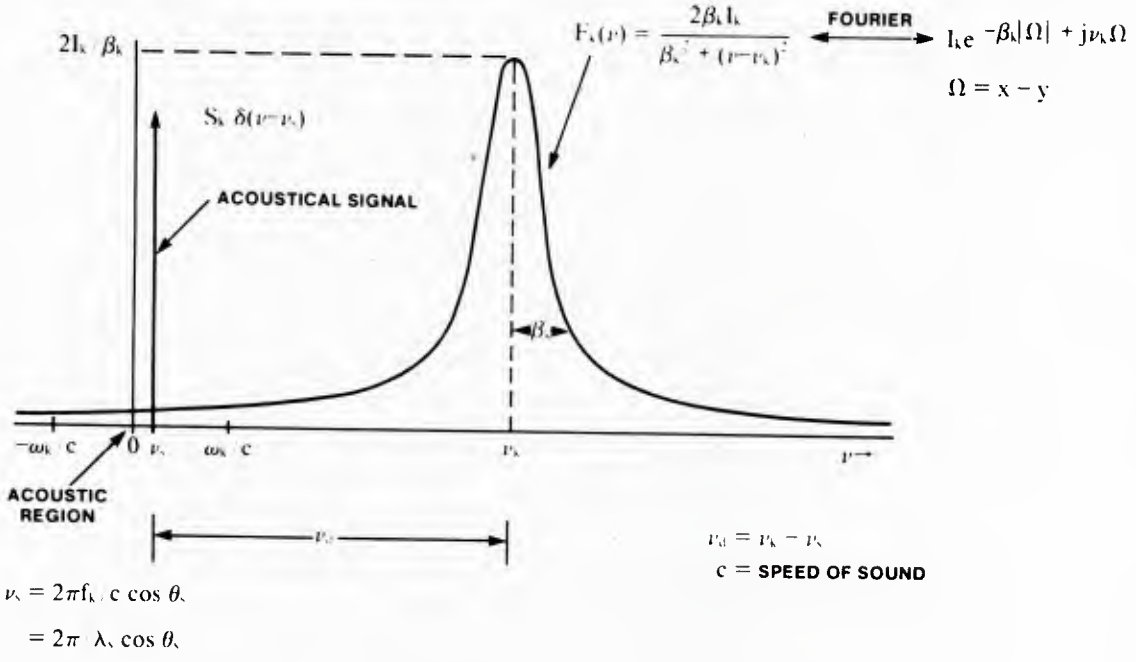

Fig. 2.3. Coherent Wavefront Signal and First Order-Butterworth Wavenumber Spectrum at kth Narrowband Frequency

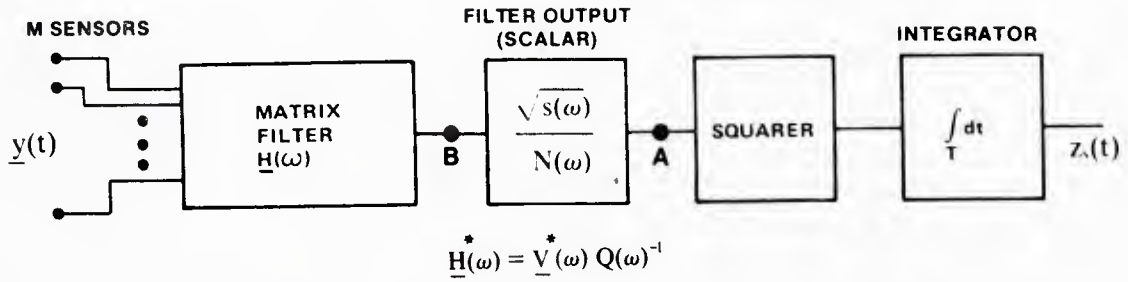

MATRIX FILTER FOR:

1) MAX S/N AT A: $\sqrt{\frac{s(\omega)}{N(\omega)}}$ **ECKART FILTER**

2) BEST FIT TO SIGNAL WAVESHAPE AT A: $\frac{\sqrt{s(\omega)}}{N(\omega)}$

Fig. 2.4. Small Signal Likelihood Ratio Test

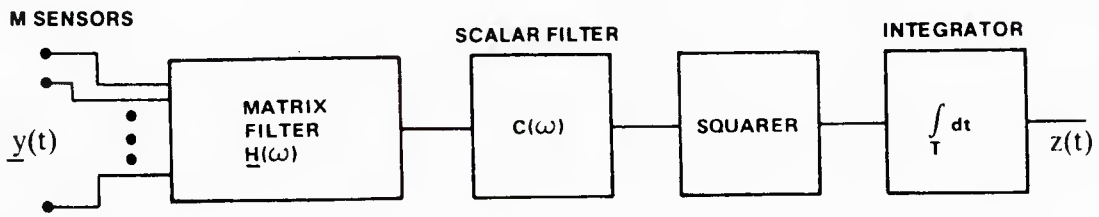

Fig. 2.5. Detector for Random Signal and Noise With Frequency Scaling

CHAPTER THREE

CONTINUOUS SPATIAL OBSERVATION

3.1 Optimal Processor Structure

This chapter deals with detection in a flow noise environment, using a continuous observation interval $[-L/2, L/2]$.

Van Trees [19, p. 316] describes a general technique of solving (2.57) for processes with rational spectra. If the noise spectrum has the form of (2.31), his procedure yields

$$g_k(x) = \frac{\sqrt{S_k}}{F_k(\nu_s)} e^{j\nu_s x} + \frac{b_o}{2}\delta(x + L/2) + \frac{c_o}{2}\delta(x - L/2), \quad -L/2 \le x \le L/2 , \tag{3.1}$$

where

$$b_o = \sqrt{S_k}\; e^{-j\nu_s L/2}\left(\frac{\beta_k + j\nu_d}{\beta_k I_k}\right)$$

and

$$c_o = \sqrt{S_k}\; e^{+j\nu_s L/2}\left(\frac{\beta_k - j\nu_d}{\beta_k I_k}\right),$$

$$\nu_d \triangleq \nu_k - \nu_s . \tag{3.2}$$

Substitution into (2.57) easily verifies that (3.1) indeed satisfies the integral equation.

According to (2.58), one constructs the spatial part of the likelihood ratio test at frequency ω_k as an inner product between $r_k(x)$ and $g_k(x)$:

$$\int_{-L/2}^{L/2} g_k^*(x) r_k(x)\,dx = \frac{b_o^*}{2} r_k(-L/2) + \frac{c_o^*}{2} r_k(+L/2) +$$

$$+ \frac{\sqrt{S_k}}{F_k(\nu_s)} \int_{-L/2}^{L/2} dx\, r_k(x) e^{-j\nu_s x} \quad . \tag{3.3}$$

The structure is shown in Fig. 3.1. We see that it is divided into two parts: a spatial-matched filter (conventional beamformer), which correlates the received process, $r_k(x)$, with a signal replica (i.e., $s_k^*(x)$) and two end-point sampling sensors, which receive the pressure field at the interval end points. The scalar $\sqrt{S_k}/F_k(\nu_s)$ represents the relative weighting necessary for the conventional processor to achieve near optimal wideband performance.

3.2 Narrowband Performance of the Optimal Spatial Processor

Nothing is lost in our understanding of narrowband optimal performance if we consider only the optimal array gain in d_o^2 from (2.91):

$$G_{ko} \triangleq \frac{I_k}{\sqrt{S_k}} \int_{-L/2}^{L/2} g_k(x)\, e^{-j\nu_s x}\, dx, \quad k = 1, 2, \ldots, N \tag{3.4}$$

$$= \frac{I_k L}{F_k(\nu_s)} + \frac{I_k}{\sqrt{S_k}} \frac{b_o}{2} e^{j\nu_s L/2} + \frac{I_k}{\sqrt{S_k}} \frac{c_o}{2} e^{-j\nu_s L/2} . \tag{3.5}$$

Substituting for b_o and c_o from (3.2), one obtains

$$G_{ko} = \frac{I_k L}{F_k(\nu_s)} + 1$$

$$= \left(1 + \frac{\beta_k L}{2}\left(1 + \frac{\nu_d^2}{\beta_k^2}\right)\right). \tag{3.6}$$

This result is intuitively appealing. If the aperture length L approaches zero, then the optimal instrumentation becomes effectively a single sensor with unity array gain:

$$G_{ko} \to 1 . \tag{3.7}$$

On the other hand, if

$$\frac{I_k L}{F_k(\nu_s)} \gg 1 \quad , \tag{3.8}$$

then

$$G_{ko} \rightarrow \frac{I_k L}{F_k(\nu_s)} = \frac{\beta_k L}{2}\left(1 + \frac{\nu_d^2}{\beta_k^2}\right), \tag{3.9}$$

which provides the intuitively satisfying observation that

$$G_{ko} = \frac{I_k}{F_k(\nu_s)1/L} = \frac{\text{Total noise power}}{\text{Noise power in band of width } 1/L \text{ near } \nu_s} \tag{3.10}$$

must exceed unity for the optimal array gain to exceed unity. In the absence of wavenumber structure for the noise in $[\nu_s, \nu_k]$ in Fig. 2.3., i.e., $\nu_d^2/\beta_k^2 \ll 1$, optimal array gain significantly exceeds unity if, and only if, $\beta_k L$ exceeds 2.

In the absence of white noise, one can achieve perfect detectability (singular detection) [19, p. 303] with optimal processing, namely

$$G_{ko} \to \infty \ , \tag{3.11}$$

if the spatial bandwidth, β_k, is exactly zero in (3.9). For flow noise, β_k cannot be zero and therefore this problem will not arise.

The result in (3.9) is very clear. Array gain with optimal processing is large if, and only if,

$$\frac{\beta_k L}{2} \left(1 + \frac{\nu_d^2}{\beta_k^2} \right) >> 1 \ . \tag{3.12}$$

For $\frac{\beta_k L}{2} >> 1$, tnis inequality always holds. For $\frac{\beta_k L}{2} < 1$, it holds only if the noise wavenumber spectrum is narrow enough, i.e., the fractional bandwidth is small enough.

There is one additional point worth making. If $\nu_d L < 1$, we shall demonstrate that a conventional beamformer cannot separate signal from noise and has an array gain near unity. The condition $\beta_k L < 1$ with large enough ν_d/β_k in (3.6), therefore, appears to offer a possibility for the optimal detector to outperform the conventional detector in this case.

3.2.1 Wideband Optimal Detection Index

A general expression for the wideband optimal detection index is obtained directly from (2.90):

$$d_o^2 = \sum_{k=1}^{N} \left| \frac{S_k}{I_k} G_{ko} \right|^2 \quad ; \tag{3.13}$$

d_o^2 is simply the sum of weignted optimal array gain from (3.6) and is therefore most heavily influenced by frequencies where the product

$$\frac{S_k}{I_k} G_{ko}$$

is largest, i.e., the beamformer output signal-to-noise ratio is highest.

Previously discussed properties of array gain obviously carry over directly to the wideband detection index. Improvement over single sensor performance is clearly substantial if (3.12) is satisfied at most frequencies.

3.3 Narrowband Performance of the Conventional Detector

The array gain for the conventional processor is derived in Appendix A:

$$G_{kc} = \frac{\frac{\beta_k L}{2}\left(1 + \frac{\nu_d^2}{\beta_k^2}\right)}{1 + \frac{\left(\nu_d^2 - \beta_k^2\right)}{\beta_k L(\nu_d^2 + \beta_k^2)}\left(1 - e^{-\beta_k L}\left(\cos \nu_d L + \frac{2\nu_d \beta_k}{\nu_d^2 - \beta_k^2} \sin \nu_d L\right)\right)}$$

$$= \frac{G_{ko} - 1}{1 + \frac{\left(\nu_d^2 - \beta_k^2\right)}{\beta_k L(\nu_d^2 + \beta_k^2)}\left(1 - e^{-\beta_k L}\left(\cos \nu_d L + \frac{2\nu_d \beta_k}{\nu_d^2 - \beta_k^2} \sin \nu_d L\right)\right)} . \tag{3.14}$$

The near optimality property of conventional processing for $\beta_k L \gg 1$ follows immediately. It is also clear that there are two distinct mechanisms of array gain degradation in (3.14). The sinusoidal terms in (3.14) vary as $e^{-\beta_k L}$ and can therefore vanish quickly when $\beta_k L > 1$.

The term

$$\frac{\nu_d^2 - \beta_k^2}{\beta_k L(\nu_d^2 + \beta_k^2)} , \tag{3.15}$$

varies as $(\beta_k L)^{-1}$ for $\nu_d > \beta_k$ and can therefore cause degradation of conventional array gain at $\beta_k L$ values appreciably less than unity. We show later that conditions $\beta_k L << 1$ and $\nu_d \leq \beta_k$, in (3.14), yield $G_{kc} \approx 1$.

There is an interesting observation to be made from (3.14). The numerator of G_{kc} is essentially equal to G_{ko} if $\nu_d L(\nu_d/2\beta_k) >> 1$. The fact that G_{ko} can be much larger than G_{kc} for $\beta_k L << 1$ indicates that the end-point sensors must achieve noise cancellation when $\beta_k L << 1$ and thus are responsible for improving performance over the performance with conventional beamforming alone.

For $\nu_d >> \beta_k$, the noise wavenumber spectrum in $[\nu_s, \nu_k]$ is very structured. Equation (3.14) then reduces to the approximate form

$$G_{kc} \simeq \frac{\frac{\nu_d L}{2}\frac{\nu_d}{\beta_k}}{1 + \frac{1}{\beta_k L}\left(1 - e^{-\beta_k L}\cos \nu_d L\right)}, \quad \nu_d >> \beta_k \quad . \tag{3.16}$$

If also

$$\frac{\nu_d L}{2}\frac{\nu_d}{\beta_k} >> 1$$

so that the optimal array gain is appreciably larger than unity,

$$\frac{G_{ko}}{G_{kc}} \simeq 1 + \frac{1}{\beta_k L}\left(1 - e^{-\beta_k L}\cos \nu_d L\right). \tag{3.17}$$

This ratio clearly exhibits minima near

$$\nu_d L = 2n\pi,\ n = 1, 2, \ldots$$

and maxima near

$$\nu_d L = (2n + 1)\pi,\ n = 0, 1, 2, \ldots.$$

At the minima, conventional array gain in (3.17) is, at most, 3 decibels below optimal if $\beta_k L << 1$. At the maxima of (3.17), with $\beta_k L << 1$, conventional array gain is far below optimal:

$$\frac{G_{kc}}{G_{ko}} \simeq \frac{\beta_k L}{2} << 1 \quad . \tag{3.18}$$

Fig. 3.2 shows the maxima and minima of (3.17) plotted as a function of $\beta_k L$. The following observations are plain. There are

no more than 3 decibels of advantage with optimal processing over conventional processing when $\nu_d L = 2n\pi$, $n = 1, 2, \ldots$. The advantage with $\nu_d L = (2n + 1)\pi$, $n = 0, 1, 2, \ldots$, is large only for $\beta_k L \ll 1$ but is no more than 3 decibels when $\beta_k L$ is only slightly larger than unity. If $\beta_k L \geq 2$, conventional array gain is, at most, 1.8 decibels below optimal. The practical implication is that the end-point sampling sensors in Fig. 3.1 provide insignificant array gain improvement when the continuous aperture L exceeds two noise correlation lengths. Thus, the long array length reduces the detection problem to near-white noise in a band of order 1/L over which the response of the conventional beamformer is significant. This result is intuitively logical. If the noise is near-white over the interval where the beamformer response is significant, then regardless of what processing is applied at the beam output, it should not significantly improve performance.

If both $\nu_d L$ and $\beta_k L$ became small, one would expect conventional array gain to approach unity because, then, all the noise power is confined to the main lobe of the beam pattern. To establish this fact more formally, we rewrite (3.14) and expand the nonalgebraic terms into an appropriate Taylor series, retaining terms to second order only:

$$G_{kc} \simeq \frac{L}{\frac{2\beta_K}{(\nu_d^2+\beta_K^2)} + \frac{2(\nu_d^2-\beta_K^2)}{L(\nu_d^2+\beta_K^2)^2} - \frac{2(1-\beta_K L+\frac{1}{2}\beta_K^2 L^2)}{L(\nu_d^2+\beta_K^2)^2}\left((\nu_d^2-\beta_K^2)(1-\frac{\nu_d^2 L^2}{2}) + 2\nu_d^2\beta_K L\right)},$$

$$0 < \beta_K L << 1 ,$$

$$\nu_d L << 1 .$$

(3.19)

Combining terms of the same order in L,

$$L^{-1} : \quad \frac{2(\nu_d^2 - \beta_K^2)}{(\nu_d^2 + \beta_K^2)^2} - \frac{2(\nu_d^2 - \beta_K^2)}{(\nu_d^2 + \beta_K^2)^2} = 0 \qquad (3.20)$$

$$L^0 : \quad \frac{2\beta_K}{(\nu_d^2 + \beta_K^2)} - \frac{2\beta_K}{(\nu_d^2 + \beta_K^2)} = 0 \qquad (3.21)$$

$$L : \quad L , \qquad (3.22)$$

yields

$$G_{kc} \simeq 1 , \quad 0 < \beta_K L << 1 , \qquad (3.23)$$

$$\nu_d L << 1 ,$$

and

$$\lim_{L \to 0} G_{kc} \simeq 1 . \qquad (3.24)$$

In the limit of $L \to 0$ (fixed β_k and ν_d), the optimal array gain must also approach unity, a fact immediately apparent from (3.6). However, when β_k is small enough so that

$$\frac{\nu_d L}{2} \frac{\nu_d}{\beta_k} >> 1 \quad ,$$

the optimal array gain can be significant even though the conventional array gain has fallen close to unity. Admittedly, this special case may have only academic value for towed array applications where $\nu_d L$ is generally much larger than unity.

These observations suggest the following strategies for choosing aperture lengths to achieve near optimal conventional array gain performance:

1. If ν_d is known, choose $L = 2\pi n/\nu_d$ with n as large as practically possible. Then, conventional performance is no more than 3 decibels below optimal.

2. If ν_d is not known exactly, again choose $L = 2\pi n/\nu_d$ with n satisfying $\nu_d/2\pi\beta_k < n$. But this is equivalent to choosing $L > 1/\beta_k$, and hence all one really needs is an array longer than the noise correlation length. Fig. 3.2 then assures one of a worst case

loss of < 3 decibels. If one can increase the array length to $L \geq 2/\beta_k$, the worst case loss is reduced to 1.8 decibels.

3.3.1 Wideband Conventional Detection Performance

Array gain in (2.63) is often used to compare performance of alternate array processing procedures. It specifies postbeamformer signal-to-noise ratio, at a given frequency, in terms of the input signal-to-noise ratio and is, therefore, independent of any linear filter connected to the conventional beamformer output (i.e., frequency scaling in Fig. 2.5).

From the arguments made in section 2.6, we know that wideband detection performance, on the other hand, is strongly dependent on such a linear filter. Hence, two detector instrumentations having identical array gains may have very different wideband detection indices. We also know that basic Eckart filtering is poorly matched to the conventional beamformer.

Much of the performance loss, as expressed by (2.77), incurred with conventional beamforming followed by basic Eckart filtering (2.76), can be recovered by the simple modification of the basic Eckart filter (2.89). The expression for the space-continuous conventional detection indices with basic and modified Eckart filtering are obtained directly from (2.77), (2.89), and (A.4):

$$d_c^2\Big|_{\substack{\text{simple}\\ \text{Eckart}}} = \frac{\left|\sum_K \frac{S_K^2}{I_K^2}\right|^2}{\sum_K \frac{S_K^2}{I_K^2}\frac{1}{G_{KC}^2}}, \tag{3.25}$$

$$d_c^2\Big|_{\substack{\text{modified}\\ \text{Eckart}}} = \sum_K \frac{S_K^2}{I_K^2} G_{KC}^2, \tag{3.26}$$

where G_{KC} is the conventional array gain on continuous $[-L/2, L/2]$ from (3.14). Again the variation of G_{KC} in (3.25) with temporal frequency causes the basic Eckart filter to perform poorly with conventional beamforming. This variation is illustrated in Fig. 3.3, using the Corcos models for β_K and ν_K from (2.32) and (2.33) with $\nu_S = 0$. Variations in array gain with frequency are directly traceable to the fact that a given aperture length equals an even multiple of a noise half wavelength at some frequencies and an odd multiple of a half wavelength at other frequencies.

Fig. 3.4 shows conventional detection indices computed from (3.16), (3.25) and (3.26) graphed together with the optimal detection index from (3.6) and (3.13). Parameter values are $\beta_K/\nu_K = \alpha = 0.01$ and $\nu_S = 0$. Detection indices are plotted against a normalized highest signal frequency, wL/U_c. Each curve is obtained by normalizing with respect to L and an assumed uniform signal-to-noise ratio in the signal band.

Specifically,

$$\frac{S_k}{I_k} = \begin{cases} S/I \text{ (a constant)}, \text{ for } k = 1, 2, \ldots, N \\ 0, \quad \text{otherwise.} \end{cases} \tag{3.27}$$

We see that wideband detection performance with conventional beamforming followed by modified Eckart filtering, as expected, is everywhere better than wideband detection performance with conventional beamforming followed by basic Eckart filtering.

As wL/U_c increases to 2π, one encounters the first conventional array gain peak (see Fig. 3.3). Hence, from (3.26), modified Eckart filtering begins to recover a large fraction of the performance loss incurred with basic Eckart filtering.

In that range the conventional detector curve, with the modified Eckart filter, lies a fairly constant 13 decibels below the optimal detector curve. On the other hand, the performance loss of the conventional detector with simple Eckart filtering, relative to optimal, ranges from 38 decibels at $wL/U_c = 2\pi$ to 48 decibels at $wL/U_c = 12\pi$. Modification of the basic Eckart filter thus recovers a substantial fraction of the performance loss even when $\beta_k L < 1$.

Note that improvement with modified Eckart filtering over basic Ekcart filtering is only 2 decibels when $wL/U_c = \pi$.

One expects limited benefit from the modified Eckart filter in this case since the variation in array gain (Fig. 3.3) is relatively small in this frequency range. In this extreme low-pass case, use of the modified Eckart filter obviously becomes less important. One could, therefore, consider using only the simple Eckart filter, $\sqrt{S_K / I_K}$, with the conventional beamformer.

One could raise the point that a simple high-pass filter preceding the squaring operation in Fig. 2.5 might be used to eliminate frequencies where array gain is smallest, i.e., the interval $[0,\pi]$ in Fig. 3.3. Since (3.25) is lowered drastically by low values of G_{KC} in even small frequency bands, elimination of such bands might secure much of the benefit available from the more complex modified Eckart filter. This suboptimal approach has interesting practical implications and is pursued in Chapter 5. The high-pass filters are relatively easy to construct and, as we shall see, are competitive with the best postbeamformer filters in (2.89).

When $\beta_K L >> 1$, $G_{KO} \simeq G_{KC}$ and the only issue then is the benefit to be gained by using the modified Eckart filter. From (3.6) and (3.14), we have

$$G_{ko} \simeq G_{kc} \simeq \frac{\beta_k L}{2}\left(1 + \frac{\nu_k^2}{\beta_k^2}\right) = \frac{\alpha L}{2U_c}\,\omega_k\left(\frac{\alpha^2 + 1}{\alpha^2}\right), \quad \beta_k L \gg 1\ , \quad \nu_k \gg \nu_s\ . \tag{3.28}$$

Using spectral functions satisfying

$$\frac{S(\omega)}{I(\omega)} = \begin{cases} \dfrac{S}{I}\ \text{(a constant), for } \omega_1 \le \omega \le \omega_2 \\ 0, \text{ elsewhere} \end{cases} \tag{3.29}$$

and assuming $T(\omega_2 - \omega_1) \gg 2\pi$ so that sums in (3.25) and (3.26) can be approximated by integrals, one obtains

$$d_o^2 \simeq d_c^2\Big|_{\substack{\text{modified}\\ \text{Eckart}}} = \frac{T}{2\pi}\frac{S^2}{I^2}\int_{\omega_1}^{\omega_2}\left(\frac{\alpha L}{2U_c}\,\omega\,\frac{(\alpha^2+1)}{\alpha^2}\right)^2 d\omega$$

$$= \frac{T}{2\pi}\frac{S^2}{I^2}\frac{L^2}{4U_c^2}\left(\frac{(\alpha^2+1)^2}{\alpha^2}\right)\left(\frac{\omega_2^3 - \omega_1^3}{3}\right), \tag{3.30}$$

$$d_c^2\Big|_{\substack{\text{simple}\\ \text{Eckart}}} = \frac{\dfrac{T}{2\pi}\dfrac{S_2}{I^2}(\omega_2 - \omega_1)^2}{\displaystyle\int_{\omega_1}^{\omega_2}\frac{d\omega}{\frac{\alpha^2 L^2 \omega^2}{4U_c^2}\,\frac{(\alpha^2+1)^2}{\alpha^2}}} = \frac{T}{2\pi}\frac{S^2}{I^2}\frac{L^2}{4U_c^2}\left(\frac{(\alpha^2+1)^2}{\alpha^2}\right)(\omega_2 - \omega_1)\omega_1\omega_2\ . \tag{3.31}$$

The ratio of the two detection indices is, therefore,

$$\frac{d_c^2\Big|_{\substack{\text{modified}\\\text{Eckart}}}}{d_c^2\Big|_{\substack{\text{simple}\\\text{Eckart}}}} \simeq \frac{1}{3}\left(\frac{\omega_2}{\omega_1} + 1 + \frac{\omega_1}{\omega_2}\right) . \tag{3.32}$$

The divergence of (3.32) for $\omega_1 \to 0$ is due to the fact that $\beta_K \to 0$ as $\omega_K \to 0$ [see (2.32) and (2.33)] so that the large $\beta_k L$ assumption is violated at the lower end of the spectrum.

Significant improvements in conventional detection are obviously available for wide bandwidth signals. For instance, if

$$\frac{\omega_2}{\omega_1} = 10 \quad ,$$

the gain in (3.32) is approximately 5 decibels, but if $\omega_2/\omega_1 = 50$, the gain is approximately 12 decibels.

According to (3.28), the required postbeamformer filter power transfer function is characterized by

$$\left|C_k\right|^2 = \frac{S_k}{I_k^2}\,\omega_k^2 \,. \qquad (3.33)$$

Thus, with $\beta_k L >> 1$, the only addition to the simple Eckart filter is a voltage gain increasing linearly with frequency. The modification is independent of U_c and, therefore, of specific operating conditions.

3.4 Summary

This chapter has compared the performance of conventional and optimal detectors, using space-continuous observations. The narrowband comparison is summarized in Fig. 3.5. Results with the Butterworth flow noise model indicate that one can achieve near optimal narrowband performance with only conventional processing in many cases of practical interest, especially if $\beta_k L >> 1$. An important observation is that one achieves this performance with an instrumentation that is relatively simple compared with the fully optimal construction. The $\beta_k L >> 1$ condition is certainly reasonable for most practical applications where overall array lengths usually exceed the flow noise correlation length.

Over such a space-continuous length, even conventional steering (beamforming) is impractical. The discussion here thus serves two purposes. First, it sets absolute bounds on performance that can be

approacned by arrays of tightly packed discrete sensors. Secondly, it leads into a later discussion of continuous sensors.

Wideband detection performance is strongly dependent on linear filtering applied to a conventional beamformer output. Two detector instrumentations having identical array gains can therefore have dramatically different detection indices. Basic Eckart filtering is poorly matched to the conventional beamformer, especially in the $\beta_k L < 1$ regime. A simple modification of the Eckart filter can very substantially enhance the performance of the detector using conventional beamforming, making it more competitive with the optimal detector. Major gains are possible with modified Eckart filtering and continuous observations when the noise has sufficient spatial structure or a reasonably wide band of frequencies is processed.

The modified Eckart filter instrumentation depends on conventional array gain, which is not usually known a priori. In the large $\beta_k L$ regime, the instrumentation reduces to a relatively simple pre-emphasis of high signal frequencies. In general, array gain is not likely to be known in advance. Hence, an adaptive modified Eckart filter is suggested. However, one needs only a single adaptive filter at the beam output. For flow noise encountered by towed arrays, the primary unknown parameter would probably be the convective noise speed. Adaptation could, therefore, be a relatively simple matter.

In Chapter 4, we revisit the binary detection problem in the context of the sampled aperture and examine detection issues surrounding spatial sampling, such as the attendant detection loss due to spatial aliasing.

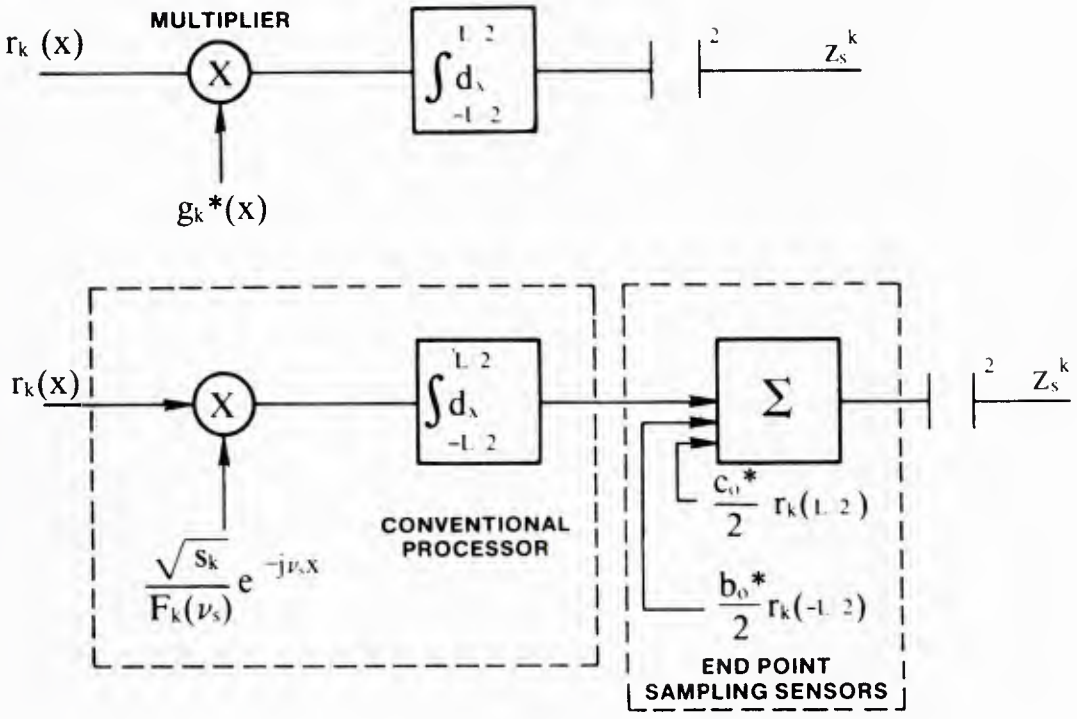

$$g_k(x) = \frac{\sqrt{s_k}}{F_k(\nu_s)} e^{-j\nu_s x} + \frac{b_o}{2}\delta(x + L/2) + \frac{c_o}{2}\delta(x - L/2)$$

$$F_k(\nu_s) = \frac{2I_k\beta_k}{\beta_k^2 + \nu_d^2} \; ; \; \nu_d = \nu_k - \nu_s$$

$$b_o = \sqrt{s_k}\; e^{-j\nu_s L/2}\frac{\sqrt{\beta_k^2 + \nu_d^2}}{I_k\beta_k} e^{j\tan^{-1}(\nu_d/\beta_k)}$$

$$c_o = \sqrt{s_k}\; e^{j\nu_s L/2}\frac{\sqrt{\beta_k^2 + \nu_d^2}}{I_k\beta_k} e^{j\tan^{-1}(-\nu_d/\beta_k)}$$

Fig. 3.1. Optimal Spatial Structure for First Order Butterworth Wavenumber Spectrum and Plane Wave Signal at kth Frequency

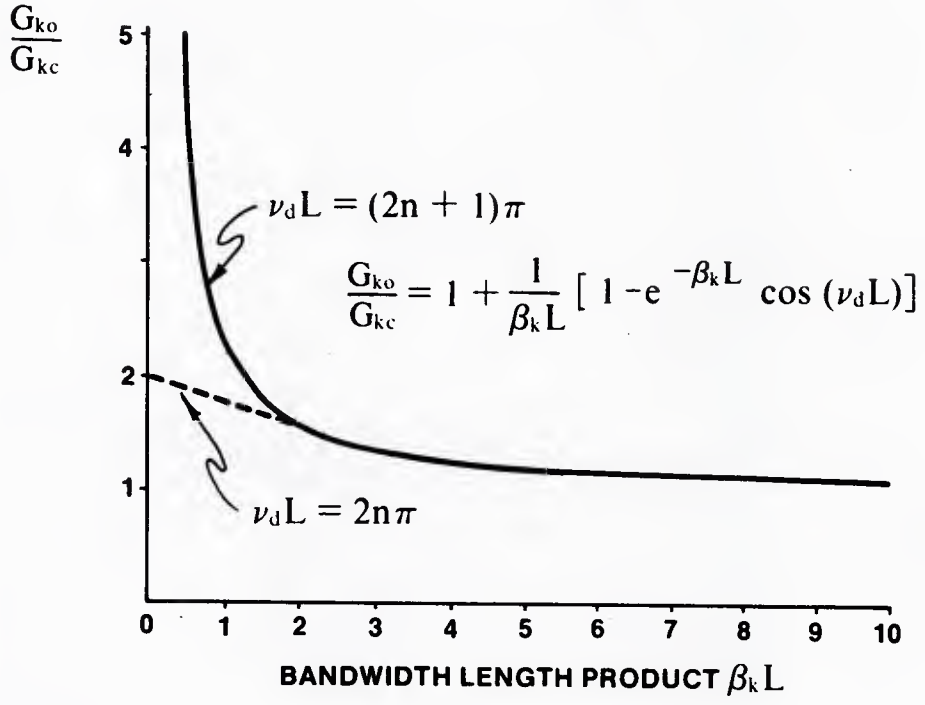

Fig. 3.2. Ratio of Optimal to Conventional Array Gain at kth Frequency ($\nu_d / \beta_i >> 1$) With $\nu_d = \nu_k - \nu_s$

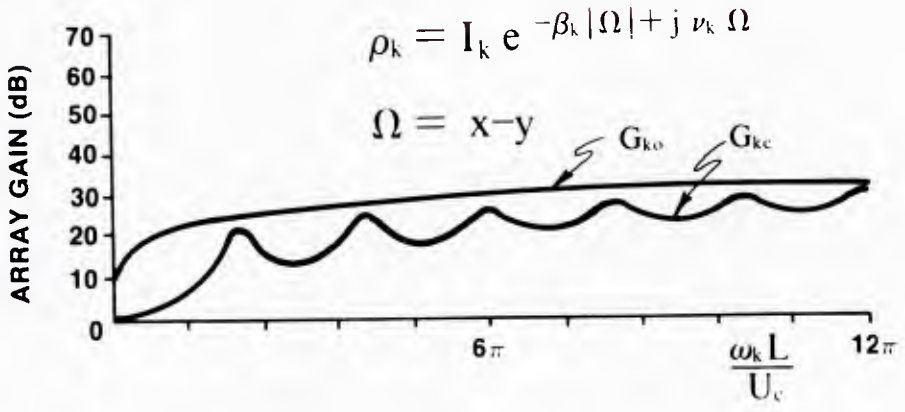

Fig. 3.3. Optimal and Conventional Array Gain Versus $\omega_k L / U_c$, $\alpha = \beta_k$ $\nu_k = 0.01$, $\beta_k L < 1$, $\nu_s = 0$

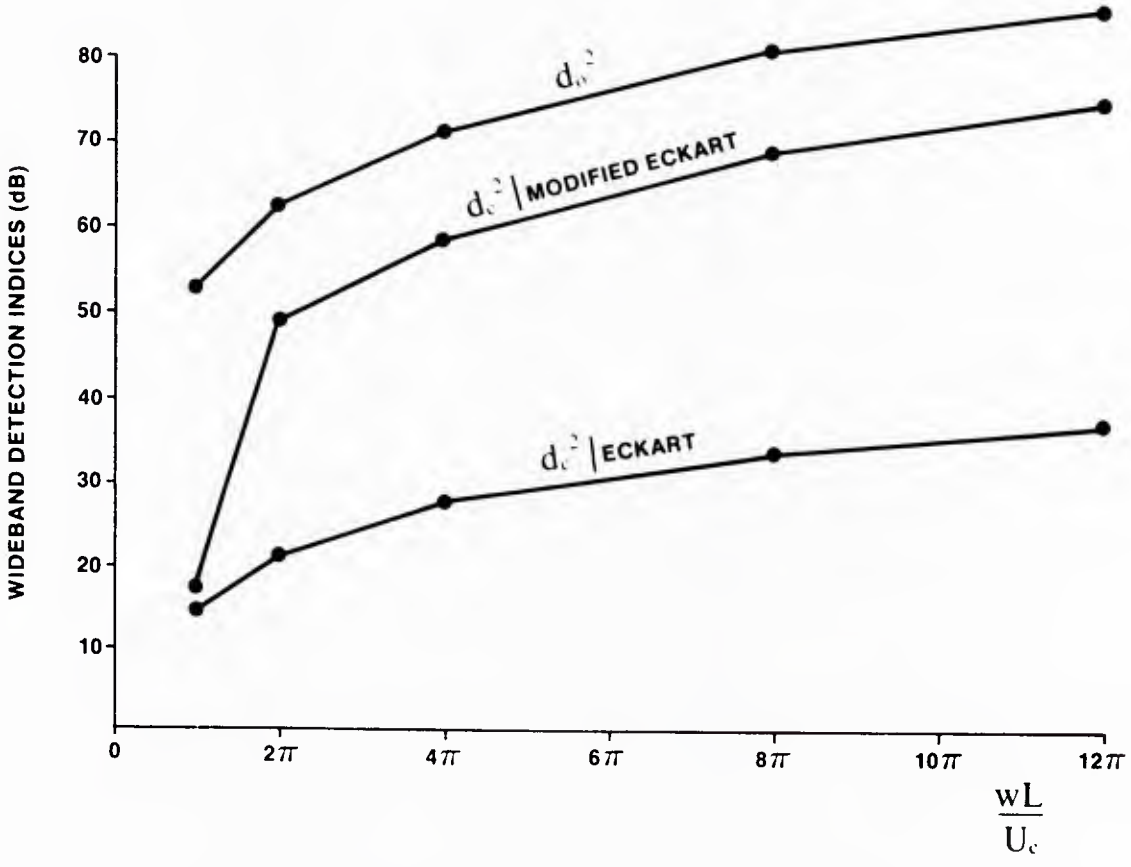

Fig. 3.4. Wideband Detection Indices Versus wL/U_c for $\alpha = \beta_k/\nu_k = 0.01$ Normalized With Respect to SNR (S/I a Constant), $\nu_s = (\omega_s/c)\cos\theta_s = 0$

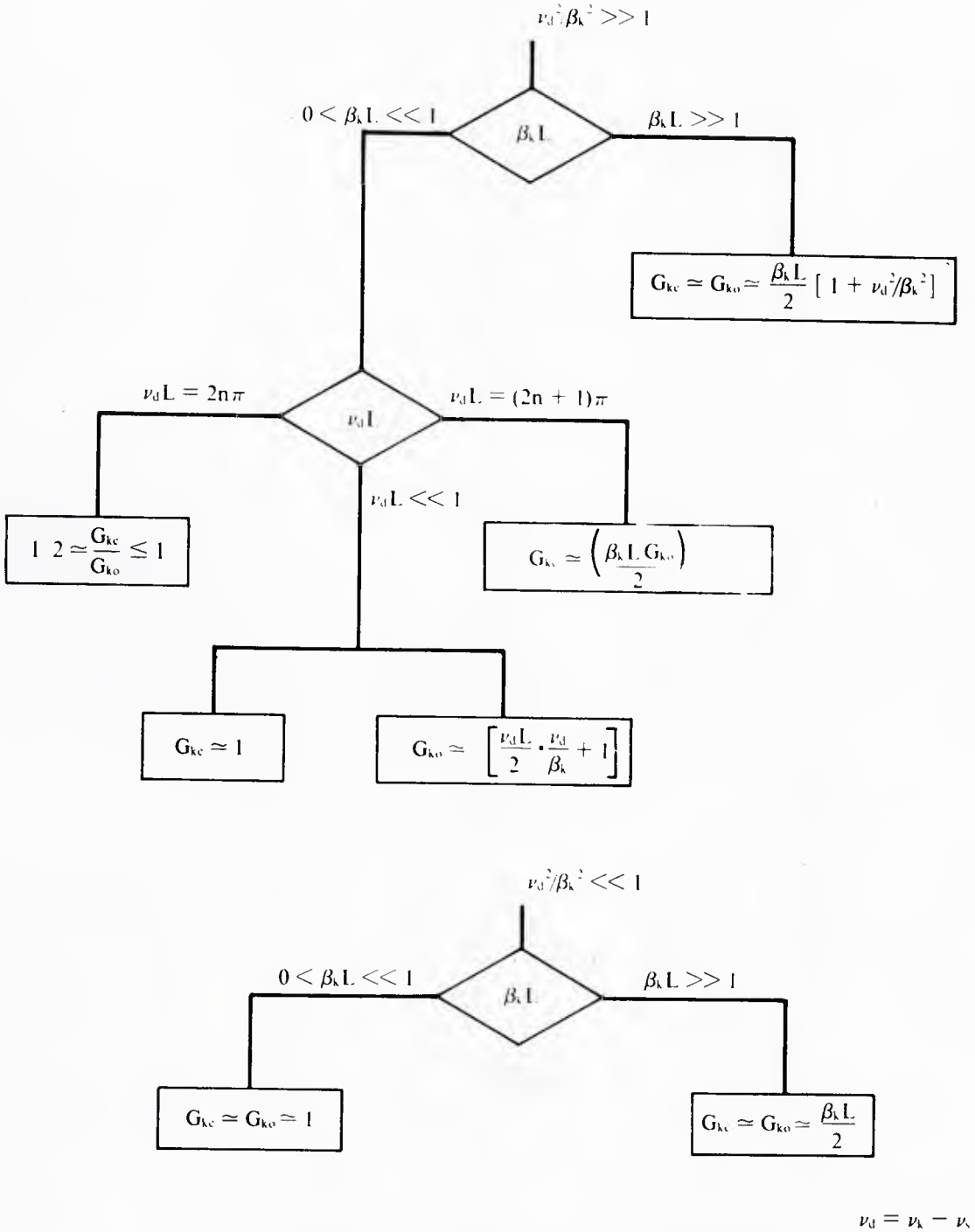

Fig. 3.5. Summary of Optimal (G_{ko}) and Conventional(G_{kc}) Array Gain Performance

CHAPTER FOUR

DETECTION PERFORMANCE WITH A UNIFORMLY SAMPLED SPATIAL APERTURE

4.1 Introduction

Continuing tne formal analysis from Chapter 3, we specify the optimal detector realization and corresponding optimal performance with discrete observations regularly spaced in $[-L/2, L/2]$.

4.2 Effects of Spatial Aliasing

Following standard procedures of sampled data analysis [35, pp. 117-120; 36; 37], the spectrum of the sampled noise process can be written as

$$F_{ka}(\nu) \triangleq \sum_{j=-\infty}^{\infty} F_k(\nu - \frac{j2\pi}{\Delta}) \ . \tag{4.1}$$

This aliased noise wavenumber spectrum arises from taking values of the homogeneous Butterworth covariance function in (2.35) at discrete, but uniform, intervals in $(-\infty, \infty)$. The wavenumber density for the sampled process is a periodic function in ν, with period $2\pi/\Delta$ obtained by summing translates of $F_k(\nu)$. Since the input noise spectrum is

not zero for $|\nu| \geq \pi/\Delta$ but covers an infinite number of wavenumbers, the spectrum of the sampled process will necessarily involve overlapping of individual terms in the summation. In all cases, the overlapping results in increased noise spectral levels and in many cases smoothes the noise spectral features. One obtains the mean square value for the sampled process by integrating the sampled spectrum over

$$\left[\frac{-\pi}{\Delta} \frac{\pi}{\Delta}\right]$$

or, more generally, over any period of length $2\pi/\Delta$. This then results in finite power even when there are delta functions in the sampled spectrum.

Notice that the spectrum for the sampled process equals the original spectrum if, and only if, Δ is made extremely small so that discrete observations pass in the limit to continuous observations.

For our Butterworth wavenumber model (in Fig. 2.3), the exact level of the aliased flow noise at ν_s is found by simply substituting (2.31) into (4.1). One can then express the ratio of the sampled flow noise spectrum, at the signal wavenumber, to the flow noise spectrum with continuous observations as

$$\frac{F_{ka}(\nu_s)}{F_k(\nu_s)} = 1 + \sum_{j=1}^{\infty} \frac{2\,(\beta_k^2 + \nu_d^2)}{(\beta_k^2 + \nu_d^2 + j^2\,\nu_c^2)^2 - \dfrac{4j^2\,\nu_c^2\,\nu_d^2}{\beta_k^2 + \nu_d^2 + j^2\,\nu_c^2}},$$

$$\nu_d \triangleq \nu_k - \nu_s, \quad \nu_c \triangleq \frac{2\pi}{\Delta},$$

$$= 1 + \sum_j \frac{2(\beta_k^2 + \nu_d^2)\,(\beta_k^2 + \nu_d^2 + j^2\,\nu_c^2)}{\beta_k^4 + \nu_d^4 + j^4\,\nu_c^4 + 2\,\beta_k^2\,\nu_d^2 + 2j^2\,\beta_k^2\,\nu_c^2 - 2\,j^2\,\nu_d^2\,\nu_c^2}$$

$$= 1 + \sum_j \frac{2(\beta_k^2 + \nu_d^2)\,(\beta_k^2 + \nu_d^2 + j^2\,\nu_c^2)}{(\nu_d^2 - j^2\,\nu_c^2)^2 + \beta_k^2(\beta_k^2 + 2\nu_d^2 + 2\,j^2\,\nu_c^2)}$$

$$= 1 + \sum_{j=1}^{\infty} \frac{2(1 + \beta_k^2/\nu_d^2)(1 + \beta_k^2/\nu_d^2 + j^2\,\nu_c^2/\nu_d^2)}{(1 - j^2\,\nu_c^2/\nu_d^2)^2 + \beta_k^2/\nu_d^2(2 + \beta_k^2/\nu_d^2 + 2j^2\,\nu_c^2/\nu_d^2)}. \tag{4.2}$$

If the fractional spatial bandwidth is assumed small, i.e., $\beta_k/\nu_d \ll 1$, (4.2) becomes

$$\frac{F_{ka}(\nu_s)}{F_k(\nu_s)} \approx 1 + \sum_{j=1}^{\infty} \frac{2\,(1 + j^2\,\nu_c^2/\nu_d^2)}{(1 - j^2\,\nu_c^2/\nu_d^2)^2 + \beta_k^2/\nu_d^2\,(2 + 2j^2\,\nu_c^2/\nu_d^2)}$$

$$= 1 + \sum_{j=1}^{\infty} \frac{1}{\dfrac{(1 - j^2\nu_c^2/\nu_d^2)^2}{2(1 + j^2\,\nu_c^2/\nu_d^2)} + \beta_k^2/\nu_d^2}\,,$$

$$\beta_k/\nu_d \ll 1. \qquad (4.3)$$

The series in (4.3) converges, a fact easily established by the Limit Comparison Test of elementary calculus.

It follows from (4.3) that

$$\frac{F_{ka}(\nu_s)}{F_k(\nu_s)} \begin{cases} \approx 1, \text{ for } \nu_c \gg \nu_d \\ > 1 + \dfrac{\nu_d^2}{\beta_k^2}, \text{ if } j^2\,\dfrac{\nu_c^2}{\nu_d^2} = 1 \text{ for some } j\,. \end{cases} \qquad (4.4)$$

Equation (4.3) may be used to compute the increase in noise level at ν_s caused by regular sampling. From (4.4), this increase is clearly very large if the sampling interval Δ is an integer multiple of

$$\frac{2\pi}{\nu_d}\,,$$

which approximates the noise wavelength

$$\lambda_K = \frac{2\pi}{\nu_K}, \text{ when } \nu_K >> \nu_S .$$

With $\Delta = 2\pi/\nu_d$, the high wavenumber noise folds down (aliased) onto the signal, making it impossible to separate the two by spatial processing. Analogous with sampling in time, noise reconstruction from the sampled values would look like low wavenumber acoustic components. Thus signal-to-noise ratio is drastically reduced relative to continuous observations. At frequencies for which Δ is a multiple of $2\pi/\nu_K$, noise adds coherently between sensors. Noise components at these frequencies can easily dominate beam output noise power.

By contrast when $\Delta = \pi/\nu_d$, (4.3) yields

$$\frac{F_{Ka}(\nu_S)}{F_K(\nu_S)} \simeq 2.4 , \tag{4.5}$$

which is an increase in noise level at ν_S of approximately 3.8 decibels relative to continuous observations. We shall show that this increased noise level is <u>all</u> that happens in the transition from continuous to discrete observations. Hence, the best array gain, with discrete observations, at this spacing, is only a factor of 2.4 [3.8 decibels] below the best array gain with continuous observations.

The conclusions inferred from (4.3) are of fundamental importance in the towed array application where ν_K is usually much larger than ν_s. One avoids the aliasing problem, in this case, with an extremely tight sensor sampling interval. The aliasing problem is reduced to a minor effect by choosing

$$\Delta << \frac{2\pi}{\nu_K}$$

or, equivalently,

$$\nu_c >> \nu_K ,$$

which demands a very large number of sensors or telemetry channels. This may not be convenient, or even possible, in practice. Such intervals, as remarked earlier, have a typical length scale in inches.

The influence of spatial aliasing is illustrated in Fig. 4.1, where the sampled Butterworth noise spectrum from Fig. 2.3 is shown for several uniform sampling intervals, with the postulated signal at ν_s. The wavenumber spectrum of the sampled process is clearly periodic with regular sensor spacing. As a tool for demonstrating effects of spatial aliasing noise, fractional bandwidth, in Fig. 4.1, has been purposely exaggerated compared with the typical spectrum in Fig. 1.2. Thus, Fig. 1.2 gives an incomplete picture of the effective flow noise spectra one would expect with discrete arrays.

Sampled (aliased) spectra in Figs. 4.1b-c are obviously distortions of the original noise spectrum in Fig. 4.1a. Uniform sampling causes high wavenumber components to fold down onto lower wavenumbers. This wavenumber folding, generated strictly by spatial sampling, clearly increases the noise level and, hence, can severely degrade signal-to-noise ratio at ν_s.

Fig. 4.1d shows an example where the spatial interval is sufficiently large so that the noise is nearly uncorrelated between sensors. For this sampling interval, the sum in (4.1) scaled by ν_c becomes a Rieman sum, which represents a reasonable approximation to the sampled process spectrum level: $2\pi(I_K/\beta_K)$. The resultant spectrum for the sampled process is nearly wavenumber white, with a spectrum level that obviously exceeds the peak level, $2I_K/\beta_K$, for continuous observations in Fig. 4.1a. Of course, the power spectrum, at a sensor, obtained by integrating (4.1) over any periodic interval, $[\nu_c]$, equals I_K, which, from our remarks in Chapter 1, increases with increased tow vessel speed. Conventional beamforming is optimal at this spacing, but signal-to-noise ratio, at the beam output, is very poor compared to the signal-to-noise ratio with continuous observations. A common practice is to space sensors at a half acoustic wavelength, which is often much larger than $2\pi/\beta_K$. Hence, detection capability, with such spacings, is seriously degraded compared with detection capability with tighter sensor spacings.

One infers from this that processing with discrete observations always results in unavoidable spatial aliasing, making it impossible to achieve the signal-to-noise ratio attainable with continuous observations.

If a wide band of frequencies is processed, there will probably be frequencies at which the noise at a conventional beamformer output is the coherent sum of noises received at various sensors. High beamformer output noise levels, at these frequencies, drastically degrade detection performance unless the appropriate postbeamformer filter in (2.89) is used.

The narrowband version of the sampling theorem [21, pp. 34-35], requiring a sampling rate of $2\pi/\beta_K$, is irrelevant here because reconstruction of the unsampled noise spectrum cannot be accomplished from raw spatial samples taken at that rate. Once discrete sensors are introduced, spatial aliasing loss has happened and is irreversible.

4.3 Detector Performance

General expressions for the optimal and conventional array gains of discrete arrays are given by (2.65) and (2.69), respectively. Expressions for the detection indices are given by (2.74), (2.77), and (2.79).

With regular sensor spacing, the normalized parameter, $\tilde{\rho}_k = \rho_k(\Delta)/I_k$, in (2.34), completely describes the noise covariance matrix Q_k. For a linear array of M regularly spaced sensors separated by a distance Δ, the exponential form of (2.34) leads to the Toeplitz matrix:

$$Q_k = \begin{bmatrix} 1 & \rho_k & \rho_k^2 & \cdots & \rho_k^{M-1} \\ \rho_k^* & \ddots & \ddots & \ddots & \vdots \\ \rho_k^{*2} & \ddots & \ddots & \ddots & \rho_k^2 \\ \vdots & \ddots & \ddots & \ddots & \rho_k \\ \rho_k^{*M-1} & \cdots & \rho_k^{*2} & \rho_k^* & 1 \end{bmatrix} . \qquad (4.6)$$

The inverse of (4.6) is therefore the <u>banded</u> matrix:

$$Q_k^{-1} = \frac{1}{1 - |\rho_k|^2} \begin{bmatrix} 1 & -\rho_k & & & O \\ -\rho_k^* & 1+|\rho_k|^2 & \ddots & & \\ & \ddots & \ddots & \ddots & \\ & & \ddots & 1+|\rho_k|^2 & -\rho_k \\ O & & & -\rho_k^* & 1 \end{bmatrix} , \qquad (4.7)$$

which, incidentally, specifies the optimal matrix filter shown in

Fig. 4.2, as computed from (2.50). The filter is the discrete analog of the optimal structure for continuous observations in Fig. 3.1.

The optimal and conventional array gains are computed (see Appendix B) in a straightforward manner from (2.65) and (2.69):

$$G_{ko} = \frac{M}{1-\left|\hat{\rho}_k\right|^2}\left(1 + (1 - \frac{2}{M})\left|\hat{\rho}_k\right|^2 - (1 - \frac{1}{M})(\hat{\rho}_k + \hat{\rho}_k^{*})\right), \tag{4.8}$$

$$G_{kc} = \frac{M}{\frac{1 - \left|\hat{\rho}_k\right|^2}{\left|1 - \hat{\rho}_k\right|^2} - \frac{2}{M} R_e\left(\frac{\hat{\rho}_k(1 - \hat{\rho}_k^{M})}{(1 - \hat{\rho}_k)^2}\right)}, \tag{4.9}$$

$$\hat{\rho}_k = e^{-\beta_k \Delta + j\nu_d \Delta},$$

$$\nu_d = \nu_k - \nu_s .$$

Since $1/\beta_k$ is the noise correlation distance, it follows that

$$\hat{\rho}_k^{M} \to 0$$

once the total array length $L = (M - 1)\Delta$ exceeds the noise correlation distance. The approximate representation of conventional array gain is, therefore,

$$G_{kc} \approx \frac{M}{\dfrac{1 - |\hat{\rho}_k|^2}{|1 - \hat{\rho}_k|^2} - \dfrac{2}{M} R_e\left(\dfrac{\hat{\rho}_k}{(1 - \hat{\rho}_k)^2}\right)} \quad . \tag{4.10}$$

When $M \to \infty$, (4.8) and (4.10) approach the same limit for fixed Δ:

$$G_{kc} \approx G_{ko} \approx \frac{M}{1 - |\hat{\rho}_k|^2}\left(1 + |\hat{\rho}_k|^2 - 2R_e(\hat{\rho}_k)\right) \quad . \tag{4.11}$$

Note that (4.11) is a strong function of ω_k as long as $\beta_k \Delta << 1$, i.e., as long as the sensor spacing is much smaller than the noise correlation distance.

More interesting than the limit for fixed Δ is the behavior as M varies but $(M - 1)\Delta = L$, a fixed length chosen so that $\beta_k L >> 1$. To deal with this problem, we form the ratio of (4.8) and (4.10):

$$\frac{G_{ko}}{G_{kc}} \simeq \left[\frac{|1 - \hat{\rho}_k|^2 + \dfrac{2}{M}\left(R_e(\hat{\rho}_k) - |\hat{\rho}_k|^2\right)}{1 - |\hat{\rho}_k|^2}\right]\left[\frac{1 - |\hat{\rho}_k|^2}{|1 - \hat{\rho}_k|^2} - \frac{2}{M} R_e\left(\frac{\hat{\rho}_k}{(1 - \hat{\rho}_k)^2}\right)\right],$$

$$\beta_k L >> 1 \; . \tag{4.12}$$

After some algebraic simplication, this reduces to

$$\frac{G_{ko}}{G_{kc}} \simeq 1 + \frac{2}{M}\left[\frac{|\hat{\rho}_k|^2}{1 - |\hat{\rho}_k|^2}\right] - \frac{4}{M^2}\left[\frac{R_e(\hat{\rho}_k) - |\hat{\rho}_k|^2}{1 - |\hat{\rho}_k|^2} R_e\left(\frac{\hat{\rho}_k}{(1 - \hat{\rho}_k)^2}\right)\right]. \tag{4.13}$$

With the definition of $\hat{\rho}_k$ from (4.9), (4.13) appears to be a function of the four parameters β_k, ν_k, Δ, and M. However, with the constraints

$$M = \frac{L}{\Delta} + 1 \tag{4.14}$$

and

$$\beta_k L = \text{constant},$$

there remain only two independent variables, ν_k and M. For any fixed M, the ratio G_{ko}/G_{kc}, considered as a function of ν_d, exhibits a maximum $[G_{ko}/G_{kc}]$ max. Fig. 4.3a plots these maxima as a function of M for various values of $\beta_k L > 3$ ($\hat{\rho}_k^M < 0.02$). Once $\beta_k L$ exceeds 1 by a significant factor, the ratio of array gains barely deviates from unity for all possible M, hence all possible sensor spacings.

It is relatively easy to show that the exact expression for optimal array gain in (4.8) approaches the array gain with continuous observations in (3.6) in the limit as $\Delta = L/M - 1 \to 0$ with L fixed.

Inserting the definition of $\hat{\rho}_k$ in (4.8), we obtain the following equivalent expression:

$$G_{ko} = \frac{1}{1 - |\hat{\rho}_k|^2}\left[M\left(1 + e^{-2\beta_k\Delta} - 2e^{-\beta_k\Delta}\cos(\Delta\nu_d)\right) - 2\left(e^{-2\beta_k\Delta} - e^{-\beta_k\Delta}\cos(\Delta\nu_d)\right)\right],$$

$$\nu_d \triangleq \nu_k - \nu_s \,. \qquad (4.15)$$

For Δ small enough so that $\beta_k\Delta \ll 1$ and $\Delta\nu_d \ll 1$, one can expand the exponentials and the cosines into Taylor series:

$$\begin{aligned} G_{ko} \approx \frac{1}{2\beta_k\Delta}\Bigg[& M\left[1 + 1 - 2\beta_k\Delta + \frac{(2\beta_k\Delta)^2}{2!} + \ldots\right. \\ & \left. - 2\left(1 - \beta_k\Delta + \frac{(\beta_k\Delta)^2}{2!} + \ldots\right)\left(1 - \frac{(\Delta\nu_d)^2}{2!} + \frac{(\Delta\nu_d)^4}{4!} + \ldots\right)\right] \\ & - 2\left[1 - 2\beta_k\Delta + \frac{(2\beta_k\Delta)^2}{2!} + \ldots\right. \\ & \left. - \left(1 - \beta_k\Delta + \frac{(\beta_k\Delta)^2}{2!} + \ldots\right)\left(1 - \frac{(\Delta\nu_d)^2}{2!} + \frac{(\Delta\nu_d)^4}{4!} + \ldots\right)\right]\Bigg]. \end{aligned} \qquad (4.15a)$$

Then performing the required multiplication and collecting terms, we arrive at

$$G_{ko} \simeq 1 + \frac{M\beta_k\Delta}{2} + \frac{M\beta_k\Delta}{2}\frac{\nu_d^2}{\beta_k^2} + \ldots + \text{terms in } \Delta^2 \text{ and higher} -$$

$$- \frac{\Delta\nu_d}{2\beta_k} - \frac{3\beta_k\Delta}{2} . \qquad (4.15b)$$

Taking the formal limit of (4.15b) as $\Delta \simeq L/M \to 0$ with L fixed and $L = (M - 1)\Delta \approx M\Delta$, we obtain

$$\lim_{L/M \to 0} G_{ko} = \frac{\beta_k L}{2} + \frac{\beta_k L}{2}\frac{\nu_d^2}{\beta_k^2} + 1 = \frac{\beta_k L}{2}\left(\frac{\nu_d^2}{\beta_k^2} + 1\right) + 1$$

$$= \frac{I_{kL}}{F_k(\nu_s)} + 1 , \qquad (4.15c)$$

which is identical to the result in (3.6).

In section 3.1, we observed that spatial sampling increases the level of the noise wavenumber spectrum at the signal wavenumber, ν_s. The increase was described by the factor $(F_{ka}(\nu_s))/(F_k(\nu_s))$ in (4.3). We now demonstrate by example that the same factor characterizes the decrease in array gain, at least for $\beta_k L >> 1$, i.e.,

$$\frac{G_{ko}}{G_{ko}|_{cont}} = \frac{F_k(\nu_s)}{F_{ka}(\nu_s)} \quad . \tag{4.16}$$

Fig. 4.3b snows two curves: (1) G_{ko} from (4.8) and (2) $G_{ko|cont}$ from (3.6) multiplied by the ratio $(F_k(\nu_s))/(F_{ka}(\nu_s))$ from (4.3). Both are plotted, using the Corcos model for β_k and ν_k in (2.32) and (2.33), for M = 100, α = 0.01, and ν_s = 0. The two curves are indistinguishable over the entire range shown, indicating that the aliasing noise fully accounts for tne array gain degradation as one makes the transition from continuous to discrete observations.

4.3.1 Numerical Examples

Numerical examples can now be computed from (4.8) and (4.9). Again we use the Corcos model values for β_k and ν_k from (2.32) and (2.33) and, in the interest of algebraic simplicity, we assume a broadside signal arrival. No loss of generality is implied because one can always choose tne origin of tne wavenumber space at the signal wavenumber.

Fig. 4.4a shows (4.11) normalized by M plotted as a function of $\omega_k \Delta / U_c$ for α = 0.01, i.e., a fractional bandwidth of 0.01. The

low array gain at $(\omega_k \Delta/U_c) = 2\pi n$, $n = 1, 2, \ldots$, is due to the fact that at these points the noise components at sensors within one correlation distance $(1/\beta_k)$ of each other are very nearly in phase. Hence, subarrays of this length have an array gain close to one. Since the entire array can be decomposed into $\beta_k L$ such subarrays, the total array gain at $\omega_k \Delta/U_c = 2\pi n$ is only of the order $\beta_k L$ and the normalized array gain of Fig. 4.4a is $G_{ko}/M \approx \beta_k \Delta$. (More exact calculations from (4.11) yield $G_{ko}/M \approx \beta_k \Delta/2$). It is important to remember that poor performance at $\omega_k \Delta/U_c = 2\pi n$, $n = 1, 2, \ldots$, results from the fact that the noise components add coherently at these frequencies and can therefore easily dominate the beamformer output. By eliminating these undesirable frequencies, the modified Eckart filter of (2.89), i.e., the filter optimized for its actual input signal plus noise spectra, achieves dramatically improved detector performance.

To get an idea of the extent of the approximation in (4.11), normalized but exact curves from (4.8) and (4.9) are plotted in Fig. 4.4b for $M = 100$ and $\alpha = 0.01$. Observe that once $\omega_k \Delta/U_c > \pi$, the difference between G_{ko} and G_{kc} quickly becomes trivial. With $\alpha = 0.01$ and $M = 100$, $\beta_k L = (99/100)(\omega_k \Delta/U_c)$. Thus, the two curves coincide once $\beta_k L \geq \pi$. More detailed examination of (4.8) and (4.9) in the expanded interval $[0.\pi]$ in Fig. 4.4c shows that G_{kc} actually oscillates about the curve in Fig. 4.4b with spatial frequency $M\nu_k$ and thus can be as much as 3-4 decibels below the

average in the vicinity of $\Delta\omega_k/U_c = \pi/10$. Conventional processing, in this expanded region, is obviously closer to optimal when $\Delta\nu_k$ is an odd multiple of π/M. Oscillations decay essentially to zero at

$$\omega_k \Delta/U_c = \pi/2 \ .$$

Because of the approximate equality of G_{ko} and G_{kc}, the detection index of the conventional detector using the modified Eckart filter, $\left(\sqrt{S_k}/N_k\right)G_{kc}$, [see (2.89)] is approximately equal to d_o^2 under the conditions leading to (4.11). On the other hand, if one only uses the simple Eckart filter, $\sqrt{S_k}/N_k$, i.e., the filter matched to the input signal and noise spectra, in conjunction with a conventional beamformer, one can expect drastically degraded performance. Specifically, let

$$\frac{S_k}{N_k} = \frac{S_k}{I_k} = \begin{cases} \frac{S}{I} \quad \text{(a constant), for } 0 \le \omega_k \le w \\ 0 \ , \text{ elsewhere} \ . \end{cases} \tag{4.17}$$

Then, from (2.74) and (2.77),

$$\frac{d_o^2}{d_c^2}\Bigg|_{\substack{\text{simple} \\ \text{Eckart}}} = \frac{1}{N^2} \sum_k \sum_e \frac{G_{ko}^2}{G_{ec}^2} \approx \frac{1}{N^2} \sum_k \sum_e \frac{G_{ko}^2}{G_{eo}^2} \ , \tag{4.18}$$

where $N = Tw/2\pi$ is the number of frequency components in the signal band.

As we have already seen, at very low frequencies the $\beta_k L >> 1$ assumption would be violated so that $G_{ec} < G_{eo}$. Hence, the ratio of (4.18) is a somewhat conservative estimate of the performance loss.

Fig. 4.5 (uppermost plot) shows (4.18) plotted as a function of α, using array gain functions approximated by 4.11 with

$$\frac{w\Delta}{U_c} = 2\pi \ . \tag{4.19}$$

Once $w\Delta/U_c \geq 2\pi$, the ratio of detection indices becomes insensitive to the precise value of w, as one might expect from the near-periodic structure of Fig. 4.4a. Only when w increases sufficiently so that $(\alpha/U_c)w\Delta >> 1$ does the ratio (4.18) diminish significantly (because the high frequency noise components at adjacent sensors are now uncorrelated). Thus, array gain becomes frequency invariant over a major portion of the band.

More exact ratios, also shown in Fig. 4.5, using array gain functions from (4.8) and (4.9), show clearly that the approximation in (4.18) is very optimistic for noise fractional bandwidths less than 0.01. We also see that the detection index for conventional beamforming with modified Eckart filtering is, at most, 6 decibels below the detection index with optimal array processing. The inaccuracy of (4.18) becomes unimportant in Fig. 4.5 when α increases to 0.1, where, presumably, most of the frequency components in bandwidth w satisfy the large $\beta_k L$ condition.

For small arrays, the approximations leading to (4.11) are inappropriate and one must again deal with the exact (4.8) and (4.9). This is done in the remaining figures. Array gains are plotted as functions of $\omega_k \Delta / U_c$. Wideband detection indices are based on spectra of the form defined by (4.17).

Fig. 4.6a shows the optimal and conventional array gains for a 2 sensor array with $\alpha = 0.01$. At $\omega_k \Delta / U_c = (2n + 1)\pi$, $n = 0, 1, 2, \ldots$, the sensors are spaced a half wavelength apart so that conventional beamforming acnieves optimal noise cancellation. For full wavelength spacing, the noise components at the sensors are in phase, just as the signal components, and no signal processor can enhance signal-to-noise ratio. For these reasons, the curves coincide at all integral multiples of π, and the array gain at even multiples of π is 0 decibels.

Fig. 4.6b shows the wideband detection indices for the same 2 sensor array and fractional bandwidtn, $\alpha = 0.01$, plotted as a function of the normalized signal bandwidth $w\Delta/U_c$. The upper curve corresponds to the optimum detector, the middle curve to tne detector with conventional beamforming followed by modified Eckart filter, and the lower curve to the detector with conventional beamforming followed by the simple Eckart filter. For

$$\frac{w\Delta}{U_c} < \frac{\pi}{2} \quad ,$$

tne modified Eckart filter yields very little performance improvement and the loss relative to optimal performance is serious (22-30 decibels). However, once

$$\frac{w\Delta}{U_c} > \pi \quad ,$$

the conventional detector with a modified Eckart filter comes within 9 decibels of the optimal detector, whereas the conventional detector with a simple Eckart filter falls 25-31 decibels below the optimum. In this range, the separation of the three curves does not vary drastically, indicating tnat relative performance is insensitive to the specific values of w and U_c.

Figs. 4.7-4.10 snow the dependence of array gain on α for a fixed 2 sensor array. With $\alpha = 1$, the noise is near-white and both conventional and optimal processors have an array gain close to 2 decibels. As the fractional bandwidth of the noise decreases, the maximum array gain increases sharply. The minimum must, of course, remain 0 decibels for the reasons mentioned in the discussion of Fig. 4.6a.

Fig. 4.11 shows the dependence of the wideband indices on α. The array gains required for the computation were taken from Figs. 4.7-4.10 and the normalized signal bandwidth was held fixed at $w\Delta/U_c = 2\pi$. Once α is small enough so that the difference between d_o^2 and $d_c^2|_{Eckart}$ becomes significant, use of the modified Eckart filter recovers a major fraction of the loss.

The final series of curves deals with the effect of the number of sensors, M, on relative performance. Fig. 4.12 shows the array gains for 3- and 5-element arrays with $\alpha = 0.01$. Conventional and optimal array gains are approximately equal near the M - 1 frequencies satisfying

$$\frac{\omega_K \Delta}{U_c} = \frac{2\pi}{M} p \ , \ p = 1, 2, \ldots (M - 1) \ . \qquad (4.20)$$

Fig. 4.13 gives the wideband detection indices normalized with respect to the assumed constant signal-to-noise ratio in (4.17) and M as functions of M for $w\Delta/U_c = 2\pi$. Once again, use of the modified

Eckart filter recovers much of the loss incurred in using conventional beamforming with a simple Eckart filter. The extent of that recovery grows with M, becoming complete when $\beta_K(M - 1)\Delta = \beta_K L >> 1$ so that performance is characterized by Fig. (4.5).

4.4 Summary

We examined spatial aliasing with arrays of uniformly spaced sensors and found aliasing to be the major cause of detection loss attendant on discrete observations. Attendant loss in array gain relative to array gain with continuous observations is directly traceable to the increased noise level, due to aliasing, at the signal wavenumber.

When $\beta_K L >> 1$, a condition usually satisfied by towed arrays in flow noise, conventional array gain is essentially optimal with uniform sensor spacing. Detection performance, in this case, is, however, limited by spatial aliasing, which must degrade the signal-to-noise ratio. Thus, signal detectability is degraded relative to the case with space-continuous data. Spatial aliasing is avoided only if spatial observations are effectively continuous, with extremely small sensor intervals so that discrete observations pass in the limit to continuous observations. For the flow noise problem, sensor spacings on the order of inches are required to approach the continuous mode of operations.

As with continuous observations in Chapter 3, use of a relatively simple modification of the Eckart filter can very substantially enhance the performance of a detector using conventional beamforming, making it more nearly competitive with the optimal detector. Major gains can, of course, be made only when a reasonably wide band of frequencies is processed and the noise has sufficient spatial structure so that optimal and conventional array gains vary significantly with frequency. The flow noise associated with towed arrays has the general form of the model used in the examples. While its relative bandwidth need not be as low as 0.01, it would probably be sufficiently concentrated in wavenumber space to make the modified Eckart filter attractive for wideband detection.

A clear drawback of the modified Eckart filter is its dependence on the (conventional) array gain and hence on the spatial structure of the noise field (except for the continuous line array discussed in Chapter 3). This structure is not likely to be known in advance, so that some form of adaptation is required.

Here again, one needs only a single adaptive filter rather than the set of M filters required for optimal processing of data from M sensors. For flow noise encountered by towed arrays, the primary unknown parameter would probably be U_c, a quantity closely related to tow speed. Adaptation could, therefore, be a relatively simple matter; one could, for example, estimate the noise spectrum at the conventional beamformer output by simply estimating U_c.

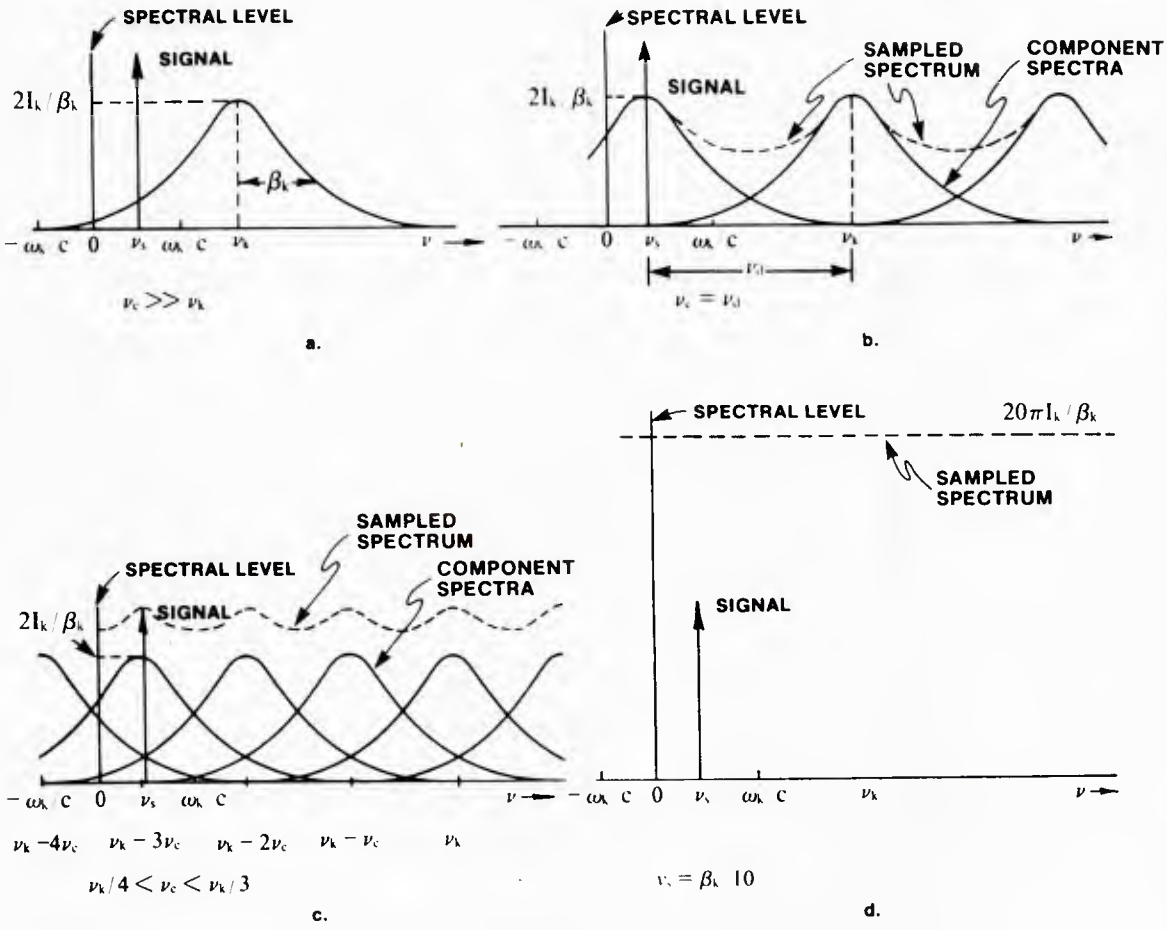

Fig. 4.1. Wavenumber Spectral Overlap

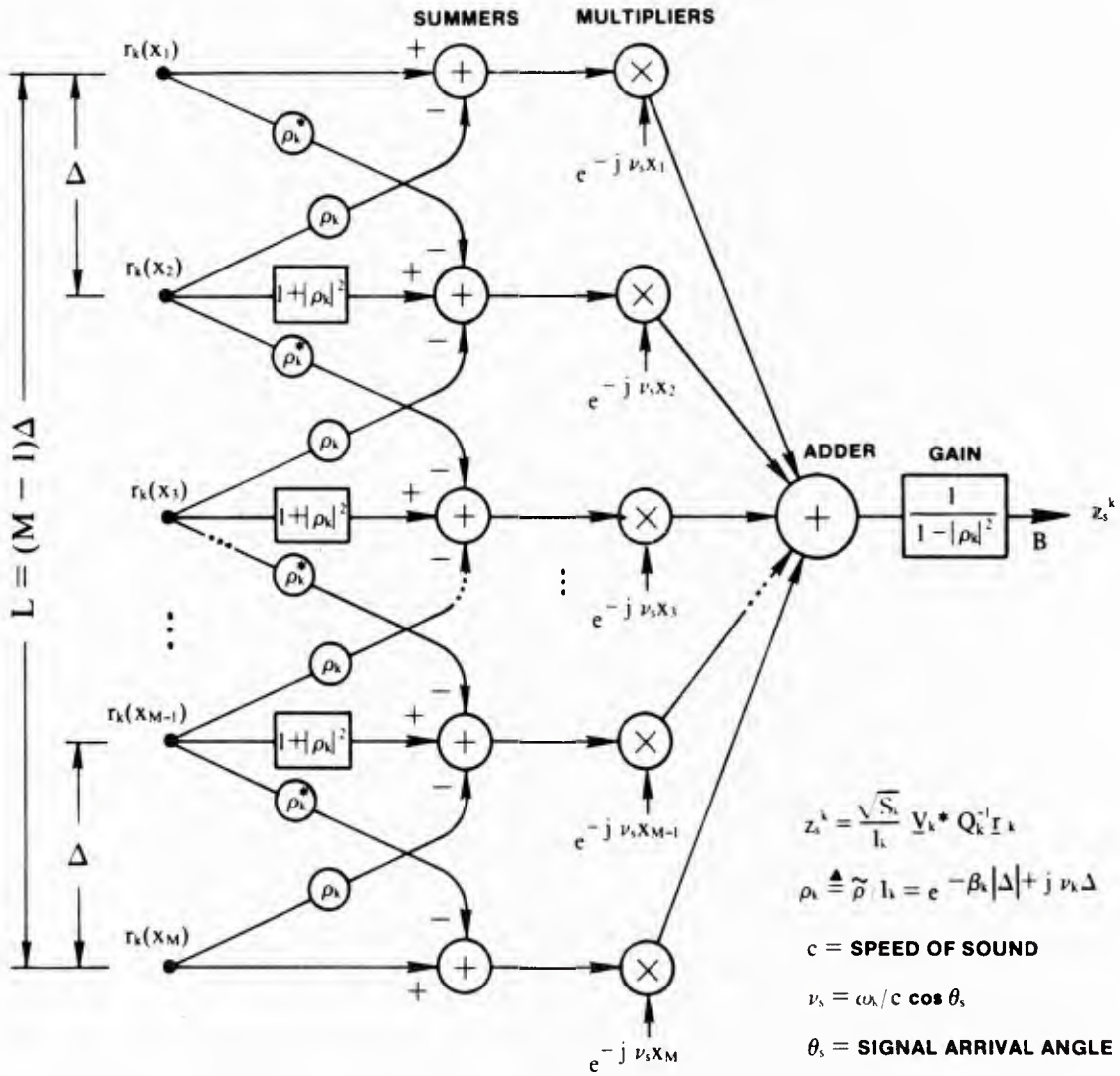

Fig. 4.2. Optimal Linear Combiner for M Equally Spaced Sensors in [-L/2, L/2] With Butterworth Noise Model

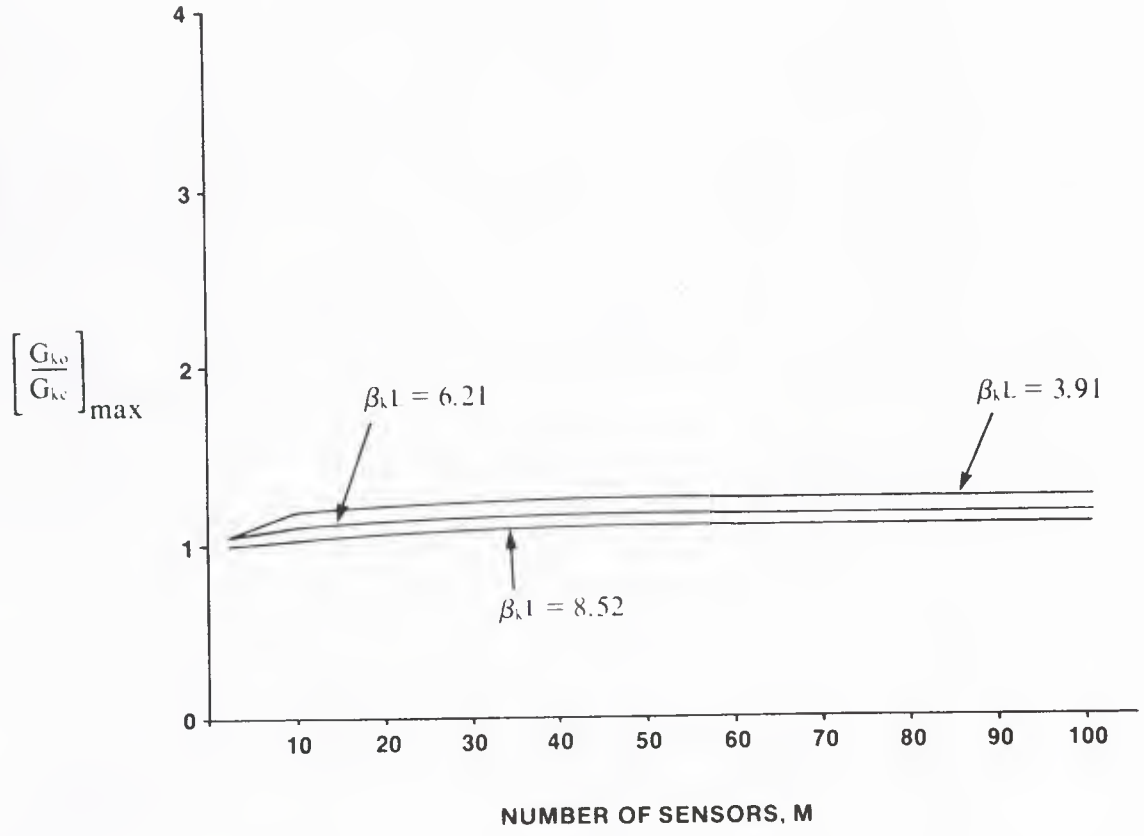

Fig. 4.3a Maximum Ratio of Optimal to Conventional Array Gain

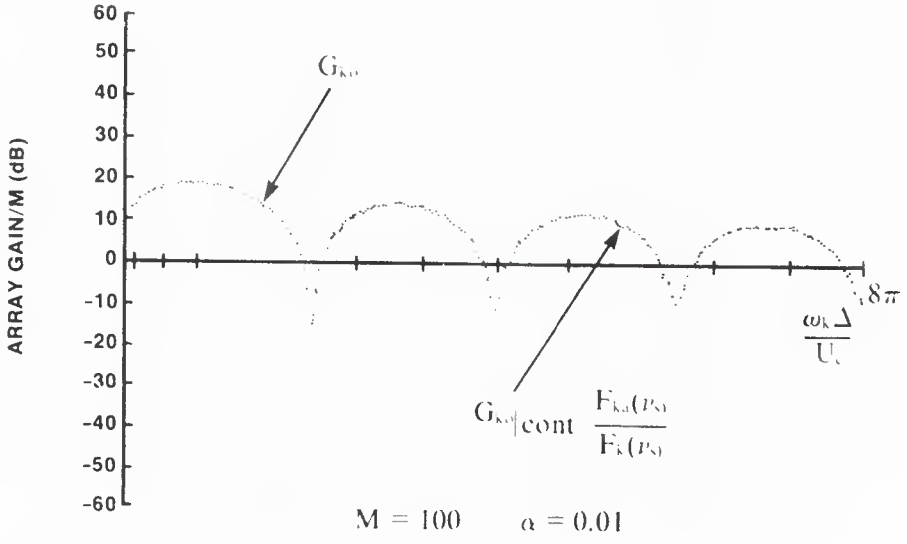

Fig. 4.3b Optimal Array Gain With Spatial Aliasing Corrections on Optimal Array Gain With Continuous Observations

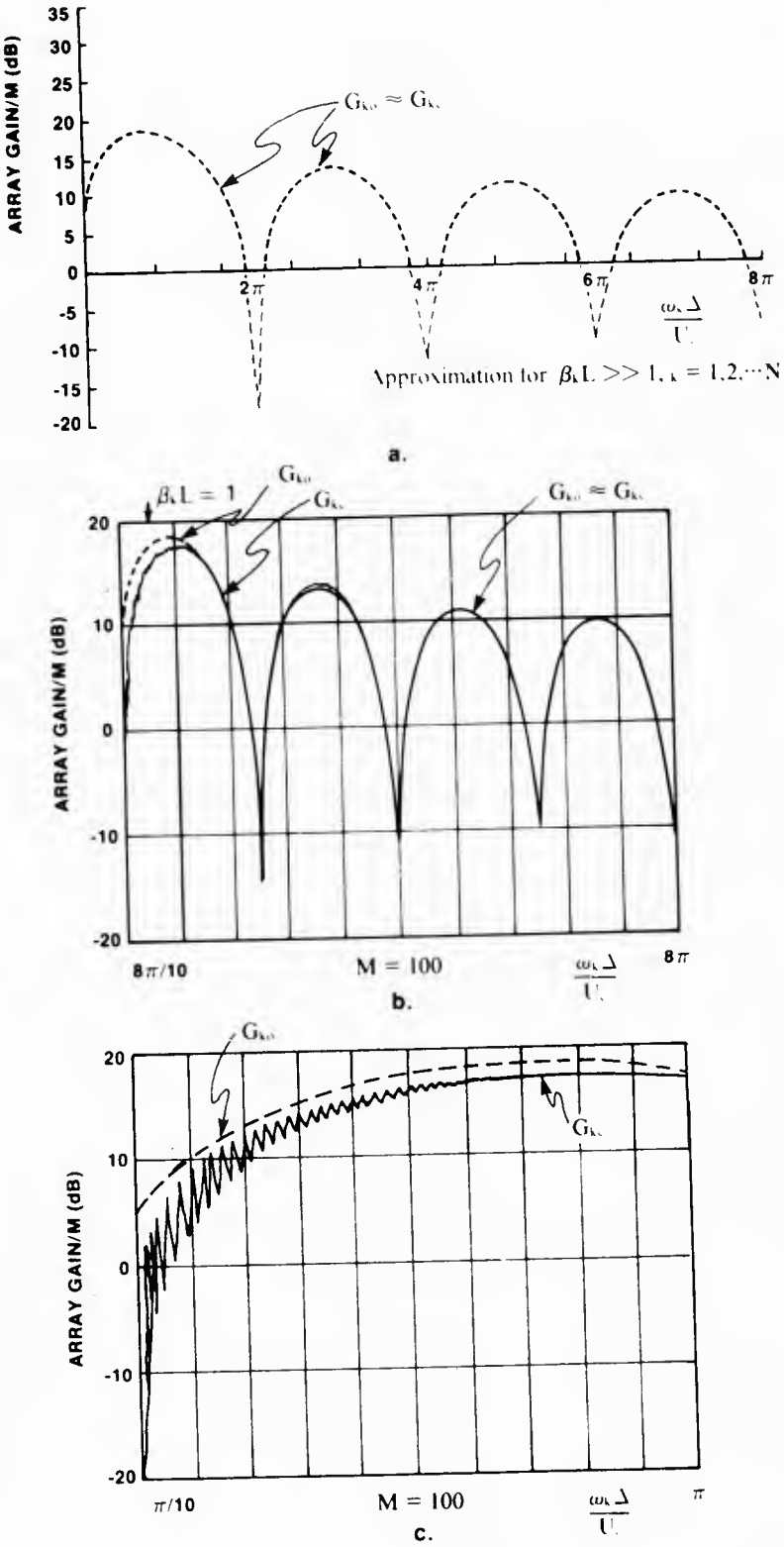

Fig. 4.4. Optimal and Conventional Array Gain Versus $\omega_k \Delta / U_c$ for $\alpha = 0.01$, $L = (M-1)\Delta$

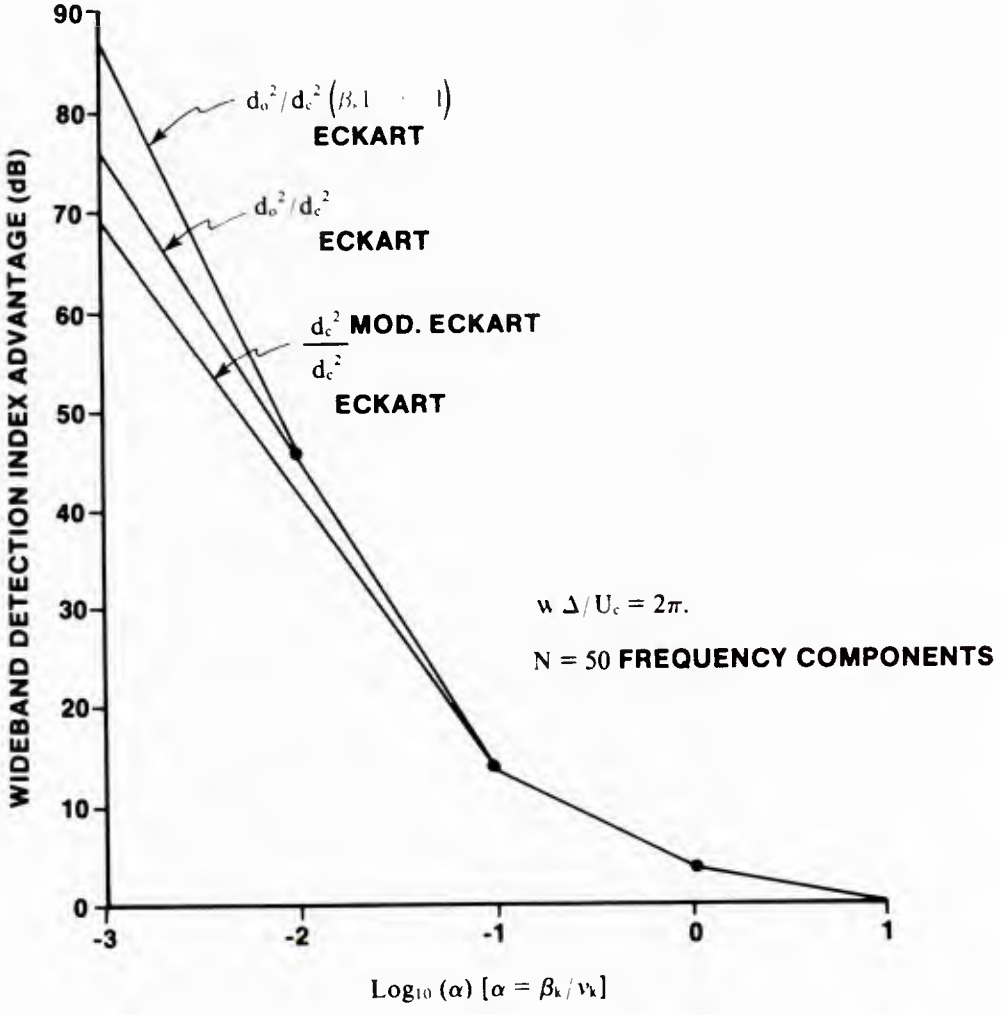

Fig. 4.5. Wideband Detection Index Advantage With Modified Eckart Filtering Over Simple Eckart Filtering

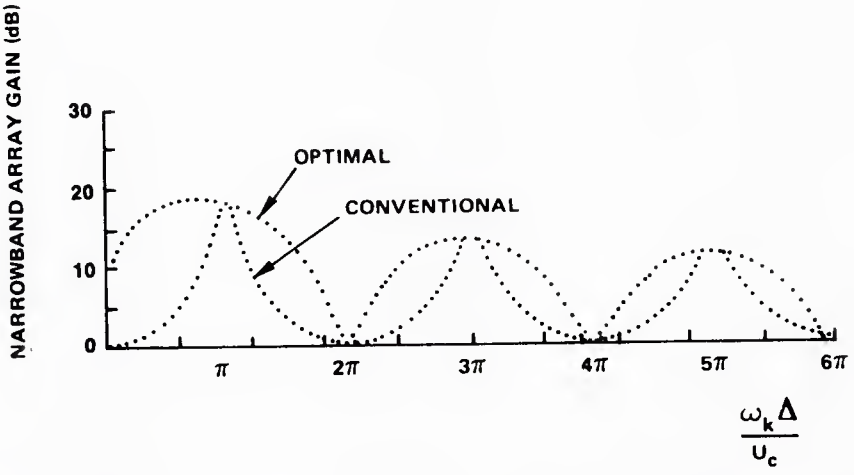

Fig. 4.6a. Optimal and Conventional Array Gain for a 2 Sensor Array With $\alpha = 0.01$

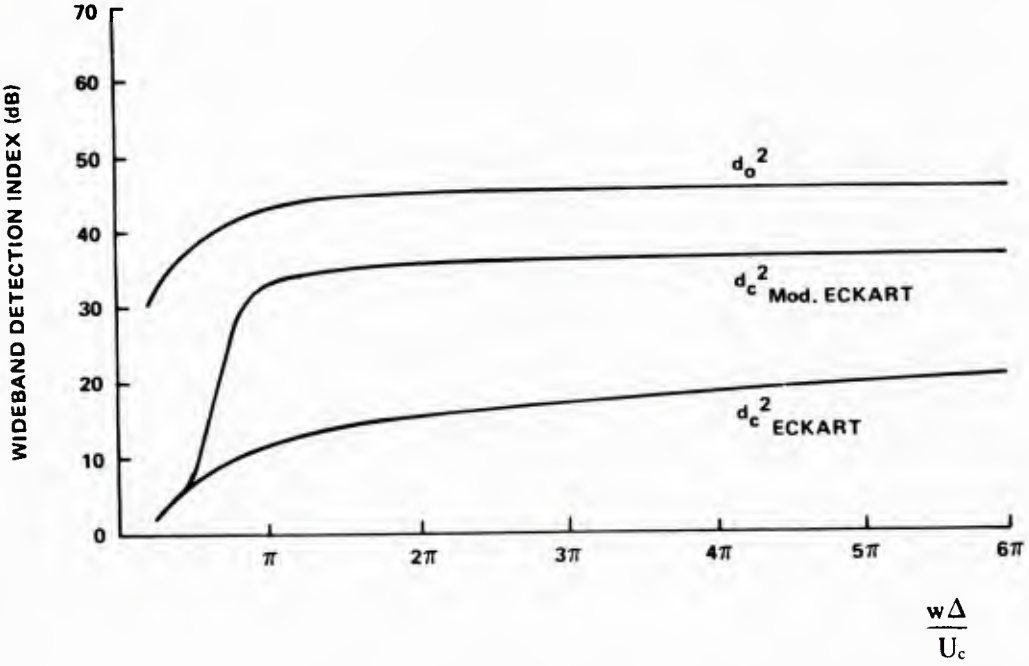

Fig. 4.6b. Wideband Detection Indices for 2 Sensors With $\alpha = 0.01$ Plotted as a Function of Normalized Bandwidth, $\frac{w\Delta}{U_c}$

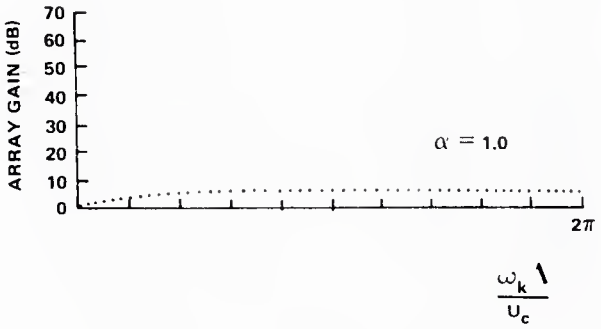

Fig. 4.7.

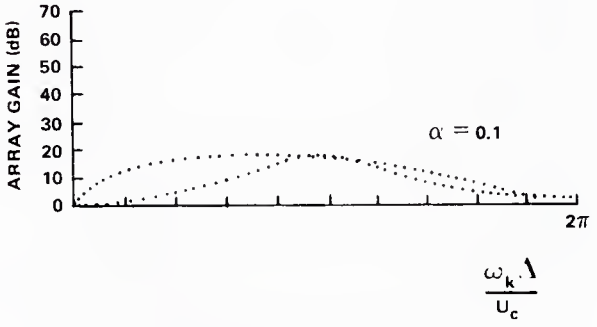

Fig. 4.8.

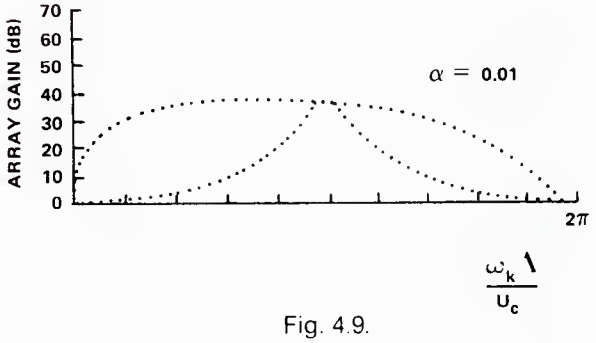

Fig. 4.9.

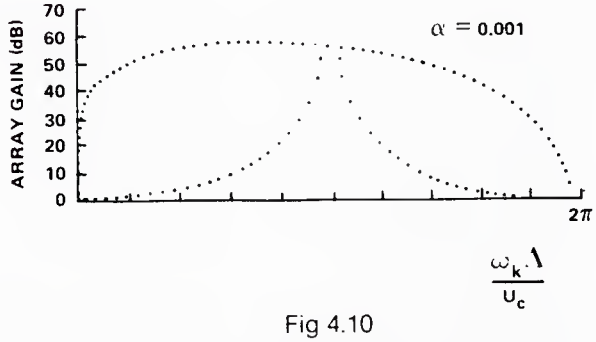

Fig 4.10

Fig. 4.7. - 4.10. Array Gain Dependence on $\alpha = \beta_k / \nu_k$ for a 2 Sensor Array, M = 2

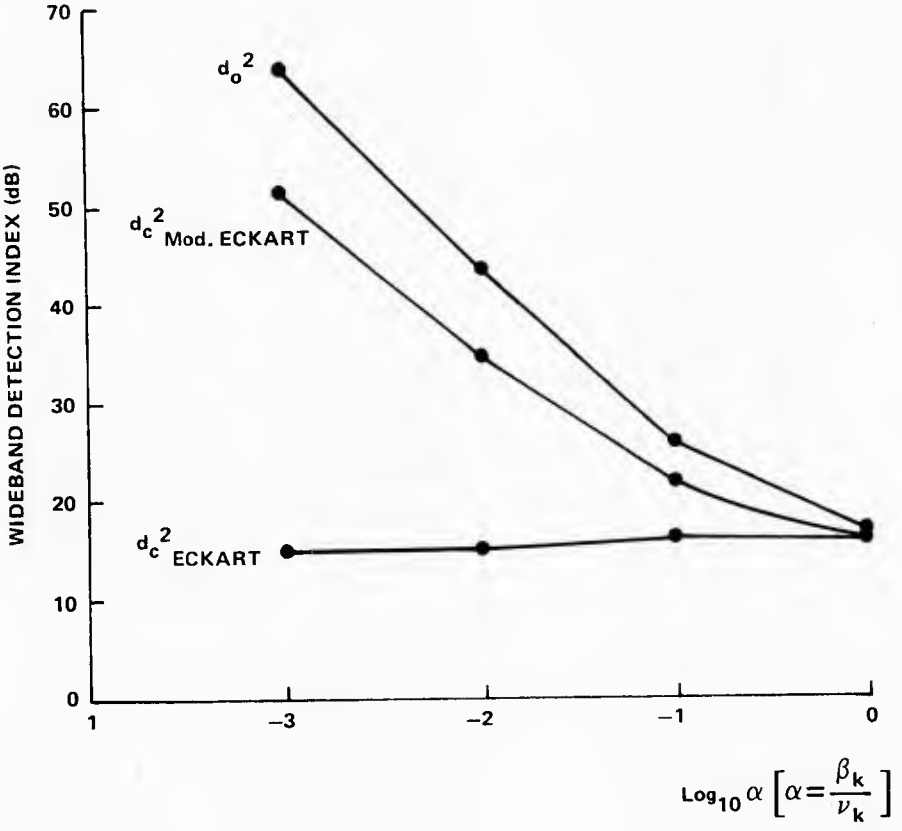

Fig. 4.11. Wideband Detection Indices Versus $\alpha = \beta_k / \nu_k$ With w $\Delta / U_c = 2\pi$ and M = 2 Sensors

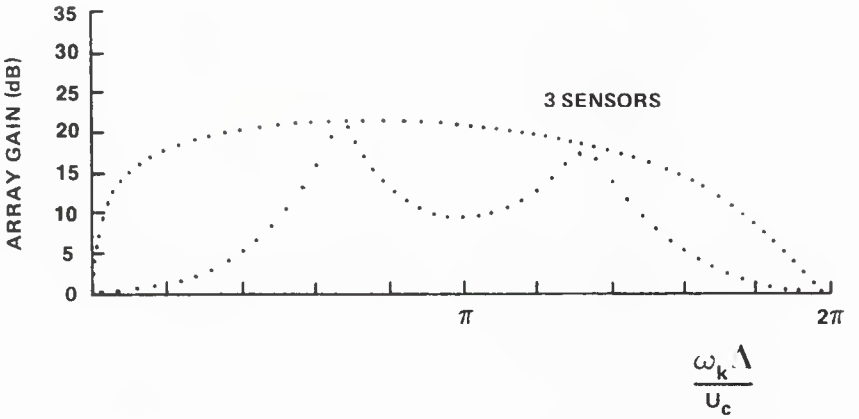

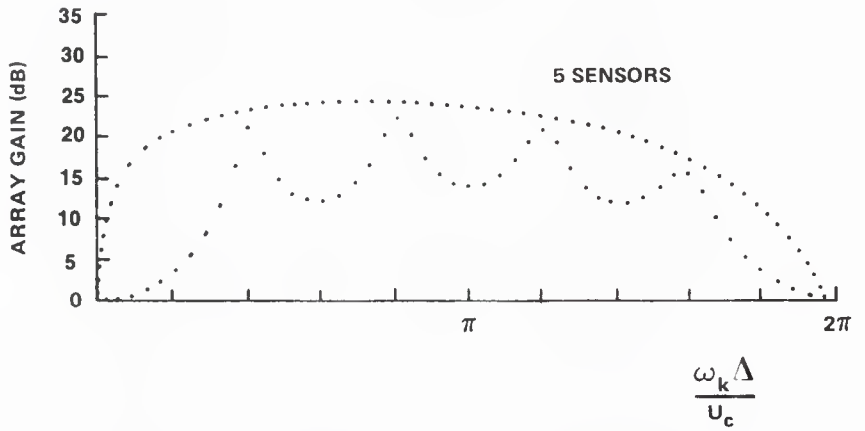

Fig. 4.12. Array Gain for 3 and 5 Sensors, $\alpha = \beta_k / \nu_k = 0.01$

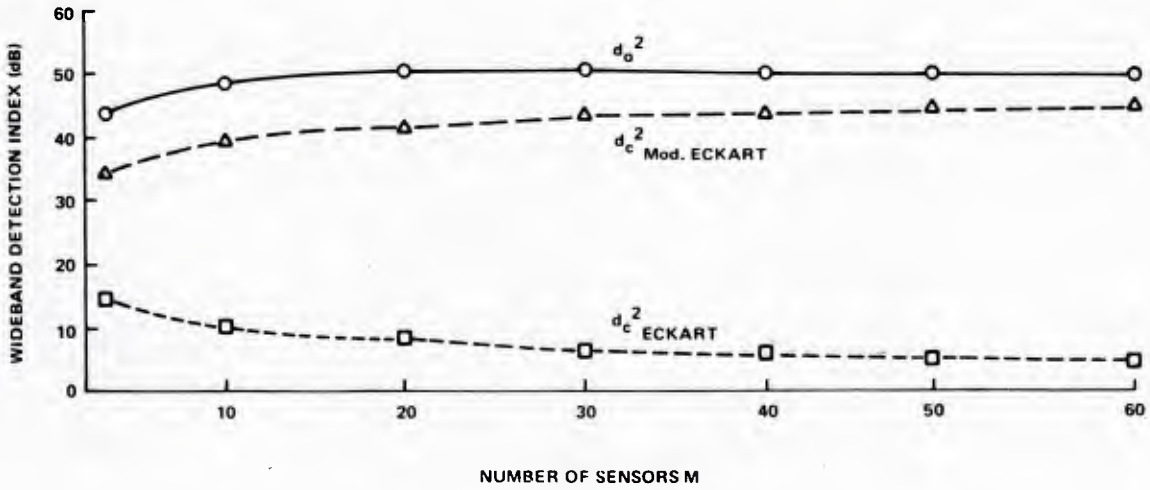

Fig. 4.13. Normalized Detection Indices Versus Number of Sensors, M With $\alpha = \beta_k$, $\nu_k = 0.01$ and $w\Delta / U_c = 2\pi$

CHAPTER FIVE

ARRAY DESIGN CONSIDERATIONS

5.1 Introduction

In Chapters 3 and 4 array geometry was given. We must now deal with criteria that affect the choice of geometry in practice. In the continuous case, the primary constraint is that the introduction of continuous phase shifts is impractical so that one must ideally work with sensor lengths small compared with acoustic wavelengths.

In the discrete case, the primary constraint is a limitation on the number (M) of available sensors. The number must often be small enough so that uniform spacing over the available aperture results in the flow noise being independent from sensor to sensor, yielding an array gain of only M. By using groups of tightly spaced sensors, one can get a much higher array gain at certain frequencies and hence achieve greatly improved detector performance (either optimal or conventional).

5.2 Space-Continuous Sensors

The first detector structure we consider is shown in Fig. 5.1. It consists of conventional beamforming on N_1 space-continuous

uniformly sensitive sensors (extended sensors) of length 1. Spatial aliasing is thus avoided at the extended sensor level but, of course, not at the beamformer input level. Extended sensors are separated by distance D, which we assume to be sufficient for the noise to be statistically independent between extended sensor outputs. Hence, conventional beamforming, which simply steers extended sensor outputs to align signal components, is formally optimal.

For most of the discussion, equally spaced subapertures are assumed. This assumption is unnecessary. It is simply convenient. All of the arguments to follow remain valid for irregularly spaced subapertures. The main requirement is that the outputs of subapertures are uncorrelated under the noise-only hypothesis. It is important to keep in mind that, if the noise is uncorrelated between subarrays, the subarrays may be distributed in the observation interval in any manner whatever, leaving the results unchanged.

In passing, we emphasize that one is driven to this type of array construction because of constraints on the number of sensors. Otherwise, one could, in principle, fully populate the observation interval with a large number of equally spaced extended sensors of very small length and thus achieve near optimal performance with simple conventional beamforming as in Chapters 3 and 4, as long as the overall $\beta_k L$ product is sufficiently larger than unity.

Appendix B derives the overall array gain for the structure shown in Fig. 5.1 as a direct extension of the results obtained in Chapter 3. The array length is now l, but no steering is possible within the space-continuous extended sensor. Hence,

$$G_{kT} = N_1 \, S_c^{\,2} \, G_{kc}\Big|_{\text{sub c}} \quad , \tag{5.1}$$

where

$$G_{kc}\Big|_{\text{sub c}} \triangleq \frac{\frac{\beta_k l}{2}\left(1 + \nu_k^{\,2}/\beta_k^{\,2}\right)}{1 + \frac{\left(\nu_k^{\,2} - \beta_k^{\,2}\right)}{\beta_k l\left(\nu_k^{\,2} + \beta_k^{\,2}\right)}\left(1 - e^{-\beta_k l}\left(\cos \nu_k l + \frac{2\nu_k\beta_k}{\left(\nu_k^{\,2} - \beta_k^{\,2}\right)} \sin \nu_k l\right)\right)} \tag{5.2}$$

is the array gain for the extended sensor. There should be no confusion between (5.1) and (5.2). The quantity, $S_c^{\,2} \, G_{kc \text{ sub}}$ in (5.1) is the unsteered array gain. Equation (5.2) gives the array for a broadside-looking direction. Except for the replacement of ν_d by ν_k (no steering), (5.2) is analogous to the array gain for the entire (steered) array in Chapter 3 (3.14) and is common to all channels. Therefore,

$$S_c^{\,2} = \left(\frac{\sin \frac{1}{2}\nu_s}{\frac{1}{2}\nu_s}\right)^2 \tag{5.3}$$

is the wavenumber response of the extended sensor to signal. N_1 is the array gain factor from conventional beamforming on the N_1 extended sensors, with noise between sensor outputs statistically independent.

The principles and reasons behind using modified Eckart filtering, rather than simple Eckart filtering, in Fig. 5.1 are exactly the same as in Chapter 3. The modified Eckart (postbeamformer) filter, C_k, from (2.89) should be chosen according to its input signal and noise spectra, not the signal and noise spectra at each sensor.

Let us now consider that the signal-to-noise ratio is constant over the signal band:

$$\frac{S_k}{I_k} = \begin{cases} S/I \text{ (a constant)} , \; k = 1, 2, \ldots, N \\ 0, \text{ elsewhere} , \end{cases} \qquad N = Tw/2\pi . \tag{5.4}$$

Then, using conventional beamforming on the extended sensor outputs ($\underline{H}_k = \underline{V}_k$ in Fig. 5.1) and simple Eckart filtering, $C_k = \sqrt{S_k}/I_k$, we obtain from (2.77) and Appendix B

$$d_c^2\Big|_{\substack{\text{simple}\\ \text{Eckart}}} = \frac{\left(\frac{S}{I}\right)^2 N_1^2 \left|\sum_k S_c^2\right|^2}{\sum_k \left(\frac{1}{G_{kc}\big|_{\text{sub c}}}\right)^2} \quad . \tag{5.5}$$

From (5.3) and the properties of the "sinc" function,

$$S_c = \frac{\sin\left(\frac{\omega_k l \cos\theta_s}{2c}\right)}{\frac{\omega_k l}{2c}\cos\theta_s} \leq 1, \; k = 1, 2, \ldots, N \; . \tag{5.5a}$$

Hence,

$$\sum_k S_c^2 \leq N \; . \tag{5.5b}$$

Equality applies in (5.5a) and (5.5b) only when $\theta_s = \pi/2$. In such a case, the signal arrives broadside to the array axis. Hence, the conventional detection index in (5.5) is degraded relative to a system using conventional beamforming with steering within the extended sensors. The degradation is clearly large if the signal bandwidth is concentrated largely outside the mainlobe response in (5.3). Conversely, one nearly avoids this degradation if the largest signal frequency is well inside the mainlobe of (5.3). For this latter case, the extended sensor length is much smaller than any signal wavelength along the array.

Using a common modified Eckart filter, $C_k = \sqrt{S_k}/I_k \; G_{kT}$, in conjunction with the conventional beamformer, in Fig. 5.1, we obtain from (2.79), (5.1), and (5.4)

$$d_c^2\Big|_{\substack{\text{modified}\\ \text{Eckart}}} = \left(\frac{S}{I}\right)^2 \sum_k \left|G_{kT}\right|^2$$

$$= \left(\frac{S}{I}\right)^2 N_1^2 \sum_k S_c^4 \, G_{kc}^2\Big|_{\text{sub c}} . \tag{5.6}$$

As in (5.5), performance in (5.6) is degraded relative to performance with steering within extended sensors, insofar as the signal bandwidth is outside the mainlobe of (5.3). In many ways, the discussion is the same here as in Chapter 3. The idea of not steering witnin extended sensors, which causes signal power suppression prior to conventional beamforming, is the main difference.

Here, as in Chapter 3, we might expect conventional beamforming followed by modified Eckart filtering to recover a substantial part of the performance loss incurred with simple Eckart filtering and conventional beamforming. This turns out to be false in some cases, e.g., when $S_c^2 << 1$ throughout the processed frequency band. Note that the best frequency filter, in this case, requires the weight of the common subaperture gain, including S_c^2 in (5.3), in addition to the simple Eckart filter, $\sqrt{S_k}/I_k$.

From (5.1) we see that G_{kT} varies directly with the extended sensor broadside array gain in (5.2) and extended sensor response to signal. Therefore, the sum in the denominator of (5.5) is affected most heavily by frequencies where extended sensor array gain is small, e.g., at frequencies satisfying

$$v_k = (2n + 1)\pi \ , \ n = 0, 1, 2, ... \qquad (5.7)$$

At these frequencies, l is an odd multiple of the noise half wavelength, evaluated at ω_k.

The sum in (5.6) is influenced most heavily by frequencies where $G_{kc}\big|_{sub\ c}$ is large and relatively little by frequencies satisfying (5.7). Simple Eckart filtering is, once again, poorly matched to conventional beamforming if there is significant extended sensor array gain variation with frequency, quite apart from the effect of S_c^2 in (5.3). Arguments made in Chapter 3 in connection with steered aperture thus provide us with a basis for discussion here.

Consider first that extended sensor length is much smaller than any signal wavelength, i.e., $v_{sl}/2 << 1$ in (5.3) for $k = 1, 2, 3, ..., N$. Then from (5.5) and (5.6),

$$\frac{d_c^2\big|_{\text{modified Eckart}}}{d_c^2\big|_{\text{simple Eckart}}} = \frac{1}{N^2} \sum_{\kappa=1}^{N} \sum_{j=1}^{N} \frac{G_{\kappa c}^2\big|_{\text{sub c}}}{G_{jc}^2\big|_{\text{sub c}}} . \qquad (5.8)$$

This is the same for the entire space-continuous array as for a simple extended sensor. We, therefore, simply appeal directly to Chapter 3 for all relevant conclusions.

Conventional processing with modified Eckart filtering is better than conventional processing with simple Eckart filtering unless the extended sensor array gain is frequency independent. The extent of the improvement, previously discussed in connection with the numerical examples of Fig. 3.4, is substantial, especially for small $\beta_K l$ products and small noise fractional bandwidths, β_K/ν_K.

Hence, if one constructs an array of extended sensors that are simultaneously small compared with signal wavelengths and with the noise spatial correlation length, then modified Eckart filtering can potentially enhance performance of the conventional detector, making it more competitive with the optimal detector. Here again, as in Chapter 3, the drawback of modified Eckart filtering is the strong dependence on the extended sensor array gain in (5.2) and hence on the spatial structure of the noise field, which usually varies with conditions. In such cases, one generally needs to estimate the spectral parameters ν_K and β_K in order to construct the modified

Eckart filter from (5.2): remember, for the Corcos flow noise model, convective noise speed, U_c, is sufficient for this construction.

We next consider cases for detection performance with conventional beamforming when S_c^2 in (5.3) is not equal to 1 over the entire signal band. We shall confine this discussion to the large $\beta_k l$ regime, where extended sensor response to signal tends to be more of a problem.

We ask if there is substantial detection enhancement possible with modified Eckart filtering at the beamformer output when there is no steering, within extended sensors, to align the signal properly? When the answer is yes, we ask if this enhancement is about the same as the enhancement accomplished, under the same conditions, with steering within extended sensors? If so, then why bother to steer? Performance loss due to signal suppression at the extended sensor level could then be recovered at the beam output with appropriate scalar filtering. It turns out that, in general, the answer to the initial question is no.

We show this using our usual noise model with β_k and ν_k given by (2.32) and (2.33) with spectral functions specified at each frequency by (3.29). Let us also assume a sufficiently large $T(\omega_2 - \omega_1)$ product so that sums in (5.5) and (5.6) can be approximated by integrals. From (5.5) and (5.6), one obtains

$$d_c^2\Big|_{\text{modified Eckart}} = \frac{T}{2\pi} N_1^2 \frac{S^2}{I^2} \frac{l^2}{4U_c^2} \frac{(\alpha^2+1)^2}{\alpha^2} \int_{\omega_1}^{\omega_2} \left(\frac{\sin(\frac{\omega l}{2c} \cos\theta_s)}{\frac{\omega l}{2c} \cos\theta_s} \right)^4 \omega^2 d\omega \tag{5.9}$$

and

$$d_c^2\Big|_{\text{simple Eckart}} = \frac{T}{2\pi} N_1^2 \frac{S^2}{I^2} \frac{l^2}{4U_c^2} \frac{(\alpha^2+1)^2}{\alpha^2} \frac{\left| \int_{\omega_1}^{\omega_2} \left(\frac{\sin(\frac{\omega l}{2c} \cos\theta_s)}{\frac{\omega l}{2c} \cos\theta_s} \right)^2 d\omega \right|^2}{\int_{\omega_1}^{\omega_2} \frac{1}{\omega^2} d\omega}$$

$$\beta_k l \gg 1 , \tag{5.10}$$

which, again, are simple extensions of our results in Chapter 3.

Making the changes of variables

$$u = \frac{\omega l}{2c} \cos\theta_s , \quad du = \frac{l}{2c} \cos\theta_s \, d\omega, \quad u_1 = \frac{\omega_1 l}{2c} \cos\theta_s ,$$

$$u_2 = \frac{\omega_2 l}{2c} \cos\theta_s , \tag{5.11}$$

with c = speed of sound, we have the ratio

$$\left.\frac{d_c^2\big|_{\text{modified Eckart}}}{d_c^2\big|_{\text{simple Eckart}}}\right|_{\text{no steering}} = \frac{\int_{u_1}^{u_2}\left(\frac{\sin u}{u}\right)^4 u^2 du}{\left|\int_{u_1}^{u_2}\left(\frac{\sin u}{u}\right)^2 du\right|^2}\int_{u_1}^{u_2}\frac{du}{u^2} \quad . \tag{5.12}$$

Again, when $\beta_k l >> 1$ is violated, (5.12) is an optimistic estimate of ennancement. Note that (5.12) is the same as (3.32) when the signal arrives broadside to the array, i.e., $\theta_s = \pi/2$ so that S_c^2 in (5.3) becomes 1 in the signal band.

Certainly, enhancement without steering witnin extended sensors as given by (5.12) must always be greater tnan 1. This follows directly from (5.12) by using tne Schwartz inequality:

$$\left|\int_{u_1}^{u_2}\frac{\sin^2 u}{u^2}\,du\right|^2 \le \int_{u_1}^{u_2}\frac{\sin^4 u}{u^2}\,du\int_{u_1}^{u_2}\frac{1}{u^2}du \quad , \tag{5.13}$$

$$0 < u_1 < u_2 < \infty \, .$$

Therefore,

$$\frac{\int_{u_1}^{u_2} \frac{\sin^4 u}{u^4}\, u^2\, du}{\left|\int_{u_1}^{u_2} \frac{\sin^2 u}{u^2}\, du\right|^2} \int_{u_1}^{u_2} \frac{1}{u^2}\, du \geq 1 \,. \tag{5.14}$$

Hence, (5.12) exceeds 1 for arbitrary nonzero intervals $[u_1, u_2]$. Equality applies in (5.14) when $u_2 \gg u_1$.

Under the steered condition, all $\frac{\sin u}{u}$ terms in (5.12) go to unity with the result

$$\left.\frac{d_c^2\,|\text{modified Eckart}}{d_c^2\,|\text{simple Eckart}}\right|_{\text{steered}} \simeq \frac{\int_{u_1}^{u_2} u^2 du \int_{u_1}^{u_2} \frac{du}{u^2}}{\left|\int_{u_1}^{u_2} du\right|^2}, \quad u = \frac{\omega l}{2c}, \quad \beta_K l \gg 1,$$

$$= \frac{1}{3}\left(\frac{u_2}{u_1} + 1 + \frac{u_1}{u_2}\right), \tag{5.15}$$

which is, of course, identical with (3.32).

We now want to show that failure to steer can sometimes result in serious performance loss. To demonstrate this, we have plotted the

exact equations in (5.12) and (5.15) as functions of u_2 for three fixed values of u_1. Results are shown in Fig. 5.2.

The results indicate the following main points. Performance gain provided by the modified Eckart filter in conjunction with conventional beamforming on extended sensors is nearly the same whether or not one steers within extended sensors if

$$u_2 = \frac{\omega_2 l}{2c} \cos \theta_s \leq \frac{\pi}{4} \quad . \tag{5.16}$$

Observe that each curve describing enhancement with steering departs dramatically from the corresponding curve for the nonsteered condition at $\pi/2$, which, incidentally, is where the signal response in (5.3) drops to 3 decibels below its value at $v_{s1}/2 = 0$.

If the condition in (5.16) is satisfied, the extended sensor length is small compared to signal wavelengths. Fig. 5.2 indicates that one then achieves approximately 5.12 decibels of conventional detection enhancement when $u_1 = \pi/40$, using the simple post-beamformer filter in (3.33) consisting of a voltage gain increasing linearly with frequency in the frequency interval specified by (5.16).

Fig. 5.2 also suggests that relative performance is best when the normalized lower frequency is smallest:

$$\frac{\omega_1 l}{2c} \cos \theta_s << 1 \ . \qquad (5.17)$$

Conditions (5.16) and (5.17), together, suggest the following procedure for determining suitable lengths for extended sensors. Extended sensor length l should be no longer than one-fourth of the smallest effective signal wavelength ($\lambda_{eff} = \lambda_s/\cos \theta_s$), evaluated at ω_2.

Observe that there is insignificant gain provided by the modified Eckart filter when $u_1 = \pi/4$. This is, of course, to be expected since then S_c^2 is small throughout most of the processed signal band. One can easily generalize this to the condition

$$u_1 > 1 \ .$$

For instance, with $u_1 = 2\pi$ and $u_2 = 4\pi$ inserted into (5.12), one finds that

$$\frac{d_c^2 \,|_{\text{modified Eckart}}}{d_c^2 \,|_{\text{simple Eckart}}\,|_{\text{no steering}}} \approx 1.52 \qquad (5.18)$$

This confirms that the modified Eckart filter construction in (5.1) is not used efficiently in this case.

For fixed l and incident angle θ_s, we can process frequencies up to

$$\omega_2 = \frac{\pi c}{2l \cos \theta_s} \tag{5.19}$$

and still be essentially compatible with conditions needed to use the relatively simple voltage gain postbeamformer filter in (3.33). Clearly one gains little by processing frequencies any higher than (5.19) with only this filter.

The main effect of the signal incident angle is to increase the upper frequency, ω_2, as θ_s approaches $\pi/2$, i.e., as one approaches broadside signal incidence. It is notable that, even for endfire incidence (e.g., $\theta_s = 0$), the quantity c/l is sufficiently large in most towed array applications so that ω_2 is usually of the order of hundreds of hertz.

The other region of interest in Fig. 5.2 is where the normalized frequency $(\omega_2 l/2c) \cos \theta_s$ exceeds $\pi/2$, the point where the signal response in (5.3) is down by 3 decibels from its value at $\nu_{s1}/2 = 0$.

For the case $u_1 < 1$, curves representing performance recovery for the unsteered condition, in Fig. 5.2, approach nearly constant values as u_2 exceeds $\pi/2$. On the other hand, curves representing recovery for the steered condition remain monotone, increasing with

u_2. The additional noise admitted by the simple Eckart filter makes the difference. With simple Eckart filtering following the beamformer, we are admitting less and less signal but more and more noise as u_2 increases beyond $\pi/2$. In contrast, the band limitation of S_c^2, in the Eckart filter, admits less signal and noise.

It is easy to verify that the quotient of forms containing sin u/u terms in (5.12) are less than unity and nearly invariant with u_2 when u_2 exceeds $\pi/2$. Equation (5.12) then reveals that recovery with modified Eckart filtering is traceable directly to signal frequencies near ω_1, where the large β_K product array gain in (5.2) is lowest for the broadside-looking direction; hence, the noise level admitted by the simple Eckart filter is highest. To show this, consider the case

$$u_1 = \frac{\pi}{40} \text{ and } u_2 > \frac{\pi}{2}$$

Then, from (5.12), we have

$$\frac{\int_{\pi/40}^{u_2} \frac{\sin^4 u}{u^4} u^2 \, du}{\left| \int_{\pi/40}^{u_2} \frac{\sin^2 u}{u^2} \, du \right|^2} \approx 0.35 , \qquad u_2 > \pi/2 . \tag{5.20}$$

Hence,

$$\left.\frac{d_c^{\,2}\ \text{modified Eckart}}{d_c^{\,2}\ \text{simple Eckart}}\right|_{\text{no steering}} \approx 0.35 \int_{\pi/40}^{u_2} \frac{1}{u^2}\,du = 0.35\left[\frac{40}{\pi} - \frac{1}{u_2}\right]$$

$$\approx 4.46\ (6.5\ \text{decibels}),$$

$$u_2 > \pi/2, \qquad (5.21)$$

which, as in Fig. 5.2, is obviously invariant with u_2, under the specified conditions.

A similar argument can be made for the other examples in Fig. 5.2. With $u_1 = \pi/10$ and $u_2 > \pi/2$, the ratio in (5.20) increases to approximately 0.49: the detector with simple Eckart filtering also encounters a proportionally smaller noise level at the low edge of the processed band with u_1 increased from $\pi/40$ to $\pi/10$. This, then, results in the relatively small performance recovery of only 1.98 decibels compared with the $u_1 = \pi/40$ case.

We visualize that substantial signal energy is rejected by the extended sensor when u_2 exceeds $\pi/2$. Processing normalized frequencies beyond $\pi/2$ is probably not worthwhile for two obvious reasons. First, one requires a relatively complicated postbeamformer

filter. Secondly, one improves performance only slightly with such a filter compared with the improvement made when processing up to only $\pi/4$. We cannot over emphasize the fact that performance, in the latter interval, is achieved with the modified Eckart filter in (3.33), consisting of a relatively simple voltage gain increasing linearly with frequency and independent of specific operating conditions. That filter, coupled with a low-pass filter cutting off at $u_2 = \pi/4$, should therefore represent a practically reasonable compromise.

There are certain narrow frequency regions where the extended sensor signal response in (5.3) introduces large variations in beam output signal power, e.g., in the vicinity of π where there are relatively large changes in the extended sensor response with frequency. Hence, performance with no steering applied within extended sensors is generally improved over performance with steering within sensors in such regions, but only by a small amount.

For instance, with $u_2 = \pi$ and $u_1 = 3\pi/4$, we have by direct numerical evaluation of (5.12) and (5.15) that

$$\left.\frac{d_c^2 \text{ modified Eckart}}{d_c^2 \text{ simple Eckart}}\right|_{\text{no steering}} \simeq 1.58 . \qquad (5.22)$$

and

$$\left.\frac{d_c^2\,|_{\text{modified Eckart}}}{d_c^2\,|_{\text{simple Eckart}}}\right|_{\text{steered}} \simeq \frac{1}{3}\left(\frac{u_2}{u_1} + 1 + \frac{u_1}{u_2}\right) = 1.03 \ . \tag{5.23}$$

We conclude from the above that the modified Eckart filter recovers some of the losses due to high frequency signal rejection. However, even in narrowband frequency regions of maximum variation of S_c^2, the recovery is so small as to make construction of the modified Eckart filter in (5.6) unattractive.

When the $\beta_k l$ product is sufficiently larger than 1 and the unused aperture space in Fig. 5.1 is a small fraction of the available observation interval L, then

$$N_1 l \simeq L \ .$$

It follows from (5.6) with $v_s l/2 << 1$ that

$$d_c^2\,|_{\substack{\text{modified}\\ \text{Eckart}}} \simeq \sum_k |d_{ko}|^2 = \sum_k \left|\frac{S_k}{I_k}\,\frac{\beta_k L}{2}\left(1 + \frac{v_d^2}{\beta_k^2}\right)\right|^2 \tag{5.24}$$

is nearly the optimal detection index for interval L computed in Chapter 3.

5.3 Discrete Sensor Subarrays

The constraints here are very different. There is no longer any reason to demand

$$l << \lambda_s \tag{5.25}$$

and optimal processing within each subarray is at least potentially possible. Also,

$$l >> 1/\beta_K \tag{5.26}$$

is no longer a natural condition, particularly with small numbers of sensors in the subarrays. The major constraint is that the total number of sensors (M), limited by practical considerations, is too small to fill the available aperture. Clearly, with unlimited sensors and channels, we could fully populate the array and achieve near optimal performance with conventional processing on individual equally spaced sensors so long as $\beta_K L >> 1$. What we are trying to do here is to get the noise cancellation and reduced spatial aliasing available with small sensor spacings while retaining large overall aperture lengths for tracking purposes.

The general overall array gain for this detector structure with conventionally processed clusters (subarrays)(see Fig. 5.3), derived in Appendix B and applicable to irregularly spaced subarrays, is

$$G_{kD} = N_1 \, G_{kc}\Big|_{sub}$$

$$= \frac{M_1 N_1}{1 + 2 \sum_{i=1}^{M_1 - 1} \left(1 - \frac{i}{M_1}\right) e^{-\beta_k i \Delta} \cos(\Delta i \nu_d)} \quad . \quad (5.27)$$

Equation (5.27) is analogous to the array gain for the entire array in (4.9), Chapter 4. The basic discussion, numerical results, and conclusions there are thus relevant here (see Figs. (4.6a), 4.7, 4.10, and 4.12). The detection index for the detector structure in Fig. 5.3 is obtained from (2.86), with array gain from (5.27):

$$d_c^{\,2}\Big|_{\text{modified Eckart}} = \sum_{k=1}^{N} \left(\frac{S_k}{I_k}\right)^2 G_{kD}^{\,2}$$

$$= N_1^{\,2} \sum_{k=1}^{N} \left(\frac{S_k}{I_k}\right)^2 G_{kc}^{\,2}\Big|_{sub} \quad . \quad (5.28)$$

Except for the factor N_1^2, this is analogous to the detection performance with full array processing in Chapter 4. Hence, the analogous expression for the relative wideband performance gain for the conventional detector with a modified Eckart filter over the conventional detector with simple Eckart filtering serves as a useful measure of improvement here. With signal and noise spectra satisfying (5.4),

$$\frac{d_c^2\Big|_{\substack{\text{modified}\\\text{Eckart}}}}{d_c^2\Big|_{\substack{\text{simple}\\\text{Eckart}}}} = \frac{1}{N^2} \sum_{k=1}^{N}\sum_{l=1}^{N} \frac{G_{kc}^2\Big|_{sub}}{G_{lc}^2\Big|_{sub}^2} \quad . \tag{5.29}$$

Performance examples with the Corcos model shown in Fig. 4.5, 4.6b, 4.11, and 4.13 are directly applicable to (5.29). The modified Eckart filter recovers much of the loss incurred when simple Eckart filtering follows conventional beamforming on subarrays for the same reasons as in Chapter 4. Substantial recovery is possible when a reasonable wide band of frequencies is processed and there are large variations in subarray array gain with frequency. As in Fig. 4.13, where detection indices are normalized by the square of the product of the total number sensors used times S/I in (5.4), i.e., $(N_1M_1\ S/I)^2$, the extent of the recovery increases with M_1.

Analogous to processing over the full array, one can improve detection performance, especially in the small $\beta_k l$ regime, with the detector structure in Fig. 5.3, by using optimal processing within clusters (see Fig. 4.2). Such an instrumentation involves complex weighting and phase shifting of sensor outputs and results in an expression for overall array gain given by

$$G_{kD} = N_1 \, G_{ko}\Big|_{sub} = \frac{M_1 N_1}{1 - e^{-2\alpha\omega_k \Delta/U_c}} \left(1 + \left(1 - \frac{2}{M_1}\right)e^{-2\alpha\omega_k \Delta/U_c} - \right.$$

$$\left. - 2\left(1 - \frac{1}{M_1}\right)e^{-\alpha\omega_k \Delta/U_c} \cdot \cos\left(\frac{\omega_k \Delta}{U_c}\right)\right) ,$$

$$\nu_s << \nu_k ,$$

(5.30)

which differs from the expression for full array processing in (4.8) only by the appearance of $M_1 N_1$ in place of M. This expression then can be applied directly to (2.79) to obtain the detection index for the detector structure, as in Fig. 5.3, with conventional beamforming on optimally processed cluster outputs:

$$d_o^2 \triangleq N_1^2 \sum_k \frac{S_k^2}{I_k^2} \, G_{ko}^2\Big|_{sub} . \qquad (5.31)$$

We emphasize that optimal processing within clusters is usually realized with a substantial increase in instrumentation complexity, especially if M_1 is large. One obviously minimizes this complexity with 2 sensor clusters (i.e., $M_1 = 2$, in Fig. 4.2).

Most practical instrumentations will depend on the actual spatial structure of the noise field, which usually varies with towed array conditions (e.g., tow vessel speed). Therefore, adaptive instrumentations are anticipated for either optimal or conventional processing within clusters, in conjunction with conventional beamforming followed by the best postbeamformer filter. Modified Eckart filtering, with conventional processing within clusters, avoids excessive instrumentation complexity associated with optimally processed clusters (see Fig. 4.2) since it demands only a single adaptive frequency scaling at the conventional beamformer output for homogeneous noise. From Chapter 4 (see Fig. 4.12), the general post-beamformer filter construction, in the latter case, requires $M_1 - 1$ bandpass filter parameters (center frequencies) with M_1 sensors per cluster. For sufficiently large M_1, we shall demonstrate that a single ideal bandpass filter with simple Eckart filtering, at a conventional beam output, recovers a large fraction of the detection loss incurred when only simple Eckart filtering is used at a beam output.

5.4 Subarray Size and Separation

The issue of optimum subarray (group) size and subarray separation with a limited number of available sensors remains to be examined. Fig. 5.4 shows normalized detection indices for the detector with conventional beamforming on optimally or conventionally processed clustered sensors as a function of $M_1 = M/N_1$ sensors per cluster, using overall array gain expressions from (5.27) and (5.30), with detection indices in (5.28) and (5.31). There are $N = Tw/2\pi = 50$ positive frequencies in the signal band and $w\Delta/U_c = 2\pi$. Signal-to-noise ratio is again assumed uniform in the signal bandwidth as specified in (5.4). Hence, signal-to-noise ratio and the $M = N_1M_1$ fixed number of available sensors are conveniently normalized out of the results. In all curves shown, $\beta_K l = \beta_K(M_1 - 1)\Delta < 1$. As one should expect, the detection index with optimal processing on clustered sensors (d_o^2) is always larger than the detection index with conventional processing within clusters ($d_c^2|_{\text{modified Eckart}}$). We see that all curves for both d_o^2 and $d_c^2|_{\text{modified Eckart}}$ increase monotonically with M_1, with the largest improvement variation occurring from one to two sensors. From the monotonic behavior, one concludes that detection performance is best when M_1 is as large as is practically possible. Given a fixed M number of available sensors, $M = N_1M_1$, one obviously maximizes M_1 by minimizing the number of clusters, N_1. If M_1 is taken large enough so that $l = (M_1 - 1)\Delta$ exceeds the noise correlation length ($l \gg 1/\beta_K$), then the results

of Chapter 4 indicate that conventional processing on the clustered sensors is near optimal. To achieve the large β_k l condition obviously requires either many sensors per cluster or greater sensor spacings within the cluster; with the parameters of Fig. 5.4, the required M_1 is greater than 16.

Note that performance is always better when available sensors are clustered instead of simply spread out uniformly over the observation interval if the latter arrangement makes the noise uncorrelated from sensor to sensor. Relative wideband performance, with uncorrelated noise (i.e., $M_1 = 1$ in Fig. 5.4), is 10 log (N) = 17 decibels for N = 50 positive frequencies. The detection index, in this case, is substantially below any of the detection indices obtained with tightly grouped sensors.

Since good detection calls for large M_1, hence small N_1, whereas localization demands $N_1 \geq 3$ [39] - [42], a logical choice is $N_1 = 3$ with $M_1 = M/3$ uniformly spaced sensors per conventionally processed cluster. Specifically, one would locate a cluster at the observation interval end points, with a cluster at the interval midpoint. It should be clear that regular cluster spacing is not necessary. The important restriction is that the noise is uncorrelated between cluster outputs.

The only argument for doing something other than simple conventional processing on clustered sensors is to recover the

difference between d_o^2 and $d_{c|\text{modified Eckart}}^2$ in Fig. 5.4. Again, one accomplishes this performance recovery with optimal processing within clusters. If the optimal cluster approach is elected, then 2 sensor clusters offer a relatively simple optimal instrumentation over the $M_1 >> 1$ optimal instrumentation. The complexity advantage over selecting $M_1 > 2$ is obvious. Physically, it is probably easier to instrument many 2 sensor clusters than fewer clusters with many sensors per cluster. The obvious disadvantage with $M_1 = 2$ is the tradeoff of approximately 6 decibels of performance in this example relative to the optimal performance with $M_1 = 16$.

To clarify the functional dependence of the detection indices on M_1, Fig. 5.4d presents the results for $\alpha = 0.001$ on log-log scales. We see that conventional beamforming on optimally processed clusters increases by approximately 3 decibels with each doubling of sensors per cluster for $2 \leq M_1 < 8$. For larger M_1, the optimal clustering curve saturates approximately at 70 decibels, which, after careful examination of (5.28), is seen to be approximately $N/\alpha^2\pi^2(50/\alpha^2\pi^2)$.

The curve for conventional detection performance with the modified Eckart filter increases with a slope of approximately one-half. Performance, in this case, increases as $\sqrt{M_1}$ while instrumentation complexity increases proportionally with $M_1 - 1$. In general, we require $M_1 - 1$ bandpass filter center frequencies to construct the postbeamformer filter (e.g., see Fig. 4.12). From this,

we infer that, given fixed M, the performance/complexity ratio for conventionally processed clustered sensors increases as $1/\sqrt{M_1}$ when M_1 is relatively small.

Since all subarrays have the same array gain, one only needs a single filter (introduced after the final beamformer). The complexity one is then concerned with is that of frequency dependence of the subarray gain. However, the problem associated with complexity of the postbeamformer filter may be less severe than it seems. Fig. 4.12 suggests that array gain fluctuations within one 2π interval of $\omega_K \Delta/U_c$ become smaller as the number of sensors, M_1, increases. If this is true, then the postbeamformer filter only needs to eliminate the normalized frequency neighborhoods of $\omega_K \Delta/U_c = 2n\pi$, $n = 0, 1$.

To demonstrate this, we have computed the detection indices in (5.28), (5.31), and (2.77), using array gains from (5.27) and (5.30), with an ideal symmetrical bandpass filter of unit amplitude, centered at $\omega_K \Delta/U_c = \pi$, applied to the output of the conventional beamformer. Detection indices are plotted in Fig. 5.5 on the vertical axis versus percent of filter bandwidth to total processing bandwidth $w\Delta/U_c = 2\pi$.

All curves are normalized by the square of the number of total sensors times the assumed constant signal-to-noise ratio:

$$\left(M_1 N_1 \frac{S}{I}\right)^2 .$$

The number, M_1, of sensors used is 25, and the noise fractional bandwidth, in each case, is 0.01.

The following observations are plain. The detector with conventional beamforming on optimally processed clustered sensors achieves the highest performance value. The penalty paid for using simple Eckart filtering following conventional beamforming is a 33-decibel loss in detection performance relative to conventional detector performance with the modified Eckart filter when the percent bandwidth of the bandpass filter is sufficiently large (i.e., 96 percent) to include aliased frequencies in the neighborhoods of $\omega_K \Delta / U_c = 0$ and 2π (e.g., see Fig. 4.12). Aliased frequencies are clearly eliminated as the width of the bandpass filter relative to 2π decreases. Specifically, the uncomplicated bandpass filter brings the detector with conventional beamforming followed by simple Eckart filtering to approximately 2.5 decibels below the performance with modified Eckart filtering when the percent of total bandwidth is 50. At the percent of total bandwidth of 50, optimal detection index and detection index of the conventional detector with modified Eckart filtering essentially achieve their maximum values for this example. In contrast, performance of the conventional detector with simple Eckart filtering begins to degrade as the filter bandwidth widens to admit frequencies in aliased neighborhoods, near $\omega_K \Delta / U_c = 0$ and $w\Delta / U_c = 2\pi$. Finally, as the bandpass filter width relative to 2π decreases to 0.16, conventional detection indices converge on each other, as they must in the extreme of very narrowband processing.

Changing conditions naturally lead to adaptive instrumentations. One thus needs only a single adaptive modified Eckart filter with conventional processing on clustered sensors with homogeneous noise. On the other hand, optimal processing within clusters requires adaptive processing on N_1M_1 sensors. Practically speaking, a modified Eckart filtering adaptive instrumentation is probably best implemented, at least with the Corcos flow noise model, by constructing bandpass filters at a beam output requiring knowledge of only the noise speed, U_c. For a large number of sensors, a single bandpass filter centered symmetrically on $\omega_k\Delta/U_c = \pi$ may suffice. Again, one needs only noise speed, U_c, to construct such a filter.

There is one other degree of freedom -- the choice of the interval Δ. As one increases Δ, one increases $w\Delta/U_c$. The evidence in Chapter 4 indicates that increases in $w\Delta/U_c$ beyond 2π have little influence on $d_c^2|_{\text{modified Eckart}}$ (see Fig. 4.6b) because of the near periodicity of G_{kc} with $\omega_k\Delta/U_c$. By increasing Δ, one can make $|\beta_k| > 1$, thus ensuring that $G_{kc} \simeq G_{ko}$, as in Fig. 4.4, and recapturing all of the differences between d_o^2 and $d_c^2|_{\text{modified Eckart}}$ in Fig. 5.4. This would lead to the following prescription for array design: divide the sensors into three clusters. Choose the sensor separation in each cluster such that $|\beta_k| = 1$ at the lowest frequency and highest noise speed. Then all one needs is a simple conventional beamformer with one modified Eckart filter at the output to achieve

near optimal performance. This near optimal performance is slightly poorer than the performance obtainable with tighter spacing of sensors, but the implementation is much simpler. The only negative factor is the complexity of the modified Eckart filter, which, as we have demonstrated, may be avoided if one uses a simple bandpass filter at the beamformer output.

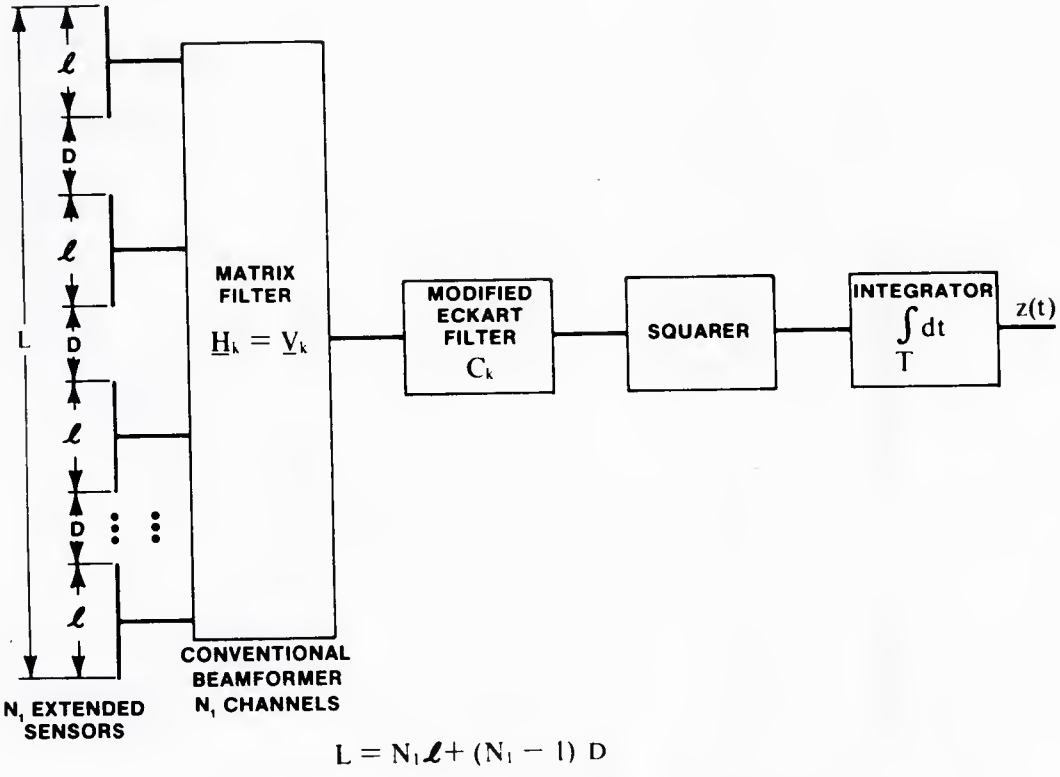

Fig. 5.1. Conventional Detector Structure With Conventional Beamforming on N_1 Space-Continuous Extended Sensors

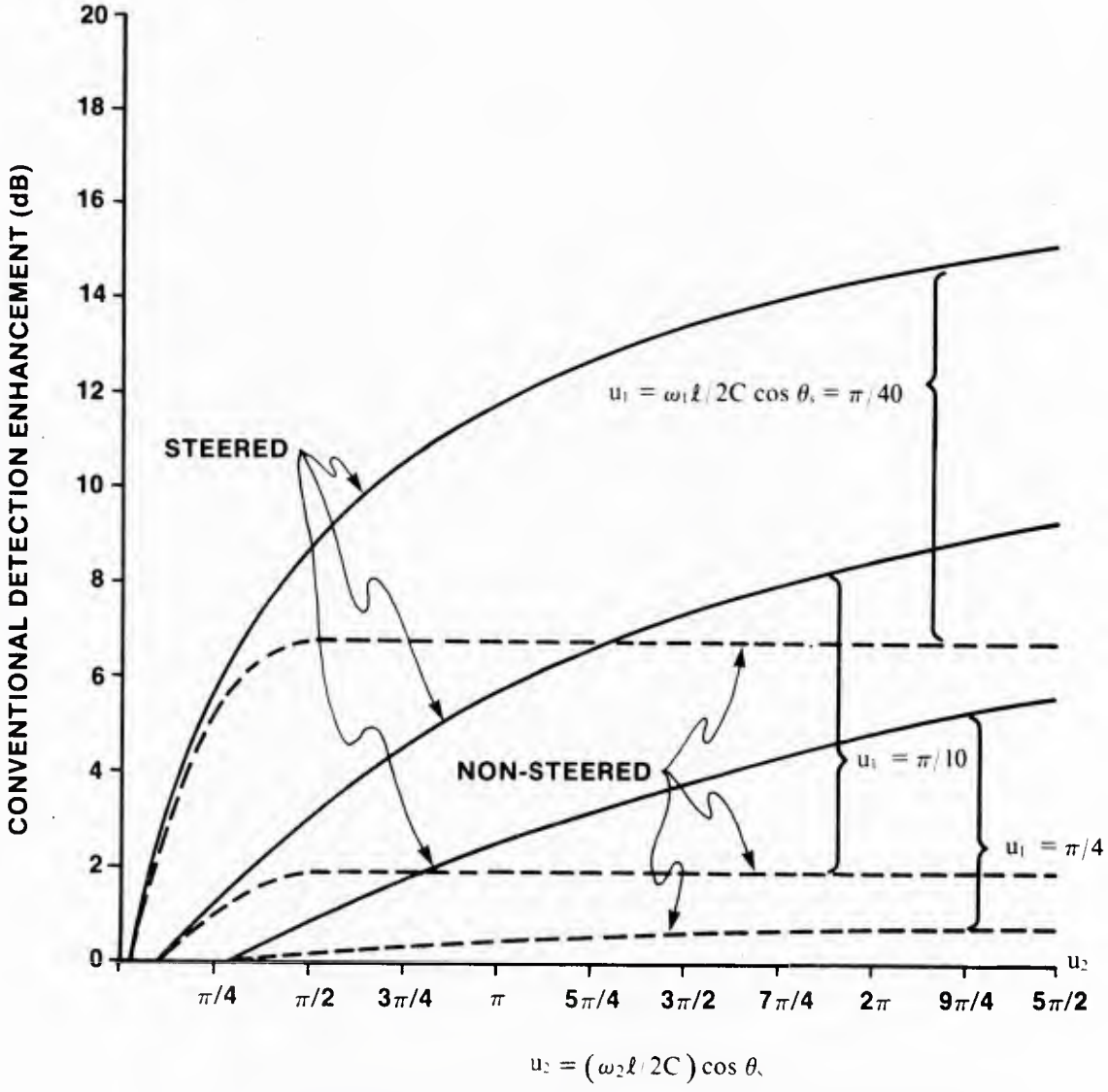

Fig. 5.2. Conventional Detection Enhancement With Conventional Beamforming on Extended Sensors

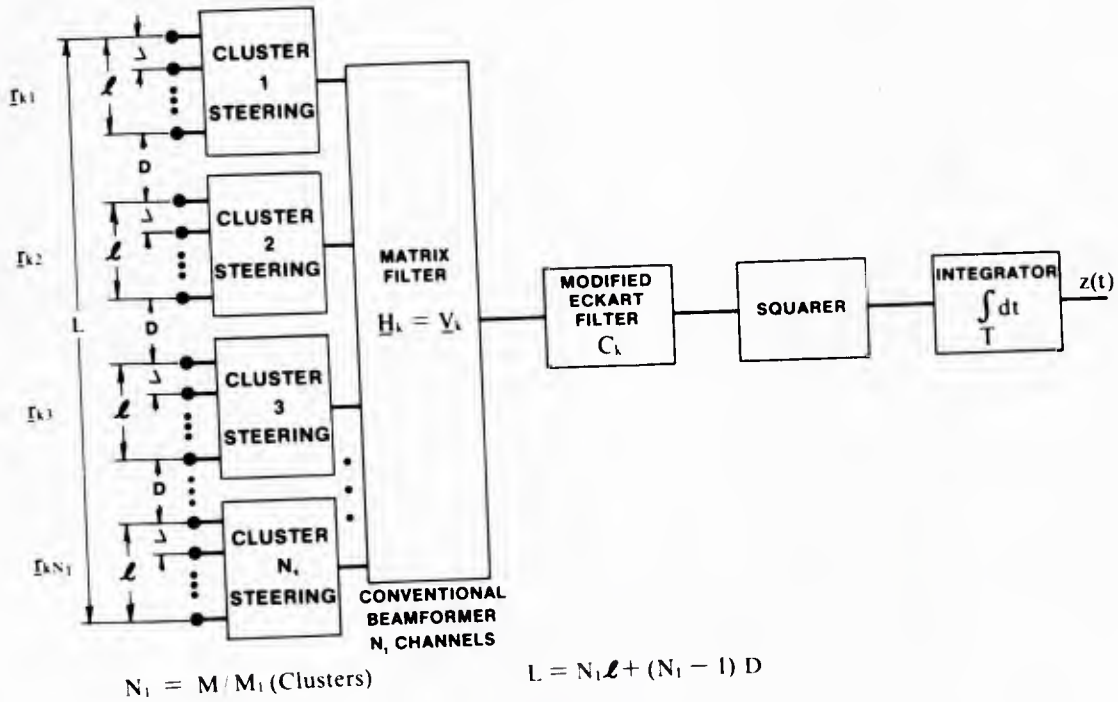

Fig. 5.3. Conventional Detector Structure With Conventional Beamforming on N_1 Subarrays of Discrete Sensors
$\ell = (M_1 - 1)\Delta$, $M = N_1 M_1$ Sensors

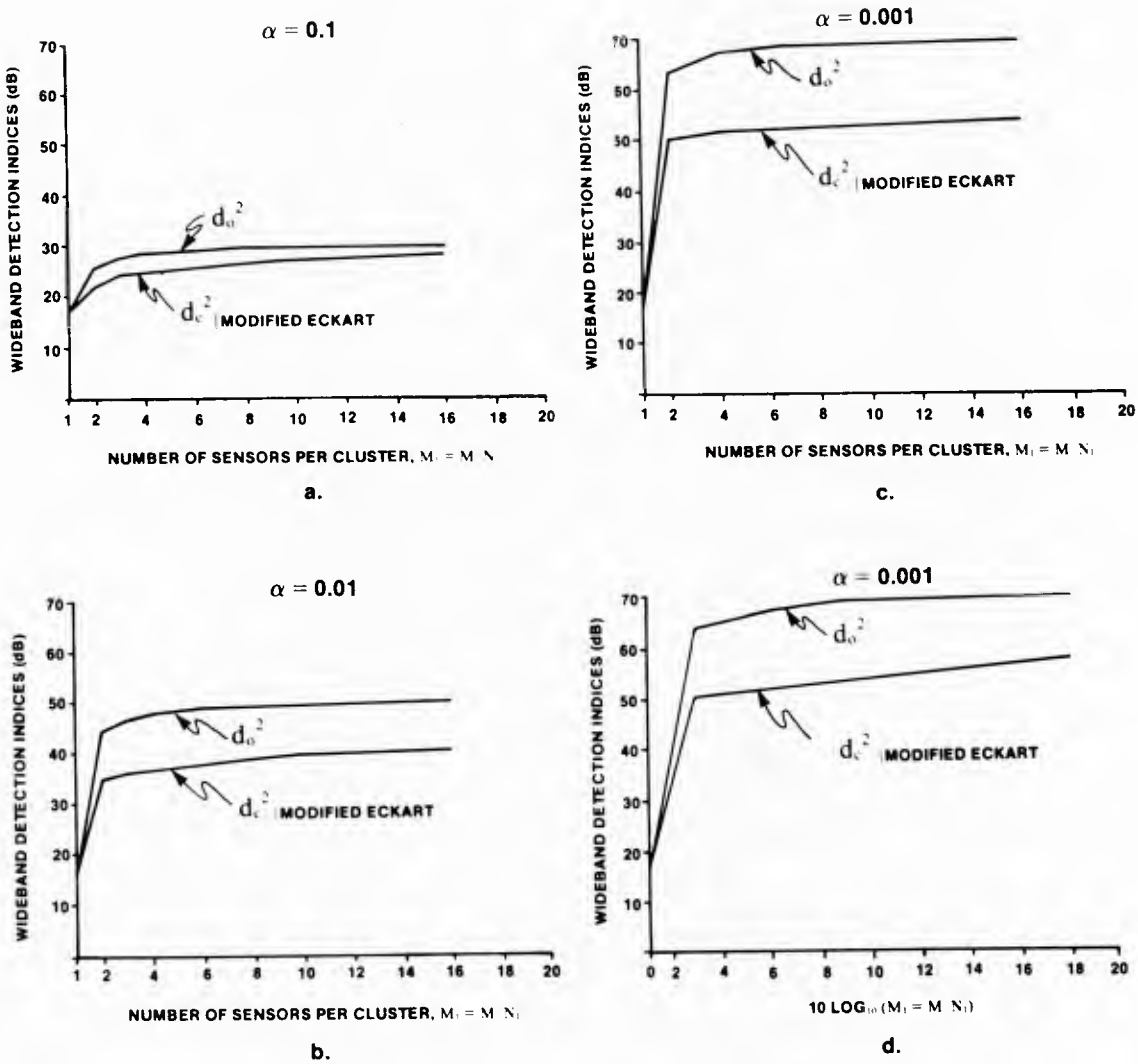

Fig. 5.4. Conventional Wideband Detection Indices for Optimal and Conventional Processing Within Clusters, $w\Delta/U_c = 2\pi$, $\alpha = \beta_k$, w_k, $M = N_1 M_1$ and $S_k / I_k = S / I$ (Constant), $k = 1,2,\cdots N$ Positive Frequencies

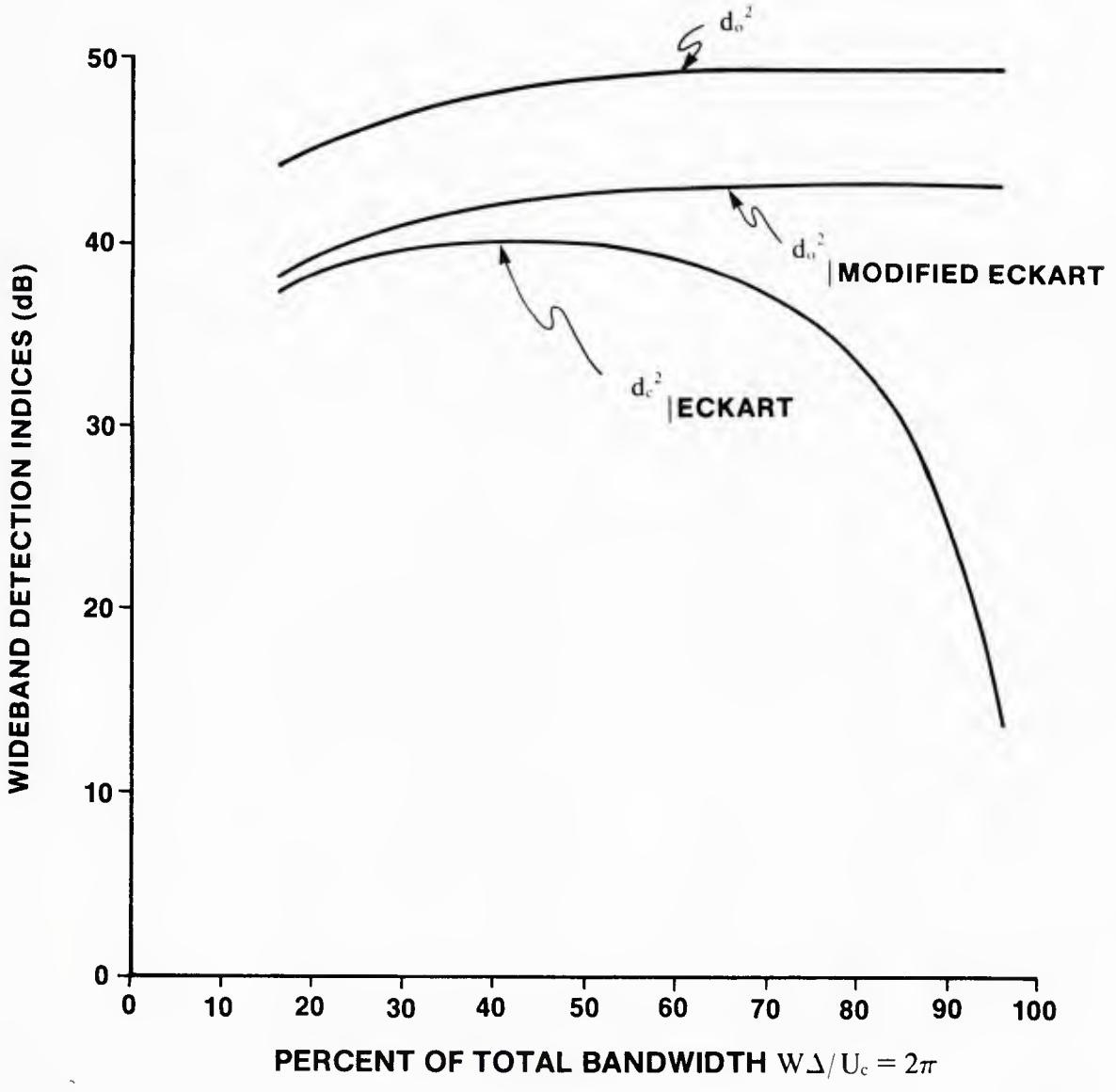

Fig. 5.5. Wideband Detection Indices Versus Percent of Total Band, $\Delta w / U_c = 2\pi$ With Symmetric Bandpass Filter Centered at $\omega_k \Delta / U_c = \pi$, Constant Signal to Noise in [0, w_s], and N = 50 Positive Frequencies

CHAPTER SIX

CONCLUSIONS

6.1 Summary of Results

A systematic approach has been developed as a means of characterizing optimal and conventional space-time detection of a target in a flow-noise-dominated environment. We derived the optimum structure for a stationary Gaussian signal and Gaussian spatially "colored" flow noise characterized as both stationary in time and homogeneous in space. Signal and noise were assumed independent of each other. We imposed the additional constraint that the signal propagated as a plane wave from a known direction. The signal wavefront was assumed to travel across the array in a time short compared with the observation interval T, with signal statistics satisfying $Tw >> 1$. If, in addition, the noise traveled its correlation length in a time short compared to T and T was large compared with the noise correlation length, the space-time detection problem became a problem of spatial processing at independent signal frequencies. This then enabled us to focus our attention on the spatial aspects of the optimal processor and its performance at independent signal frequencies under tne assumption of small signal-to-noise ratio at each sensor.

The wideband processor and its performance followed from appropriately weighted sums of corresponding narrowband components at the independent signal frequencies.

We formulated exact expressions for the likelihood ratio test for discrete and continuous observations. In each case, the optimal instrumentation and its performance were related to the temporal and spatial properties of signal and Butterworth rational flow noise model. We then analyzed, in some detail, optimal performance and also the best possible performance advantage attainable with optimal processing over conventional processing (detector with conventional beamforming) in the modeled flow noise environment.

In passing from discrete to continuous but finite length observations, we established that the uncorrelated noise component formally has a spectrum level of zero. Hence, only wavenumber-colored flow noise remained to limit detection when one had continuous observations. The optimal processor structure was found by solving a nontrivial Fredholm integral equation of the first kind encountered in the binary detection problem. It was shown to consist of a conventional beamformer in addition to appropriately weighted end-point sampling sensors located at each end of the finite observation interval.

We found that the product of the spatial bandwidth and array length ($\beta_k L$) is a very important spatial parameter. Array gain with conventional beamforming alone was shown to be at most 1.8 decibels below optimal with the first-order Butterworth model if the array length exceeds two noise correlation lengths. This very important result states that once the large $\beta_k L$ condition holds, nothing more can be done with any other processor to significantly improve array gain over what has already been accomplisned by the conventional beamformer alone. The detection problem thus must be reduced to that of near spatially white noise in a band of order 1/L, over which the response of the conventional beamformer is significant.

We indicated that substantial array gain improvement is possible, over conventional beamforming alone, if one implements end-point sampling sensors in addition to conventional beamforming. However, end-point sensors require a relatively complex instrumentation, and they significantly improve performance only when the array length is much less than the noise correlation length. Such a condition is probably best avoided in many towed array applications by simply extending the observation interval (array length) beyond the noise correlation distance.

Even the idea of conventional steering (beamforming) is likely to be impractical over any space-continuous length. Therefore, the formulation of space-continuous arrays with any steering at all probably represents an unrealistic idealization. Its purpose is merely to establish absolute performance bounds. Such bounds are used as benchmarks for comparisons with the performance of other array geometry. Of course these performance bounds can never be reached with any other array geometry whatsoever.

A key development step noted that array gain, a frequently used measure of performance, is independent of a linear transfer function connected to the beamformer output, but wideband detection or tracker performance is strongly dependent on linear filtering applied to a conventional beamformer output. For flow noise, usually concentrated at high wavenumbers, optimal and conventional detectors can, therefore, have dramatically different wideband detection indices, even when conventional array gain is itself nearly optimal.

We nave shown that much of the performance loss due to the use of conventional beamforming can be recovered by optimal postbeamformer scalar frequency filtering. For continuous observation intervals, long compared with noise correlation length, the best postbeamformer filter can reduce the difference between optimal and conventional (beamformer) detector performance to a negligible amount. For the Corcos flow noise model, the best postbeamformer filter

instrumentation, in this case, is a simple modification of the basic Eckart filter, consisting of relatively simple pre-emphasis of high signal frequencies. A remarkable property of this best postbeamformer filter, from Appendix A, is its optimality for a large class of noise wavenumber spectra of the form

$$\frac{I_K}{\beta_K} \; \tilde{Q}_K \left(\frac{\nu_K - \nu}{\beta_K} \right) ,$$

where ν_K and β_K are linear functions of frequency ω_K. We note that this class of spectra includes the simple single pole Butterworth wavenumber spectrum at one extreme and an infinite pole Gaussian wavenumber spectrum at the other.

In Chapter 4, we examined the likelihood ratio test and its performance with arrays of uniformly spaced sensors in the absence of uncorrelated noise. We justified omitting uncorrelated noise with arrays by arguing that performance predictions without the uncorrelated noise represent the upper bound performance advantage achievable with optimal processing over conventional processing. Even the smallest amount of uncorrelated noise tends to make the noise wavenumber spectrum flatter, thus bringing the conventional beamformer closer to optimal.

We demonstrated that spatial aliasing is ideally all that happens when one goes from continuous to equally spaced discrete observations. Aliasing causes high wavenumber noise components to fold down onto lower acoustic wavenumbers. This necessarily increases the noise level in the neighborhood of the acoustic signal wavenumber and hence degrades signal-to-noise ratio relative to continuous observations. If one utilizes the common practice of spacing sensors at half acoustic wavelengths, which is often much larger than the flow noise correlation length, then the sampled noise wavenumber spectrum becomes essentially flat. Conventional beamforming is nearly optimal at this spacing, but beam output signal-to-noise ratio is extremely poor since the level of the sampled noise spectrum is very much larger than the noise level with continuous observations.

The best performance attainable with continuous observation is nearly achieved with arrays of extremely tight sensor spacings. Such spacings must be smaller than flow noise wavelengths, which typically have a length scale in inches. One avoids spatial aliasing if, and only if, spatial observations are continuous. Once we have chosen to discretize the observation interval, detection performance is lost. No amount of processing applied subsequently can recover this lost performance.

Aliasing of high wavenumber noise is related directly to variations of array gain with frequency when the noise is correlated between sensors. The minima of these variations occur at frequencies where sensor separations are such that the noise components add coherently. The maxima occur at frequencies where noise components at adjacent sensors are out of phase and, therefore, tend to cancel naturally. Noise components at the former frequencies can dominate the conventional beamformer output. The optimal detector, therefore, outperforms the detector with conventional beamforming and simple Eckart filtering by large amounts. If the undesirable frequencies are eliminated, the best postbeamformer filter, optimized for its actual input signal-to-noise ratio, achieves dramatically improved wideband performance of the detector using conventional beamforming. This performance becomes nearly optimal when conventional array gain is nearly optimal at all signal frequencies.

This treatment of arrays suggests that the use of a relatively simple modification of the Eckart filter can very substantially enhance the performance of a detector using conventional beamforming, making it more nearly competitive with the optimal detector. Major gains can, of course, be made only when a reasonably wide band of frequencies is processed and the noise has sufficient spatial structure (i.e., small fractional bandwidth) so that optimal and conventional array gains vary significantly with frequency. The flow noise associated with towed arrays has the general form of the model

used in this study. While its fractional bandwidth need not be as low as the values considered, it would probably be sufficiently concentrated in wavenumber space to make the modified Eckart filter attractive for wideband detection.

A clear drawback of the modified Eckart filter with arrays is, of course, its dependence on the (conventional) array gain and hence on the spatial structure of the noise field. This structure is not likely to be known in advance so that some form of adaptation is required. However, one needs only a single adaptive filter at a beam output. For arrays, this suggests a significant reduction in processing requirements compared with the set of M filters usually required for optimal processing of data from M sensors. For flow noise encountered by towed arrays, the primary unknown parameter would probably be convective noise speed, U_c, a quantity closely related to tow speed. Adaptation could, therefore, be a relatively simple matter.

In Chapter 5, we dealt with criteria that affect the choice of geometry in practice. With continuous observations, the primary constraint is that the introduction of continuous phase shifts is impractical so that one must work with sensor lengths that are small compared with acoustic wavelengths.

The impracticality of continuous phase shifts led us to consider a detector with conventional beamforming on space-continuous subarrays (extended sensors) where steering within a sensor is abandoned.

Our results with the simple Butterworth model suggest that conventional beamforming on a fully populated (filled) array of individual equally spaced extended sensors, with lengths sufficiently small compared with signal wavelengths, nearly achieves the best possible array gain performance if the array length is sufficiently larger than the noise correlation length. One then nearly achieves best wideband detection index if, in addition, the array length exceeds the noise correlation length at the lowest processed signal frequency.

An alternate array geometry uses, in general, irregularly spaced extended sensors so that the noise is uncorrelated between sensor outputs. Then conventional beamforming on extended sensor outputs followed by modified Eckart filtering can come close to optimal wideband performance, provided that each extended sensor length is less than one-fourth of the smallest acoustic signal wavelength along the array. Processed signal bandwidth is thus kept wholly inside the frequency interval where the extended sensor response to the signal is near unity. Extended sensors are effectively steered in this case.

If each extended sensor length also exceeds the noise correlation length at the lowest signal frequency and, in addition, the unused

aperture between extended sensors is a small fraction of the entire observation interval, then conventional beamforming on equally spaced extended sensors, in conjunction with best postbeamformer filtering, nearly achieves the best detection index attainable with continuous observations on the entire observation interval.

For this special case of extended sensor lengths, long compared with the (Butterworth) noise correlation length and simultaneously short compared with signal wavelengths, the modification to the simple Eckart postbeamformer filter, analogous to full array processing, is a simple voltage gain increasing linearly with frequency. Again, this postbeamformer filter remains optimal as the input noise wavenumber spectra ranges over the large class of input noise spectra mentioned earlier in connection with full array processing.

We considered the important sonar issue of the constraint of a limited number of point sensors in a given observation interval. The number must often be small enough so that uniform spacing over the available aperture results in flow noise being independent from the sensor. Otherwise, one can nearly achieve the optimal performance with conventional beamforming on a filled array of tightly but equally spaced sensors if the array length exceeds the noise correlation length. By using groups (clusters) of tightly spaced sensors, one can get a much higher array gain at certain frequencies and hence achieve greatly improved detector performance (either optimal or conventional).

Again, the best postbeamformer frequency filter must be applied to the conventional beamformer output.

With conventional beamforming on subarrays (clusters) of tightly grouped discrete sensors, conventional steering and optimal processing within clusters are potentially possible. Thus, there is no requirement that the subarray length exceed the noise correlation length in order to achieve optimal array gain at the cluster level.

The subarrays are separated so that the noise is uncorrelated between them. Again, the best postbeamformer frequency filter, which incorporates the common subaperture array gain and simple Eckart filtering, recovers much of the wideband detection loss incurred by simple Eckart filtering following conventional beamforming on subarrays. Substantial recovery of detection performance is possible at the beam output when a reasonably wide band of frequencies is processed so that there is a large variation in subarray gain over frequency.

We noted that detection performance with a fixed number of sensors is maximized when the number of sensors within a cluster is maximum. Good detection calls for a large number of sensors in a cluster, whereas localization criteria demand a minimum of three clusters. The logical choice is one cluster at each end of the observation interval with the remaining cluster at the midpoint of the

observation interval. Cluster separation, however, need not be uniform. The important restriction is that the noise is uncorrelated between cluster outputs. The suggested array construction of clustered sensors with conventional steering within clusters thus achieves greatly improved detection and localization performance over conventional beamforming on available sensors spread over the observation interval. This latter case, with flow noise independent from sensor to sensor, yields an array gain of only M, the total number of sensors used.

Optimal processing within a cluster always improves detection performance over simpler conventional steering within clusters, especially if the cluster length is much less than the noise correlation length at most signal frequencies. However, there is a substantial cost in complexity, especially if the number of sensors per cluster is greater than 2. Thus, an efficient detector structure uses conventional beamforming on outputs of optimally processed 2 sensor clusters distributed in the observation interval in any manner whatever, with noise uncorrelated between cluster outputs. The best postbeamformer filter, in this case, consists solely of the simple Eckart filter chosen from signal and noise spectra at each sensor.

One can exercise the sensor separation degree of freedom. If one chooses uniform sensor separation within each cluster, such that the cluster length exceeds the noise correlation length at the lowest

signal frequency and fastest tow speed, then all one needs is a simple conventional beamformer on outputs, with one modified Eckart filter at the beamformer output, to achieve near optimal wideband detection index.

6.2 Concluding Remarks

We modeled flow noise as a single pole rational Butterworth spectrum. If, instead, we used a rational spectrum with higher order poles, then the solution of the Fredholm integral equations encountered in our detection problem with continuous observations contains Dirac delta functions and their derivatives at the interval end points. It follows that the likelihood ratio test then requires data samples and derivatives of the data at the interval end points. This naturally increases the complexity and sensitivity of the test over the test specified with the first-order Butterworth model. However, asymptotic optimality of the conventional array gain, with the plane wave signal, still holds approximately if the array length is sufficiently larger than the noise correlation length. The plane wave signal model of known location can be shown to satisfy approximately the Fredholm integral equation for more general noise wavenumber spectra, provided the array length is sufficiently larger than the noise correlation length [2, 19, pp. 204-207].

With continuous observations and rational noise spectral models, one easily argues that the likelihood ratio test designed with assumed noise spectral forms can be very sensitive to the functional form of actual noise spectra. Finite power flow noise, considered to be in the class of rational spectra, can be expressed as a ratio of polynomials, with difference $p - q > 1$ between the order of the denominator and numerator polynomials. If one restricts processing to the conventional beamformer alone, then its performance will probably not vary much over the class of rational noise spectra once the total array length sufficiently exceeds the noise correlation length.

However, this is not true for strictly optimal processors designed on the basis of an assumed functional form for the flow noise. Performance with the optimum processor, requiring derivatives of the end-point data, can vary drastically over the class of rational spectra if the actual noise spectra deviate from the assumed form, particularly if the order of the assumed functional form in the optimal design exceeds the order of the actual noise spectra. This suggests a way to make the theoretical optimal processor "robust" (less sensitive). One makes the optimal processor more robust by reducing or eliminating the order of the data differentiation at the interval end points. With rational noise spectra, one achieves this with lowest order optimal processor designs, such as the first-order Butterworth wavenumber spectrum used in this study. This then suggests that in any practical problem where actual noise spectra are

seldom known, it is probably wise to instrument optimal processors assuming the lowest possible (nontrivial) order functional form for the noise spectra.

6.3 Suggestions for Future Work

In almost all cases, we have obtained exact solutions to our formulation of the binary detection problem in flow noise. As usual, there remain unresolved issues, a partial list of which follows:

1. We have not established mathematically (for wavenumber spectra more general than the first-order Butterworth) that conventional beamforming on a plane wave signal with arrays of discrete sensors is asymptotically optimal when the array length is sufficiently large compared with noise correlation length. Our mathematical analysis and numerical computations indicate that conventional beamforming is nearly optimal when the array length exceeds two noise (Butterworth) correlation lengths. If one can establish this for general noise spectra, one can assert that beams not carrying the signal cannot be used to significantly reduce noise on target-carrying beams if the array length is long compared to the noise correlation length. Under these circumstances, only the signal-carrying beams are relevant for detection.

2. We have not considered the complete sensitivity problem, specifically amplitude and phase error tolerance, which will surely impact any of our predicted performance values. This is a basic issue for any paper study. We feel, however, that consideration of this issue will serve to reinforce the argument for conventional beamforming followed by modified Eckart postbeamformer filtering. It frequently happens in practice that such suboptimum instrumentations are least sensitive to error tolerances. In contrast, optimal instrumentations are usually more complex to build than the simpler conventional processor and, typically, are more sensitive to error tolerances.

APPENDIX A

DETECTION INDEX WITH CONTINUOUS OBSERVATIONS

The space-continuous form of the conventional detection index for detector structure in Fig. 2.5, with frequency scaling, is obtained directly from (2.78):

$$d^2 = \frac{\left| \sum_{k=1}^{N} |C_k|^2 \; S_k \; \underline{H}_k^* \; \underline{V}_k \; \underline{V}_k^* \; \underline{H}_k \right|^2}{\sum_{k=1}^{N} |C_k|^4 \; N_k^2 \; \left| \underline{H}_k^* \; Q_k \; \underline{H}_k \right|^2} . \qquad \text{(A.1)}$$

Inserting $\underline{H}_k = \underline{V}_k$, the conventional detection index with frequency scaling is

$$d^2 = \frac{\left| M^2 \Delta^2 \sum_{k=1}^{N} |C_k|^2 \; S_k \right|^2}{\sum_{k=1}^{N} |C_k|^4 \; N_k^2 \left| \sum_{i=1}^{M} \sum_{l=1}^{M} \underline{V}_i^* \; Q_{il} \; \underline{V}_l \; \Delta_i \Delta_l \right|^2} , \qquad \text{(A.2)}$$

$$\Delta^2 = \Delta_i \Delta_l ,$$

where i and l denote identical uniform sampling of interval Δ on x and y, respectively, in $[-L/2, L/2]$. With $N_k Q_{il} = q_k(x_i, y_l)$, a general sampled noise covariance function, we write (A.2) as follows:

$$d^2 = \frac{\left| M^2\Delta^2 \sum_{k=1}^{N} |C_k|^2 S_k \right|^2}{\sum_{k=1}^{N} |C_k|^4 \left| \sum_{l=1}^{M} e^{-j\nu_s x_i} \Delta_l \sum_{i=1}^{M} q_k(x_i, y_l) e^{j\nu_s y_l} \Delta_i \right|^2} . \quad (A.3)$$

Taking the limit of (A.3) as Δ_i, $\Delta_l \to 0$, with continuity conditions assumed satisfied, we obtain

$$d^2 \to \frac{\left| L^2 \sum_{k=1}^{N} |C_k|^2 S_k \right|^2}{\sum_{k=1}^{N} |C_k|^4 \left| \int_{-L/2}^{L/2}\int e^{+j\nu_s y} e^{-j\nu_s x} q_k(x,y)\,dxdy \right|^2} , \quad (A.4)$$

where

$\Delta_i \Delta_l \to dxdy$,

$M\Delta \to L \quad q_k(x_i, y_l) \to q_k(x,y)$,

$e^{+j\nu_s y_l} \to e^{+j\nu_s y}$, and

$e^{-j\nu_s x} \to e^{-j\nu_s x}$.

For sufficiently large T, the sum over k can be approximated by an integral yielding

$$d^2 \doteq \frac{T}{2\pi} \frac{\left| L^2 \int_0^W |C(\omega)|^2 \, S(\omega) d\omega \right|^2}{\int_0^W |C(\omega)|^4 \left| \iint_{-L/2}^{L/2} e^{+j\nu_s y} e^{-j\nu_s x} q(\omega;x,y) dxdy \right|^2 d\omega}, \tag{A.5}$$

where $q_k(x,y) \rightarrow q(\omega;x,y)$, $C_k \rightarrow C(\omega)$, and it is understood that ν_s is a function of radian frequency ω.

Array gain for the conventional detector structure on space-continuous $[-L/2, L/2]$ is obtained easily by considering only the ktn component of (A.4):

$$G_{kc} \triangleq \frac{L^2 I_k}{\iint_{-L/2}^{L/2} e^{j\nu_s y} e^{-j\nu_s x} q_k(x,y) dxdy}. \tag{A.6}$$

Note that (A.6) is not affected by frequency scaling, C_k. Hence, narrowband conventional array gain is not influenced by frequency scaling following conventional beamforming.

Let

$$x - y = \sigma$$
$$x + y = \gamma \; ; \tag{A.7}$$

then the unique solution for x and y is

$$x = \frac{\gamma + \sigma}{2}$$
$$x = \frac{\gamma - \sigma}{2} \quad . \tag{A.8}$$

The Jacobian of the transformation is 1/2. It follows that

$$\int_{-L/2}^{L/2}\int e^{j\nu_s y} e^{-j\nu_s x} q_k(x-y)dxdy =$$

$$\frac{1}{2}\left\{\int_{-L}^{0} d\sigma\, e^{-j\nu_s\sigma} q_k(\sigma) \int_{-L-\sigma}^{L+\sigma} d\gamma + \int_{0}^{L} d\sigma\, e^{-j\nu_s\sigma} q_k(\sigma) \int_{-L+\sigma}^{L-\sigma} d\gamma\right\}$$

$$= \int_{-L}^{0} d\sigma\, e^{-j\nu_s\sigma} q_k(\sigma)(L+\sigma) + \int_{0}^{L} d\sigma\, e^{-j\nu_s\sigma} q_k(\sigma)(L-\sigma) \tag{A.9}$$

or, the equivalent,

$$\int_{-L/2}^{L/2}\int e^{j\nu_s y}\, e^{-j\nu_s x}\, q_K(x-y)\,dx\,dy = L\int_{-L}^{L} d\sigma\; q_K(\sigma)e^{-j\nu_s\sigma}\left(1-\frac{|\sigma|}{L}\right). \tag{A.10}$$

Inserting (A.10) into (A.6), we obtain

$$G_{KC} = \frac{LI_K}{\int_{-L/2}^{L/2} d\sigma\; q_K(\sigma)e^{-j\nu_s\sigma}\left(1-\frac{|\sigma|}{L}\right)}\,. \tag{A.11}$$

Letting $\beta_K L \gg 1$,

$$\begin{aligned}\int_{-L}^{L} d\sigma\; q_K(\sigma)e^{-j\nu_s\sigma}\left(1-\frac{|\sigma|}{L}\right) &\approx \int_{-\infty}^{\infty} d\sigma\; q_k(\sigma)e^{-j\nu_s\sigma}\\ &= Q_n(\nu_s)\,,\end{aligned} \tag{A.12}$$

where we have used the Wiener-Khintchine relationship [37] between the noise spatial covariance function $q_k(\sigma)$ and its wavenumber spectrum $Q_n(\nu_s)$. Inserting (A.12) into (A.11), we have the large $\beta_k L$ conventional array gain for the general noise wavenumber spectrum $Q_n(\nu)$ with power spectrum I_κ:

$$G_{kc} \simeq \frac{L\, I_\kappa}{Q_n(\nu_s)} , \qquad \beta_k L >> 1 . \tag{A.13}$$

For the first-order Butterworth homogeneous covariance function in (2.34), we have, from (A.10), that

$$\int_{-L/2}^{L/2}\int e^{j\nu_s y}\, e^{j\nu_s x}\, q_k(x-y)\,dx\,dy = 1_k \int_{-L}^{L} d\sigma\, e^{-\beta_k|\sigma| - j(\nu_k-\nu_s)\sigma}(L-|\sigma|)$$

$$= 2I_k \int_0^L d\sigma\, e^{-\beta_k\sigma}(L-\sigma)\cos\nu_d\sigma$$

$$= 2I_k L \int_0^L d\sigma\, e^{-\beta_k\sigma}\cos\nu_d\sigma - 2I_k \int_0^L \sigma\, e^{-\beta_k\sigma}\cos\nu_d\sigma\, d\sigma ,$$

$$\nu_d = \nu_k - \nu_s . \tag{A.14}$$

These are tabulated integrals [38, Gradshteyn and Ryzhik, p. 196 no. 3, p. 198, no. 6], which combine to yield

$$\int_{-L/2}^{L/2}\int e^{j\nu_s y}\, e^{-j\nu_s x}\, q_k(x-y)\,dx\,dy$$

$$= \frac{2I_k\beta_k L}{\beta_k^2+\nu_d^2} + \frac{2I_k(\nu_d^2-\beta_k^2)}{(\nu_d^2+\beta_k^2)^2} + \frac{2I_k e^{-\beta_k L}}{(\nu_d^2+\beta_k^2)^2}\Big((\nu_d^2-\beta_k^2)\cos\nu_d L + 2\nu_d\beta_k \sin\nu_d L\Big). \qquad (A.15)$$

Inserting (A.15) into (A.6), we obtain

$$G_{kc} = \frac{L}{\frac{2\beta_k}{\beta_k^2+\nu_d^2} + \frac{2(\nu_d^2-\beta_k^2)}{L(\nu_d^2+\beta_k^2)^2} + \frac{2e^{-\beta_k L}}{L(\nu_d^2+\beta_k^2)^2}\Big((\nu_d^2-\beta_k^2)\cos\nu_d L + 2\nu_d\beta_k\sin\nu_d L\Big)} \qquad (A.16)$$

or, equivalently,

$$G_{kc} = \frac{\frac{\beta_k L}{2}\left(1+\nu_d^2/\beta_k^2\right)}{1+\frac{\left(\nu_d^2-\beta_k^2\right)}{\beta_k L(\nu_d^2+\beta_k^2)}\left(1-e^{-\beta_k L}\left(\cos\nu_d L + \frac{2\nu_d\beta_k}{\left(\nu_d^2-\beta_k^2\right)}\sin\nu_d L\right)\right)}. \qquad (A.17)$$

APPENDIX B

ARRAY GAIN

WITH DISCRETE OBSERVATIONS

For a linear array of M regularly spaced sensors in $[-L/2, L/2]$, separated by a distance,

$$\Delta = \frac{L}{M - 1} . \tag{B.1}$$

The elements of the first-order Butterworth noise covariance matrix Q_k in (4.6) from (2.34) are

$$Q_k\Big|_{rn} = e^{-\beta_k \left|(r-n)\Delta\right| + j\nu_k(r-n)\Delta} , \qquad r,n = 1, 2, \ldots, M . \tag{B.2}$$

Optimal Array Gain

Optimal array gain from (2.49) is

$$G_{ko} \triangleq \underline{V}_k^* \, Q_k^{-1} \, \underline{V}_k , \tag{B.3}$$

where the "steering vector" $\underline{V}_k$ is defined by (2.22). From (2.22) and (B.3), we obtain

$$G_{ko} = \left[e^{-j\nu_s x_1} \; e^{-j\nu_s x_2} \; \cdots \; e^{-j\nu_s x_M} \right] \frac{1}{1 - |\rho_k|^2} \begin{bmatrix} 1 & -\rho_k & & O \\ -\rho_k^* & 1+|\rho_k|^2 & \ddots & \\ & \ddots & \ddots & -\rho_k \\ O & & -\rho_k^* & 1 \end{bmatrix} \begin{bmatrix} e^{j\nu_s x_1} \\ e^{j\nu_s x_2} \\ \vdots \\ e^{j\nu_s x_M} \end{bmatrix} . \tag{B.4}$$

Diagonal elements of banded, Hermitian Q_k^{-1} contribute terms

$$\frac{M + (M - 2)\,|\rho_k|^2}{1 - |\rho_k|^2} .$$

Off diagonal elements of Q_k^{-1} contribute terms

$$\frac{(M - 1)(-\hat{\rho}_k - \hat{\rho}_k^*)}{1 - |\rho_k|^2} ,$$

$$\hat{\rho} = e^{-\beta_k \Delta + j\Delta\nu_d} ,$$

$$\nu_d = \nu_k - \nu_s .$$

Hence,

$$G_{ko} = \frac{1}{1 - |\hat{\rho}_k|^2} \left[M + (M - 2)\,|\hat{\rho}_k|^2 + (M - 1)(-\hat{\rho}_k) + (M - 1)(-\hat{\rho}_k^*) \right] \tag{B.5}$$

or, equivalently,

$$G_{ko} = \frac{M}{1 - |\hat{\rho}_k|^2} \left[1 + (1 - \tfrac{2}{M})\,|\hat{\rho}_k|^2 - (1 - \tfrac{1}{M})(\hat{\rho}_k + \hat{\rho}_k^*) \right] . \tag{B.5a}$$

Conventional Array Gain

Conventional array gain is obtained from the general expression in (2.69):

$$G_{kc} = \frac{M^2}{\underline{V}_k^* Q_k \underline{V}_k} \quad . \tag{B.6}$$

Expanding the quadratic form in the denominator of (B.6), using Q_k from (4.6), we have

$$\underline{V}_k^* Q_k \underline{V}_k = M + (M-1)\hat{\rho}_k^* + (M-2)\hat{\rho}_k^2 + \ldots + (M-(M-1))\hat{\rho}_k^{M-1} +$$

$$+ (M-1)\hat{\rho}_k^* + (M-2)\hat{\rho}_k^{*2} + \ldots + (M-(M-1))\hat{\rho}_k^{*M-1}. \tag{B.7}$$

An equivalent form for (B.7) is

$$\underline{V}_k^* Q_k \underline{V}_k = \sum_{i=-M+1}^{M-1} (M - |i|)\hat{\rho}_k^i \quad . \tag{B.8}$$

Inserting (B.8) into (B.6), we arrive at

$$G_{kc} = \frac{M}{\sum_{i=-M+1}^{M-1} (1 - \frac{|i|}{M})\hat{\rho}_k^i} \quad . \tag{B.9}$$

A more useful expression for (B.9) takes the form

$$G_{kc} = \frac{M}{1 + \sum_{i=1}^{M-1} (1 - \frac{i}{M})\hat{\rho}_k^{\,i} + (1 - \frac{i}{M})\hat{\rho}_k^{\,i*}} \tag{B.10}$$

or the equivalent

$$G_{kc} = \frac{M}{\sum_{i=0}^{M-1} (1 - \frac{i}{M})\hat{\rho}_k^{\,i} + \sum_{i=0}^{M-1} (1 - \frac{i}{M})\hat{\rho}_k^{\,i*} - 1} \; . \tag{B.10a}$$

Sums (geometric progressions) in the denominator of (B.10a) have closed forms from [38, p. 1, Equation 0.113], which, when inserted into (B.10a), yield

$$G_{kc} = \frac{M}{\frac{1 - \frac{1}{M}\hat{\rho}_k^{\,M}}{(1 - \hat{\rho}_k)} - \frac{\hat{\rho}_k(1 - \hat{\rho}_k^{\,M-1})}{M(1 - \hat{\rho}_k)^2} + \frac{1 - \frac{1}{M}\hat{\rho}_k^{\,*M}}{(1 - \hat{\rho}_k^{\,*})} - \frac{\hat{\rho}_k^{\,*}(1 - \hat{\rho}_k^{\,*M-1})}{M(1 - \hat{\rho}_k^{\,*})^2} - 1} \; , \tag{B.11}$$

$$[\rho_k \neq 1] \; .$$

A straightforward calculation yields an equivalent expression,

$$G_{kc} = \frac{M}{\frac{1 - |\hat{\rho}_k|^2}{|1 - \hat{\rho}_k|^2} - \frac{2}{M} R_e\left(\frac{\hat{\rho}_k(1 - \hat{\rho}_k^M)}{(1 - \hat{\rho}_k)^2}\right)} ,$$

$$[\rho_k \neq 1] . \qquad \text{(B.11a)}$$

Array Gain for Conventional Beamforming on Subarrays

In physical terms, the overall array gain for the clustered structure is the signal-to-noise ratio at the beamformer output divided by the signal-to-noise ratio at each sensor.

The array gain for a cluster is obtained from the general expression for array gain in (2.63):

$$G_{k_{clus}} = \frac{\underline{H}_k^* \underline{V}_k \underline{V}_k^* \underline{H}_k}{\underline{H}_k^* Q_k \underline{H}_k} . \qquad \text{(B.12)}$$

The matrix filter for each cluster steers to wavenumber ν_D:

$$\underline{H}_k^* = \left[e^{-j\nu_D x_1} \; . \; . \; . \; e^{-j\nu_D x_{M_1}} \right] , \qquad \text{(B.13)}$$

where

$$\nu_D = \frac{\omega_k}{c} \cos \theta_D \ . \tag{B.14}$$

Note, ν_D does not necessarily coincide with the signal wavenumber ν_s. One determines array gain for a cluster using

$$\underline{V}_k = \begin{bmatrix} e^{-j\omega_k \frac{\underline{\delta} \cdot \underline{x}_1}{c}} \\ \vdots \\ e^{-j\omega_k \frac{\underline{\delta} \cdot \underline{x}_{M_1}}{c}} \end{bmatrix} , \tag{B.15}$$

where now $\underline{\delta} \cdot \underline{x}/c$ is the delay at point x in the cluster relative to the origin or reference point within a cluster. For uniformly spaced sensors, assuming that the first sensor within a cluster is the reference point,

$$\underline{H}_k^* \ \underline{V}_k = \sum_{i=0}^{M_1-1} e^{(\nu_s - \nu_D) i\Delta} \quad , \quad \Delta = \frac{1}{M_1 - 1} \ . \tag{B.16}$$

It follows from (B.16) and the properties of a geometric series that

$$\underline{H}_k^* \underline{V}_k \underline{V}_k^* \underline{H}_k = \left| \sum_{i=0}^{M_1-1} e^{j(\nu_s-\nu_D)i\Delta} \right|^2 = M_1^2 \left(\frac{\sin\left(\frac{M_1\Delta(\nu_s - \nu_D)}{2}\right)}{M_1 \sin\left(\frac{\Delta(\nu_s - \nu_D)}{2}\right)} \right)^2$$

$$= M_1^2 \hat{S}^2 . \qquad (B.17)$$

If we now define

$$\frac{M_1^2}{\underline{H}_k^* \underline{Q}_k \underline{H}_k} \triangleq G_{kc}|_{sub} , \qquad (B.18)$$

then

$$G_{k_{clus}} = \hat{S}^2 G_{kc}|_{sub} . \qquad (B.19)$$

Note this is <u>not</u> the usual G_{kc} since $\nu_s \neq \nu_d$ in (B.13).

The overall array gain at the beamformer output is obtained in a similar manner from (2.63) by treating the clusters as individual sensors with noise uncorrelated between clusters. With beamformer matrix filter

$$\underline{H}_k = \begin{bmatrix} e^{-j\omega_k \frac{\underline{\delta} \cdot \underline{x}_1}{c}} \\ \vdots \\ e^{-j\omega_k \frac{\underline{\delta} \cdot \underline{x}_{N_1}}{c}} \end{bmatrix} = \underline{V}_k \ , \qquad \text{(B.20)}$$

we obtain

$$G_{KD} \triangleq \frac{N_1^2}{\underline{V}_k^* \ Q_k \ \underline{V}_k} \ G_k\big|_{clus} \ . \qquad \text{(B.21)}$$

Since the noise is uncorrelated between clusters, we have, in this case,

$$Q_k = I \qquad \text{(Identity Matrix).} \qquad \text{(B.22)}$$

Therefore,

$$G_{kD} \triangleq N_1 \ \hat{S}^2 \ G_{kc}\big|_{sub} \ . \qquad \text{(B.23)}$$

Analytically, one generates overall array gain, with correct steering within subarrays, by setting $\nu_D = \nu_s$. Hence (B.23) becomes

$$G_{kD} = N_1 \, G_{kc}\big|_{sub} \, . \tag{B.24}$$

One extends (B.23) to array gain for the space-continuous subaperture in Fig. 5.1 in the manner of Appendix A. Taking the limit in (B.23) as $\Delta \to 0$, with continuity conditions assumed satisfied on fixed l and setting $\nu_D = o$ in (B.17), we obtain

$$G_{kD} \to G_{kT} \quad N_1 \, S_c^{\,2} \, G_{kc}\big|_{sub\ c} \, , \tag{B.25}$$

where $M_1 - 1 \approx M_1$ and $M_1 \Delta \to 1$,

$$\frac{\sin \frac{M_1 \Delta \nu_s}{2}}{M_1 \sin \frac{\Delta \nu_s}{2}} \to \frac{\sin \frac{l \nu_s}{2}}{\frac{l \nu_s}{2}} = S_c \, , \tag{B.26}$$

represents the response of a space-continuous subaperture (extended sensor) with generally no steering within the sensor to the plane wave signal at ν_s unless $\nu_s = 0$. $\underline{V}_k$ in (B.13) becomes a vector of ones, in this case, and

$$G_{kc}|_{\text{sub c}} = \frac{1}{\frac{2\beta_k}{\nu_k^2+\beta_k^2} + \frac{2(\nu_k^2-\beta_k^2)}{l(\nu_k^2+\beta_k^2)^2} - \frac{2e^{-\beta_k l}\left((\nu_k^2-\beta_k^2)\cos \nu_k l + 2\nu_k\beta_k \sin\nu_k l\right)}{l(\nu_k^2+\beta_k^2)^2}} \tag{B.27}$$

or, equivalently,

$$G_{kc}|_{\text{sub c}} = \frac{\frac{\beta_k l}{2}\left(1 + \nu_k^2/\beta_k^2\right)}{1 + \frac{\left(\nu_k^2 - \beta_k^2\right)}{\beta_k l\left(\nu_k^2 + \beta_k^2\right)}\left(1 - e^{-\beta_k l}\left(\cos \nu_k l + \frac{2\nu_k\beta_k}{\left(\nu_k^2 - \beta_k^2\right)} \sin \nu_k l\right)\right)}. \tag{B.28}$$

Equation (B.28) is analogous to the array gain expression in (3.14) for the entire array. The key difference in (B.28) is that the extended sensor is <u>always</u> steered to broadside.

BIBLIOGRAPHY

1. Urick, R. J., Principles of Underwater Sound, 3rd edition, McGraw-Hill Book Company, Inc., NY, 1983.

2. Pasupathy, S., "Optimal and Conventional Processing of Space-Time Signals," Ph.D Thesis, Yale University, New Haven, CT, 1973.

3. Jorgensen, W., and G. Maidanik, "Response of a System of Point Transducers to Turbulent-Boundary-Layer Pressure Field," J. Acous. Soc. Am., vol. 43, 1968, pp. 1390-1394.

4. Kennedy, R. M., Cancellation of Turbulent-Boundary-Layer Pressure Fluctuations, NUSC Technical Report 3006, Naval Underwater Systems Center, New London, CT, 10 September 1970.

5. Nuttall, A. H., and D. W. Hyde, A Unified Approach to Optimum and Suboptimum Processing for Arrays, NUSC Technical Report 992, Naval Underwater Systems Center, New London, CT, 22 April 1969.

6. Fay, J. W., and N. L. Owsley, "Optimum Turbulent-Boundary-Layer Noise Suppression With Suboptimum Realizations," J. Acous. Soc. Am., vol. 64, 1978.

7. Proceedings of the IEEE, Special Issue on Detection Theory and Application, May 1970.

8. Bryn, F., "Optimal Signal Processing of Three-Dimensional Arrays Operating on Gaussian Signals and Noise," J. Acous. Soc. Am., vol. 34, March 1962, pp. 289-297.

9. Vanderkulk, W., "Optimum Processing for Acoustical Arrays," J. Brit. I.R.E., vol. 26, no. 4, October 1963, pp. 285-292.

10. Edelblute, D. J., J. M. Fisk, and G. L. Kinnison, "Criteria for Optimum Signal Detection Theory for Arrays," J. Acous. Soc. Am., vol. 41, January 1967, pp. 199-205.

11. Middleton, D., and H. L. Groginsky, "Detection of Random Acoustic Signals by Receivers With Distributed Elements: Optimum Receiver Structures for Normal Signal and Noise Fields," J. Acous. Soc. Am., vol. 38, November 1965, pp. 727-737.

12. Chang, J. H., "Adaptive Array Processors," Ph.D Thesis, Yale University, New Haven, CT, 1969.

13. Schultheiss, P. M., "Passive Sonar Detection in the Presence of Interference," J. Acous. Soc. Am., vol. 43, 1968, pp. 418-425.

14. Anderson, V. C., and P. Rudnick, "Rejection of a Coherent Arrival at the Array," J. Acous. Soc. Am., vol. 45, May 1969, pp. 406-410.

15. Selin, I., Detection Theory, Princeton University Press, Princeton, NJ, 1965.

16. Root, W. L., "The Detection of Signals in Gaussian Noise," in Communication Theory, A. V. Balakrishnan, ed., ch. 4, McGraw-Hill Book Company, Inc., NY, 1968.

17. Root, W. L., "Stability in Signal Detection Problems," Proc. Symp. Appl. Math., vol. 16, 1964, pp. 247-263.

18. Lewis, J. B., and P. M. Schultheiss, "Optimum and Conventional Detection Using a Linear Array," J. Acous. Soc. Am., vol. 49, 1971, pp. 1083-1091.

19. Van Trees, H. L., Detection, Estimation, and Modulation Theory, part I, John Wiley and Sons, 1968.

20. Helstrom, C. W., Statistical Theory of Signal Detection, Pergamon Press, 1960.

21. Woodward, P. M., Probability and Information Theory With Applications to Radar, Pergamon Press, 1953.

22. Strasberg, M., "Hydrodynamic Flow Noise in Hydrophones," Adaptive Methods in Underwater Acoustics, NATO ASI Series C, Math and Physical Sciences, vol. 151, 1984.

23. Blake, W. K., and D. M. Chase, "Wavenumber-Frequency Spectra of Turbulent Boundary Layer Pressure Measured by Microphone Arrays," J. Acous. Soc. Am., vol. 49, 1971, pp. 862-877.

24. Chase, D. M., "Wave Vector Structure of Turbulent Wall Pressure and Its Filtering by Normal Transmission and Spatial Averaging in Sensor Arrays," Adaptive Methods in Underwater Acoustics, NATO ASI Series C, Math, and Physical Sciences, vol. 151, 1984.

25. Bakewell, H. P., Jr., G. F. Carey, J. J. Libuha, H. H. Schloemer, and W. A. Von Winkle, Wall Pressure Fluctuations in Turbulent Flow, NUSC Technical Report 559, Naval Underwater Sound Laboratory, New London, CT, August 1962.

26. Bakewell, H. P., Jr., "Narrowband Investigations of Longitudinal Space-Time Correlation Function in Turbulent Airflow," J. Acous. Soc. Am., vol. 36, January 1964, pp. 146-148.

27. Corcos, G. M., "The Resolution of Pressure in Turbulence," J. Acous. Soc. Am., vol. 35, 1963, pp. 192-199.

28. Corcos, G. M., "The Resolution of Turbulent Pressure at the Wall of a Boundary Layer," J. Sound. Vib., vol. 6, 1967, pp. 55-70.

29. Hodgkiss, W. S., and L. W. Nolte, "Covariance Between Fourier Coefficients Representing the Time Waveforms Observed From an Array of Sensors," J. Acous. Soc. Am., vol. 59, no. 3, March 1976.

30. Bangs, W. J., "Array Processing With Generalized Beams," Ph.D Thesis, Yale University, New Haven, CT, 1971.

31. Bartlett, M. S., "An Inverse Matrix Adjustment Arising in Discriminant Analysis," Ann. Math Stat., 22, March 1951, pp. 101-111.

32. Kelly, E. J., J. S. Reed, and W. L. Root, "The Detection of Radar Echoes in Noise," J. Siam, vol. 8, no. 7, June 1960.

33. Cox, H., "Optimum Arrays and the Schwartz Inequality," J. Acous. Soc. Am., vol. 45, no. 1, 1969, pp. 228-232.

34. Cox, H., "Line Array Performance When the Signal Coherence is Spatially Dependent," J. Acous. Soc. Am., vol. 54, no. 6, 1973, pp. 1743-1746.

35. Gold, B., and C. Radar, Digital Processing of Signals, McGraw Hill Book Company, NY, 1969.

36. Blackman, R. B., and J. W. Tukey, The Measurement of Power Spectra, Dover Publications, NY, 1958.

37. Stark, H., and F. B. Tuteur, Modern Electrical Communications Theory and Systems, Prentice-Hall, Inc., Englewood Cliffs, NJ, 1979.

38. Gradsnteyn, I. S., and I. M. Ryzhik, Table of Integrals, Series, and Products, Academic Press, Inc., NY, 1980.

39. Hahn, W. R., and S. A. Tretter, "Optimum Processing for Delay-Vector Estimation in Passive Signal Arrays," IEEE Trans. on Inf. Theory, vol. IT-19, no. 5, September 1973.

40. Carter, G. C., "Passive Ranging Errors Due to Receiving Hydropnone Position Uncertainty," USN J. Underwater Acous., vol. 29, 1979, pp. 78-89.

41. Carter, G. C., "Variance Bounds for Passively Locating an Acoustic Source With Symmetric Line Array," J. Acous. Soc. Am., vol. 62, 1977, pp. 922-926.

42. Ianiello, P., and P. M. Schulthesis, "Optimum Range and Bearing Estimation With Randomly Perturbed Arrays," J. Acous. Soc. Am., vol. 68, no. 1, July 1980.

INITIAL DISTRIBUTION LIST

Addressee	No. of Copies
DIA	1
NRL (Dr. J. Hansen, Dr. R. Menton)	2
NRL USRD (Dr. L. Van Buren)	1
NOSC (Library, Code 6565)	1
DTNSRDC BETH (Code U31, -U31 (Dr. G. Maidanik, E. F. Geib))	3
NAVPGSCOL	1
NAVSEASYSCOM (63-D (CDR L. Schneider, Dr. Y. Yam, C. Smith, D. Early, Dr. C. Walker, E. Plummer); PMS-411 (W. Burgess, CDR. E. Graham))	8
NORDA (Code 113 (R. Martin))	1
SPAWAR (Code 612 (R. Mitnick, B. Ogg))	2
ONR (ONR-411 (Dr. N. Gerr), -220 (T. J. Warfield))	2
OCNR/ONT (OCNR 231, CAPT R. Fitch))	1
DARPA STO (Dr. C. Stuart)	1
Johns Hopkins APL (H. South, J. Lombarde, R. Wojcik)	3
SUBDEVGRU 12 (M. Schindler)	1
COMSUBPAC (D. Diorio, Science Advisor)	1
COMSUBLANT (B. Meyers, Science Advisor)	1
NSWC NSAP Office (Dr. S. Marshall, Director)	2
DTIC	12
ARL/Penn State, State College (Dr. S. Hayek)	1
ARL/Univ of Texas	1
MAR, INC. (Dr. L. King)	1
BBN (Dr. N. C. Martin, Dr. K. Chandirihani, H. Cox))	3
Vibrasound Research Corp. (Dr. G. F. Kuhn)	1
NOSC	1
NADC	1
NCSC	1
UCONN (Electrical Engineering Dept.)	1
URI (Electrical Engineering Dept.)	1
Northeastern Univ. (Electrical Engineering Dept.)	1
Southeastern Mass. Univ. (Electrical Engineering Dept.)	1